

**MPE-Fe(II) Footprinting: Drug Binding Sites  
on Native DNA**

Thesis by  
Michael W. Van Dyke

In Partial Fulfillment of the Requirements  
for the Degree of  
Doctor of Philosophy

California Institute of Technology  
Pasadena, California

1984

(Submitted December 28, 1983)

-ii-

To My Folks

### **ACKNOWLEDGEMENTS**

I would especially like to thank my research advisor, Peter Dervan, for all his encouragement, wisdom, and patience, which not only made this research possible but also allowed for the maturation of this being in an academic milieu. Such is a gift beyond simple measure; a lasting treasure of "portable property" as Dickens would say.

Also deserving thanks are my friends, both in the group and without, who through the time spent together, adventures and dialogues, provided the spiritual balance to the Sturm und Drang of higher education. Special note goes to those, and you know who you are, whose behavior was beyond the call of the wild and good taste. Lauds and accolades belong to those who really made this thesis possible: Debbie Chester for typing, Valerie Purvis for graphics, and Ben and Richard of Photo Lab for the pics. Financial support from the National Institutes of Health is gratefully acknowledged.

Also you have to hand it to my parents for getting the whole ball rolling, and of course it proceeds from there.

### ABSTRACT

Many small molecules, such as antibiotics used in cancer chemotherapy, are believed to execute their therapeutic action through binding to the DNA template and impeding the progress of transcription and replication. While it is possible by spectroscopic means to determine the overall affinities and stoichiometries of these small molecule/DNA interactions, the exact locations and sizes of these sites of interaction are not known. The analogous question of protein:DNA binding specificities has been answered through the use of DNase I footprinting. This technique combines DNase I cleavage of protein-protected DNA fragments and Maxam-Gilbert sequence determination methods, relying on the relatively low specificity of DNase I in a partial digestion and the ability of DNA-bound proteins to prevent phosphodiester bond hydrolysis between the base pairs they cover.

Reported within is a direct technique, MPE·Fe(II) footprinting, which allows the determination of the preferred binding sites of several small molecules on heterogeneous double helical DNAs. Methidiumpropyl-EDTA [MPE], in the presence of ferrous ion and oxygen efficiently creates single-strand breaks in double helical DNA and with significantly lower sequence specificity than DNase I. Utilizing MPE·Fe(II) as a small synthetic scissor one is capable of footprinting the preferred locations and binding site sizes of small molecules bound on native DNA.

The small molecules actinomycin D, chromomycin A<sub>3</sub>, distamycin A, echinomycin, mithramycin, netropsin, and olivomycin have been shown to demonstrate sequence specific MPE·Fe(II) cleavage inhibition, thus

allowing a determination of their preferred binding sites and site sizes. Actinomycin D was found to have a minimum site size of 3 base pairs and an absolute guanine requirement in its binding site. Distamycin A and netropsin demonstrated equivalent binding specificities, preferring contiguous A+T rich regions of 5 base pairs in length. Chromomycin A<sub>3</sub>, mithramycin, and olivomycin all shared similar binding specificities, demonstrating typically 3 base pair binding site sizes and preferring a 5'-GC-3' sequence within. Echinomycin protected a minimum of 4 base pairs; nearly all sites containing a central 5'-CG-3' sequence with 5'-COGG-3' being favored. All footprints demonstrated an opposite strand asymmetry with overprotection on the 3' end. From a collection of their preferred binding sites, binding models for these small molecules have been derived.

MPE·Fe(II) footprinting has been compared with DNase I footprinting in their ability to determine the binding specificities of both small molecules and proteins. While DNase I exhibits a slightly greater sensitivity, MPE·Fe(II) footprinting provided greater resolving capacity and importantly more precisely defined the binding locations and sizes of small molecule:DNA complexes. Both methods provided similar information in the case of a sequence-specific DNA binding protein, *lac* repressor. Investigations were also undertaken to study the effects of altered DNA conformation (Z-form DNA; binding cooperativity of different small molecules) on the interactions of small molecules with native DNA.

**TABLE OF CONTENTS**

	<u>Page</u>
<b>INTRODUCTION.....</b>	1
Interaction of Small Molecules with Nucleic Acids.....	1
Sequence Specificity of Small Molecule:DNA Interaction....	4
Methidiumpropyl-EDTA·Fe(II), [MPE·Fe(II)].....	10
Deoxyribonuclease I, [DNase I].....	12
<b>BACKGROUND.....</b>	15
Daunomycin.....	15
Actinomycin D.....	18
Netropsin and Distamycin.....	21
Chromomycin, Mithramycin, and Olivomycin.....	23
Echinomycin.....	26
Anthracyclines.....	28
Quinoxalines.....	30
Tilerones.....	30
Miscellaneous.....	32
Footprinting Small Molecules by Other Methods.....	35
<b>RESULTS AND DISCUSSION.....</b>	36
The Specificity of MPE·Fe(II) Cleavage.....	37
MPE·Fe(II) Footprinting of Small Molecules on DNA:	
Initial Studies.....	41
MPE·Fe(II) Footprinting: Opposite Strand Analyses.....	48
MPE·Fe(II) Footprinting of Chromomycin A <sub>3</sub> , Mithramycin, and Olivomycin.....	61
Comparison of MPE·Fe(II) and DNase I Footprinting.....	73

MPE·Fe(II) Footprint of the <u>lac</u> Repressor.....	85
Echinomycin Binding to DNA.....	91
Small Molecules Which Apparently Do Not Footprint.....	109
Attempted MPE·Fe(II) Footprinting of Z DNA.....	116
Investigation of Small Molecule Induced Allosteric Transitions in DNA Structure by Footprinting.....	123
Equilibrium Conditions on MPE·Fe(II) Footprinting.....	130
Comparison of MPE·Fe(II) and EDTA·Fe(II)-mediated Footprinting.....	133
Reproducibility of MPE·Fe(II) and DNase I Footprinting of Small Molecules.....	136
DNA Affinity Cleaving and MPE·Fe(II) Footprinting.....	136
Actinomycin D Binding Model.....	145
Distamycin A Binding Model.....	153
Chromomycin A <sub>3</sub> Binding Model.....	156
Echinomycin Binding Model.....	158
Footprinting of Proteins.....	162
<b>SUMMARY</b> .....	165
<b>EXPERIMENTAL</b> .....	167
DNA.....	167
Reagents.....	176
Reactions.....	182
Resolution of Data.....	189
Practical Protocols.....	197
<b>REFERENCES</b> .....	208

<b>APPENDIX.....</b>	222
Synthetic Small Molecule as Model for	
Chromomycin: DNA Interaction.....	

## INTRODUCTION

### Interactions of Small Molecules with Nucleic Acids

Many naturally occurring small molecules having molecular weights ranging from 100 to 2000 grams per mole, are antibiotics which interfere with the synthesis of nucleic acids *in vivo* and have found uses in antiviral and cancer chemotherapies.<sup>1-4</sup> A subset of these molecules interferes with nucleic acid synthesis by forming reversible complexes with a double-stranded DNA template. These drug:DNA complexes serve as impediments to alterations in the DNA structure, alterations which are necessary for the processes of transcription<sup>5</sup> and replication.<sup>6</sup> Another subset of these molecules interferes with these processes by causing permanent structural alterations in the DNA such as strand breakage, base removal, or formation of crosslinks. Examples of both types of molecules and their modes of action are shown in Figure 1.

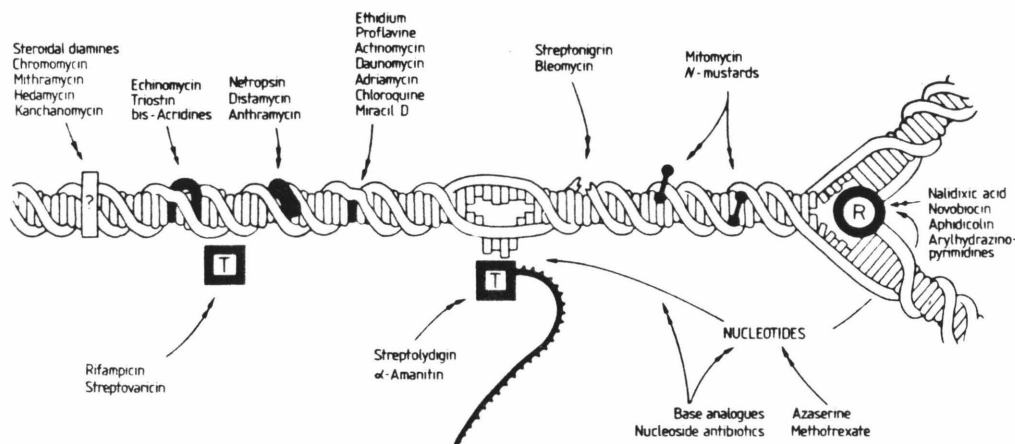


Figure 1

Sites of template interference by antibiotics and drugs. Shown is a segment of DNA on which initiation of transcription (left), transcription (center), and replication are depicted. **T** in the transcribing complex; **R** in the replicating complex. Class of molecules which affect the template capability of DNA are listed in the upper half of the figure (reproduced from Gale, et al.<sup>1</sup>).

Two general classes of interaction modes can exist between small molecules and DNA: covalent and noncovalent. Covalent binders, including such substances as mitomycin C,<sup>7</sup> cis-diamminedichloroplatinum,<sup>8</sup> anthramycin,<sup>9</sup> psoralen,<sup>10</sup> nitrogen mustard,<sup>11</sup> and various planar aromatic carcinogens,<sup>12</sup> often react by chemical or photochemical means with specific nucleotides in the DNA. These then may become labilized, eventually leading to strand scission, or may inactivate the DNA's ability to serve as a template for polymerases. The generation of interstrand crosslinks, which prevent the separation of the two strands of double helical DNA, is thought to constitute the primary lethal event for many of these covalent binding molecules.<sup>13</sup>

The second general class, those small molecules which interact noncovalently with DNA, comprised the majority of substances investigated during the course of this thesis work. Most are thought to primarily act by inhibiting the progress of RNA polymerase along an affected DNA template.<sup>2-4</sup> These small molecules may interact with DNA through the use of electrostatic forces, hydrogen bonding, and hydrophobic interactions. An example of the latter case is intercalation, where a flat planar aromatic molecule becomes inserted between the adjacent base-pairs of double helical DNA.<sup>14</sup> The base pairs of the DNA remain perpendicular to the helix axis, but the distance separating the base pairs is increased to accommodate the intercalated molecule. This results in localized unwinding of the DNA, seen as increasing the average contour length of short DNA fragments thus increasing the viscosity of a drug:DNA solution.<sup>15</sup> Binding also occurs in the major or minor grooves of DNA, where accessibility to the

hydrogen bond donators (amines) and acceptors (carbonyls and imines) on the nucleic acid bases become possible.<sup>16</sup> Inhibition of polymerase action may also be achieved by damaging the DNA through strand cleavages. These may be produced by equilibrium-binding small molecules which can generate reactive species near the DNA. Examples of these include the antibiotics bleomycin<sup>17</sup> and streptonigrin.<sup>18</sup>

These small molecules which interact with DNA may do so with some specificity as to the state, conformational structure, and/or nucleotide sequence present. DNA, as the ultimate repository of genetic information, consists of two sugar-phosphate backbones to which the bases guanine, adenine, cytosine, and thymine (including at times various methylated and glycosylated analogs) are attached by N-glycosidic linkages.<sup>19</sup> These sugar-phosphate backbones, or strands, run in an antiparallel fashion forming a double helix, with the aromatic bases guanine (G) to cytosine (C) and adenine (A) to thymine (T) hydrogen bonded together. This double helical DNA may assume a number of different conformations, dependent on ionic strength and degree of hydration present.<sup>20</sup> Examples of the A, B, and Z forms of DNA are depicted in the computer drawings as shown in Figure 2. Whereas the exact nucleotide sequence determines the amino acid sequence of the trivial protein product from a structural gene, the effect of nucleotide sequence on DNA state and solution conformations plus the effects of DNA structure on the processes of transcription, replication and their regulation is at this time not fully understood.<sup>21</sup> Knowledge of drug binding specificity to heterogeneous DNAs might help in the design of even more specific DNA binders, working towards a design of synthetic

repressors and synthetic restriction enzymes.

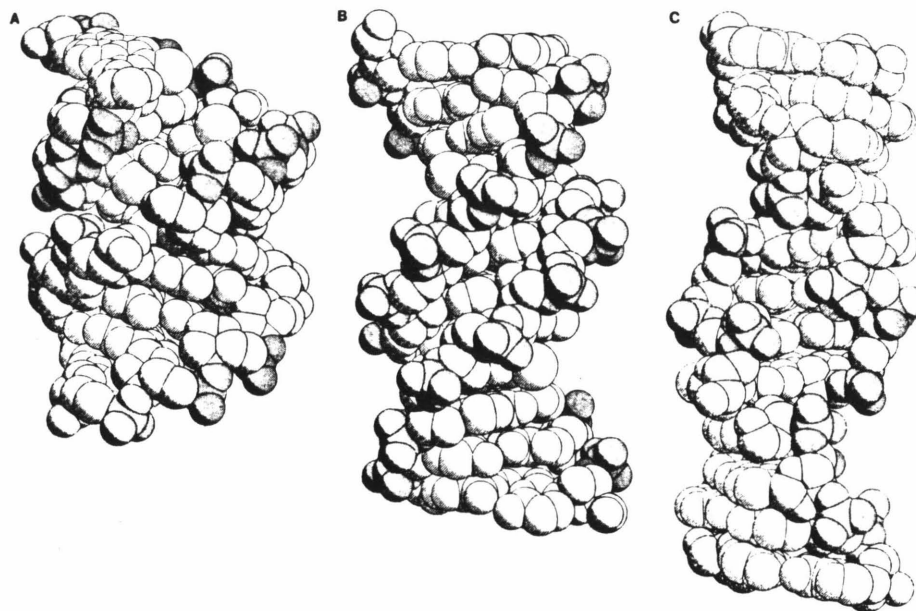


**Figure 2**

Computer generated, space filling representation of the three principal DNA conformations: A-form (A), B-form (B), and Z-form (C). Phosphates have darker, and sugars lighter, shading. In A-form, major groove is deep (top 1/2, A) while minor groove is shallow (bottom 1/2, A). B-form DNA has the minor groove in the center of the figure (B), with portions of the major groove on either side. Both A- and B-form DNAs form right-handed double helices. Z-form (C) forms a left-handed double helix, with deep minor groove running diagonally across the center of the figure.

#### **Sequence Specificity of Small Molecule:DNA Interactions**

Methods of determining the binding specificities of small molecules to DNA rely on changes in the physical parameters of these two components upon the formation of a complex. Typical of these methods include spectroscopic analyses: shift in the absorbance maxima,<sup>22</sup> changes in the magnitudes of absorbance and fluorescence,<sup>23</sup> and Cotton effects in circular dichroism;<sup>24</sup> hydrodynamic effects: increases in the thermal denaturation temperature,<sup>25</sup> decreases in buoyant density,<sup>26</sup> and

viscosity changes;<sup>14</sup> biological assays: rates for the action of DNA-dependent DNA and RNA polymerases<sup>27</sup> and protection of the DNA template to degradative enzymes.<sup>28</sup> All of these parameters may be investigated for various natural DNAs of known overall nucleotide composition or for synthetic DNA homopolymers. Correlations may then be made between percent G+C and the magnitude of the observed changes, thus providing rough information as to the base preference for their interaction with DNA. The use of synthetic repeating nucleotide DNA polymers allows the selection of a finite number of known potential binding sites and a more complete picture of the binding sequence preference.<sup>29</sup> The number of possible binding sites can be determined by the following expressions:

$$B = \frac{(4)^n}{2} \quad (n \text{ is odd})$$

or

$$B = \frac{(4)^n}{2} + \frac{(4)^{n/2}}{2} \quad (n \text{ is even})$$

where B is the number of possible binding sites and n is the number of base pairs per binding site. A representative table of the number of unique sites as a function of binding site size is provided (Table I).

Table I - Site Sizes and Numbers<sup>a</sup>

Number of base pairs in site = n	Number of unique sites possible
2	10
3	32
4	136
5	512
6	2080

a) Private communication, D. Crothers, Yale University

Although these methods make it possible to determine the overall

affinity and stoichiometry of the noncovalent binding of small molecules to DNA, the exact locations and extents of the preferred binding sites on naturally occurring heterogeneous DNA sequences are not known.

Two classic methods are capable of discretely determining the locations, sizes of binding sites, and modes of interaction between small molecules and heterogeneous DNAs. Both methods utilize short (6-12 base pair), synthetically made DNA oligomers as their binding substrates. Nucleic magnetic resonance spectroscopy (NMR), especially with the use of proton nuclear Overhauser effect (NOE) measurements, allows for the determination of intermolecular contacts between protons on the DNA and the binding ligand from which models of this solution interactions may be derived.<sup>30</sup> X-ray crystallographic analysis of small molecule:DNA complexes allows for a determination of the binding geometry in the solid state, and helps locate potential stabilizing hydrogen bonds and destabilizing steric interferences.<sup>31</sup> Neither method is suitable for the rapid assaying of the hundreds of potential binding sites present in a typical heterogeneous DNA restriction fragment under physiological solution conditions.

With the advent of chemical and enzymatic means of DNA sequencing, it has become possible to determine DNA sequences hundreds of nucleotides in length rapidly and easily.<sup>32-34</sup> In the case of double stranded DNAs, Maxam-Gilbert chemical sequencing methods are applied.<sup>33,35</sup> These rely on the partial modification and subsequent degradation of singularly end-labeled DNA restriction fragments followed by high resolution gel electrophoresis and autoradiography. Results are obtained as a series of bands on the autoradiogram corresponding to that

subset of singularly end-labeled cleavage fragments of different lengths, whose unlabeled termini are one nucleotide short of a specific modified nucleotide(s) (Figure 3). Typical selectivities are for one to two nucleotides as in the cases of the commonly observed sequencing reactions G, A>C, C, and C+T. Chemical reactions employ such reagents as dimethylsulfate and hydrazine to modify the nucleotides; piperidine is used to catalyze the strand scission reactions. Small molecules which cause modifications to the DNA that lead to strand scissions permit their sequence specificities on heterogenous DNA to be determined similarly. This has been performed for the antibiotics neocazinostatin,<sup>36</sup> bleomycin,<sup>36-38</sup> phleomycin,<sup>38</sup> tallysomycin,<sup>38</sup> adriamycin activated by NADPH cytochrome P-450 reductase,<sup>39</sup> and the alkali-labile lesions generated by aflatoxin B<sub>1</sub> activated by liver extracts.<sup>40</sup> Unfortunately with small molecules which cleave DNA it is not possible to determine what percentage of their observed specificities is due to their preferred binding interactions or to the specificity inherent in the chemical modifications they perform. Also these methods are not applicable to that majority of small molecules which bind to DNA reversibly without generating modifications on the DNA.

These difficulties arose when attempting to determine the specific binding sites on their DNA substrates for regulatory proteins such as polymerases, repressors, and other transcription factors.

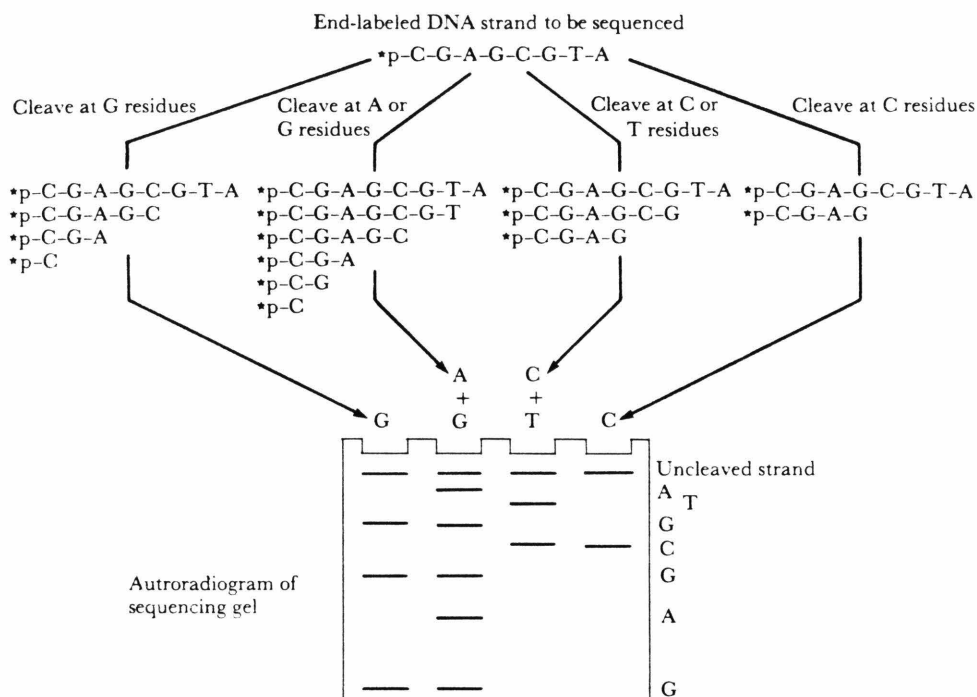


**Figure 3**

Maxam-Gilbert DNA sequencing method. Singularly end-labeled, double helical DNA is partially cleaved by specific chemical modification and piperidine treatment. Generated is a nested set of cleavage fragments whose unlabeled terminus is one nucleotide short of a modified base. Combinations of four such reactions electrophoresed in parallel allows for the determination of the DNA sequence on one strand.

Currently the best method for studying protein-DNA binding specificities is the DNase footprinting method of Galas and Schmitz.<sup>41,42</sup> This method combines partial DNase-cleavage of protein-protected DNA fragments and double-stranded DNA sequence determination techniques. Partial digestion by DNase I shows relatively little sequence specificity and the DNA-bound protein is capable of preventing cleavage of the DNA backbone between the base pairs it protects. The protein-protected DNA

sequence is expressed in the autoradiogram as a lightened region in the normal DNase I cleavage pattern. Comparison with Maxam-Gilbert sequencing lanes run in parallel allows for the exact determination of the nucleotide sequence to which the protein is bound. Cases in which this method has been employed included the lac repressor,<sup>41</sup> RNA polymerase,<sup>43</sup> and cyclic AMP receptor protein<sup>44</sup> each binding to the lactose promoter-operator region and numerous other examples.

Investigations on the interaction of Int protein with the specific site on  $\lambda$ att DNA has employed the relatively nonspecific DNA cleavers micrococcal nuclease and neocarzinostatin as substitutes for DNase I in footprinting.<sup>45</sup> Exonuclease III, an enzyme possessing 3'phosphatase and double-strand DNA specific 3' exonuclease activities, has been employed in determining the site specific binding of proteins to DNA.<sup>46</sup>

Unfortunately it is capable of only determining the 3' end of the protected fragments and therefore would have reduced sensitivity in defining two nearby binding sites on the same fragment. Regardless of the DNA cleaving agent used, whether it be nuclease or antibiotic, the problem arises as to the exact phenomenon to which this cleaver is responding to when protection afforded by protein binding is observed. For example, DNase I is known to exhibit changes in its rate of phosphodiester bond hydrolysis as a function of high level helical twist in the DNA structure.<sup>47</sup> Thus the locations of diminished DNase cleavage may be due to protein induced alterations in DNA conformation rather than steric interference. Without detailed knowledge as to the actual mechanism for cleavage and causes for specificity, complete accuracy in determining the exact location and extent of a protein binding site

cannot be obtained.

It should be possible to apply footprinting to directly determine small molecules preferred binding sites on heterogeneous DNAs. Equilibrium and kinetic binding studies indicate that different small molecules may interact simultaneously with double-stranded DNAs by either competing for similar binding sites<sup>48</sup> or by noninterfering binding at adjacent sites.<sup>49-50</sup> Thus the utilization of a small molecule which binds nonspecifically to double stranded DNA and efficiently induces cleavages may prove useful in probing the locations and extent of binding sites of small molecules on naturally occurring DNA.

**Methidiumpropyl-EDTA-Fe(II), [MPE·Fe(II)]<sup>51,52</sup>**

Recently Hertzberg and Dervan have reported the synthesis of methidiumpropyl-EDTA (MPE), (Figure 4) composed of the DNA intercalator methidium coupled to a metal chelator ethylenediaminetetraacetic acid (EDTA) by a propyl hydrocarbon linker.<sup>51</sup> The binding affinities of MPE, MPE·Ni(II), and MPE·Mg(II) to calf thymus DNA are  $2.4 \times 10^4 \text{ M}^{-1}$ ,  $1.5 \times 10^5 \text{ M}^{-1}$  and  $1.2 \times 10^5 \text{ M}^{-1}$  in 50 mM NaCl, pH 7.4.<sup>52</sup> The binding site size is 2 base pairs. MPE·Mg(II) unwinds PM2 DNA  $11 \pm 3^\circ$  per bound molecule. MPE·Fe(II) in the presence of O<sub>2</sub> efficiently cleaves DNA and with low sequence specificity. Reducing agents significantly enhance the efficiency of the cleavage reaction in the order sodium ascorbate > dithiothreitol > NADPH. Optimum ascorbate and dithiothreitol concentrations are

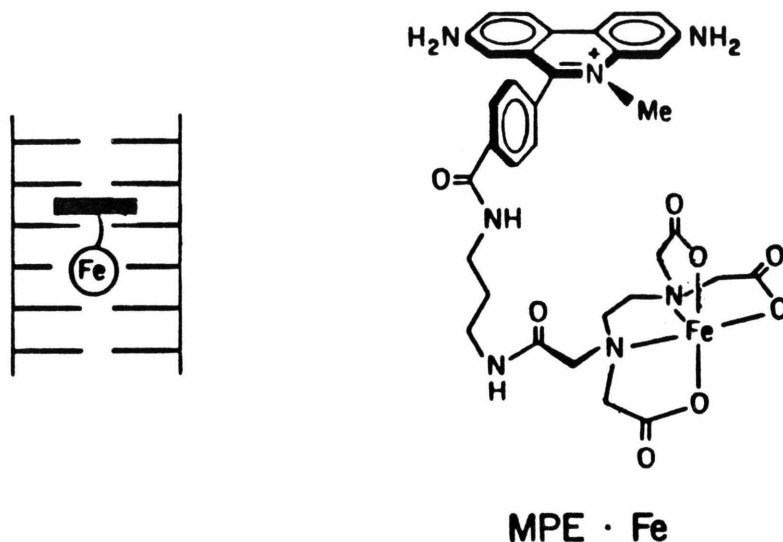
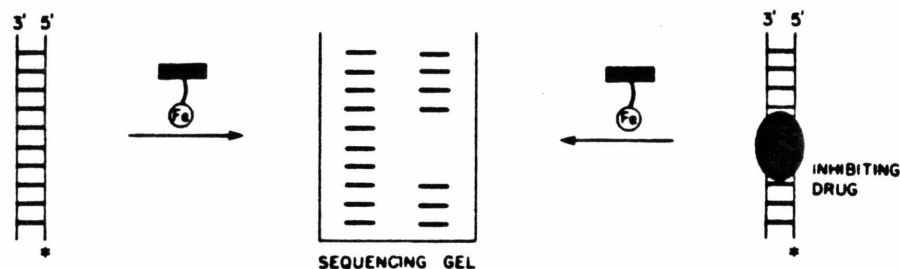


**Figure 4**

Structure of methidiumpropyl-EDTA·Fe(II) and cartoon depicting its intercalative mode of binding to DNA.

1-5 mM. Efficient cleavage of DNA with MPE·Fe(II) occurs over a pH range of 7-10 with the optimum at 7.4 (Tris·HCl buffer). Optimum cleavage time is 3.5 hours (22°C). DNA cleavage is efficient in a Na<sup>+</sup> ion concentration range of 5 mM to 1 M, with the optimum at 5 mM NaCl. The number of single strand scissions on supercoiled DNA per MPE·Fe(II) under optimum conditions is greater than stoichiometric (1.4). Metals such as Co(II), Mg(II), Ni(II) and Zn(II) inhibit strand scission by MPE. The released products from DNA cleavage by MPE·Fe(II) are the four nucleotide bases. The DNA termini at the cleavage site are 5'-phosphate and roughly equal proportions of 3'-phosphate and 3'-phosphoglycolic acid (Figure 6). The products are consistent with the oxidative degradation of the deoxyribose ring of the DNA backbone, most likely by

hydroxyl radical. This thesis reports an application of  $MPE \cdot Fe(II)$  for determining the sequence specificity of small molecule binding to heterogeneous DNA (Figure 5).



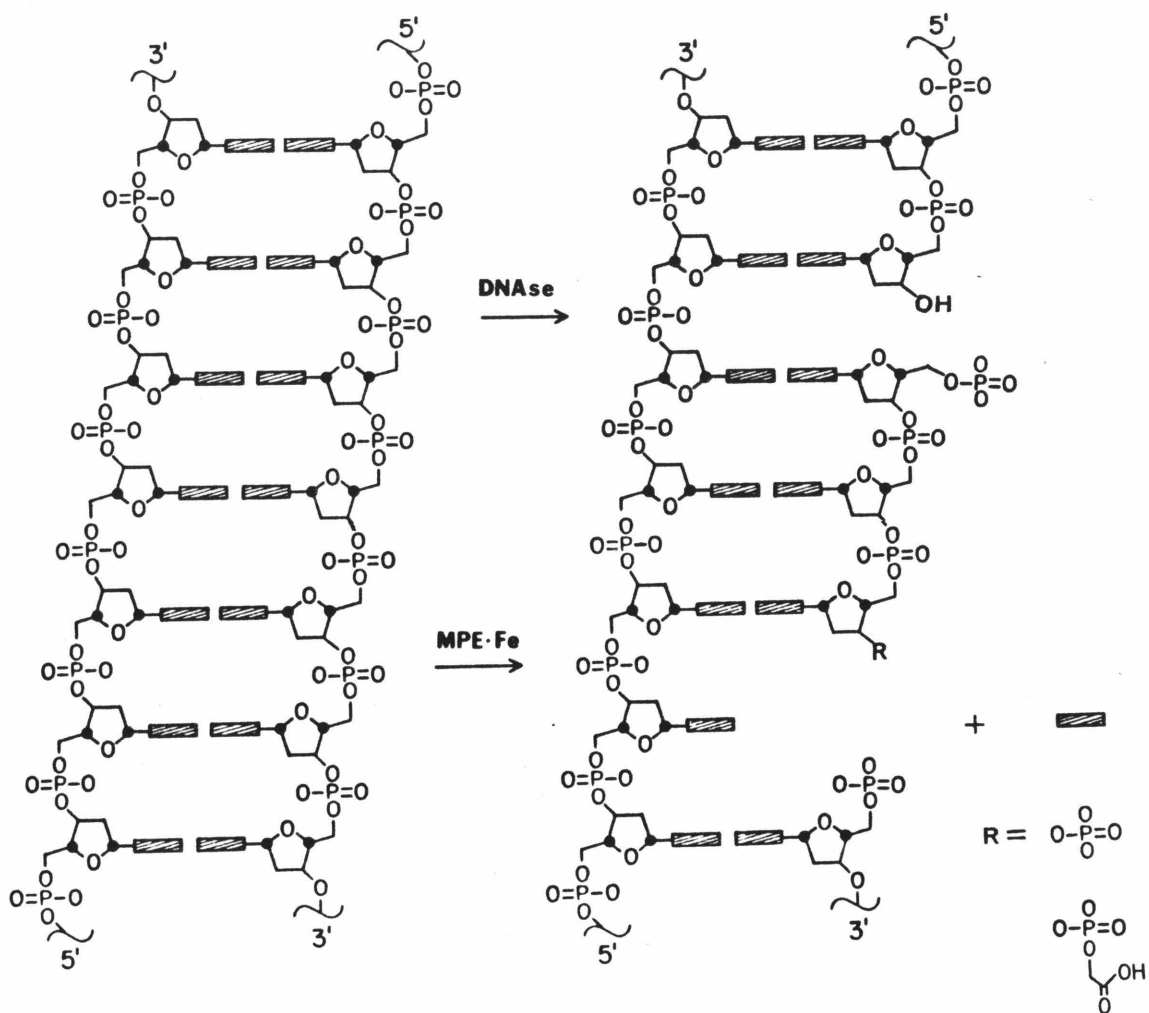
**Figure 5**

Illustration of  $MPE \cdot Fe(II)$  footprinting. Left is unprotected and right, small molecule protected double stranded DNA.

### **Deoxyribonuclease I, [DNase I]**

DNase I is the classic footprinting reagent for determining the preferred binding sites of proteins on heterogeneous, double stranded DNA. DNase I, a 30,000 dalton molecular weight protein, acts as an endonuclease cleaving either one or both strands of double helical DNA, producing 5'-phosphate and 3'-hydroxyl termini (Figure 6).<sup>53-55</sup> Cleavage sites are overestimated by 2-3 nucleotides minimally on each strand due to the internal nature of the enzyme active site. This overestimation depends on the protein being investigated.<sup>42</sup> DNA cleavage by DNase I is very efficient,  $1 \times 10^{-8}M$  DNase induces  $1 \times 10^{-6}M$  cleavages in  $2 \times 10^{-4}M$  base pairs DNA given the typical reaction conditions, 30 sec at room temperature. This is equivalent to 100 cleavages per DNase molecule. DNase I-mediated DNA cleavage

demonstrates sequence specificity in the rate of phosphodiester bond hydrolysis as a function of local helical twist.<sup>47</sup> High levels of local helical twist may be intrinsic to a given nucleotide sequence, the presence of certain flanking sequences inferring a particular conformation, or DNA structural changes induced upon small molecule and/or protein binding. The exact cause for the specificity of DNase I cleavage is not particularly well understood. Reduction of DNase I cleavage upon competing molecule binding is not uniform but appears proportional to rate of cleavage present.<sup>42</sup>



**Figure 6**

Diagram of MPE·Fe(II) and DNase I-mediated cleavages of double-stranded DNA. DNase I (top) causes a phosphodiester bond hydrolysis resulting in 3'-hydroxyl and 5'-phosphate termini. MPE·Fe(II) (bottom) cleaves through an oxidative degradation of the deoxyribose. Products are released free bases, 5'-phosphates, and either 3'-phosphates or 3'-phosphoglycolates in equal percentages.

## **BACKGROUND**

### **Small Molecules Investigated by MPE-Fe(II) Footprinting**

Reviews on the biological and physical characteristics of the antibiotics actinomycin D, chromomycin A<sub>3</sub>, daunomycin, distamycin A, echinomycin, mithramycin, netropsin, olivomycin and their interactions with nucleic acids are provided.

### **Daunomycin**

Daunomycin hydrochloride (daunorubicin, rubidomycin, and Cerubinin) is a red crystalline anthracycline antibiotic isolated from either Streptomyces peucetius or S. coeruleorubidus. It is composed of an aromatic chromophore, 7-hydroxy-9-acetyl-4-methoxy-7,8,9,10-tetrahydro-6,9,11-trihydroxy-5,12-naphthacenedione, and the amino sugar 3'-amino-2',3',6'-trideoxy- $\alpha$ -L-lyxo-hexopyranose linked by a glycoside bond at the 7 position (Figure 7). This structure was elucidated by chemical degradation studies and confirmed by x-ray crystallographic analysis of the N-bromoacetyl derivative.<sup>56</sup> Several syntheses of daunomycin and its analogs have been described. (Reviews 57,58).

Daunomycin has been shown to exhibit antibacterial,<sup>59</sup> antifungal, and antityrpanosomal properties.<sup>60</sup> In eukaryots, damage is usually nuclear in nature, consisting of changes in the nucleolus and a granular appearance in the chromatin.<sup>61</sup> Daunomycin also inhibits double-stranded DNA viruses and phages, but not single-stranded DNA or RNA viruses.<sup>59</sup> Its activity is believed to stem from its ability to interfere with the progress of RNA and DNA polymerase on a double-stranded DNA template though multiple effects are observed in

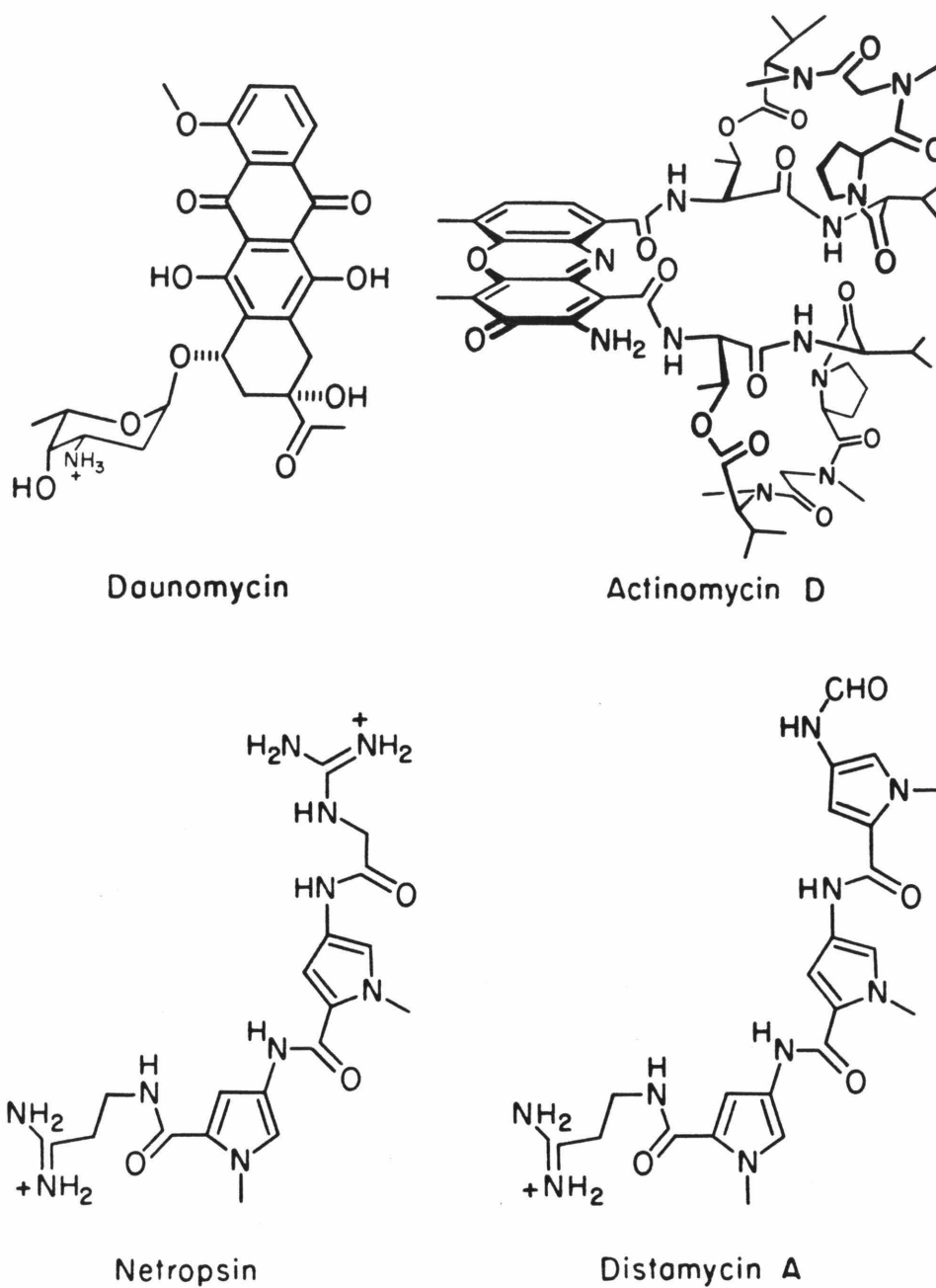


**Figure 7**

Structures of antibiotics which bind to DNA and inhibit cleavage by MPE•Fe(II).

vivo and this may not be the lethal event.<sup>62</sup> Clinically this antibiotic has been employed against acute lymphocytic and myelogenous leukemias.<sup>63</sup> Observed toxic side effects include leukopenia, thrombocytopenia, gastrointestinal distress, with the overall limiting feature being congestive heart failure.

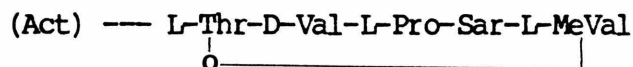
Daunomycin interacts with double-stranded DNA, but not denatured DNA, nucleotides, or RNA.<sup>64</sup> From changes in the superhelicity of  $\phi$ X174 RFI DNA, daunomycin binds with an unwinding angle of  $11^\circ$ .<sup>65</sup> Binding to DNA is dependent on the structure and stereochemistry of the amino glycoside measured.<sup>66</sup> Equilibrium dialysis experiments of daunomycin binding to various natural and homopolymers DNAs shows binding constants on the order of  $0.2-7.6 \times 10^5 \text{ M}^{-1}$  at 100 to 200 mM  $\text{Na}^+$ .<sup>67,68</sup> The binding constant decreases with increasing ionic strength. The binding site size is 3.5 base pairs for a heterogeneous DNA. Sequence specificity is for alternating purine-pyrimidine sequences, with the order for preferential binding being:  $d(A-T) > d(G-C) > dG \cdot dC > dA \cdot dT$ . For natural DNAs it shows a binding specificity of  $\alpha = 1.45$ , or slightly G+C specific. The  $\alpha$  value is defined as a measure of the relative small molecule binding affinities for DNAs of different G-C composition.<sup>69</sup> The kinetics of daunomycin association and dissociation with DNA are relatively fast,  $k_{\text{dissoc}} = 0.36$  to  $0.68 \text{ s}^{-1}$ , with this rate increasing upon increasing ionic strength.<sup>70</sup> Intercalation has been shown to proceed from the minor groove, as shown by comparisons between T2 glucosylated DNA and anthramycin-treated DNA.<sup>71</sup>

Daunomycin was thought to intercalate between the base pairs

with the amino sugar located in the minor groove where it would electrostatically interact with a DNA phosphate. X-ray crystallography of a daunomycin:hexamer crystal showed that this model is generally correct, with the DNA altering its structure to accommodate the large intercalator.<sup>31</sup> The far D ring of the anthracycline chromophore actually protrudes into the major groove, with the A ring and attached sugar in the minor groove. Hydrogen bonding may take place between the 9-hydroxyl and the N-3 of purine nucleotides or O-2 of pyrimidines. A bound water molecule appears to associate with the carbonyl O-13 and various nucleotides. The positively charged amino group does not interact with any phosphates, contrary to earlier findings. Complementary studies have been performed on daunomycin:DNA complexes in solution, using <sup>1</sup>H and <sup>31</sup>P NMR as probes.<sup>72</sup> These solution results confirmed many of the solid state observations.

#### **Actinomycin D**

Actinomycin D (C<sub>1</sub>) is a red, crystalline antibiotic isolated from the culture of Streptomyces antibiotics. Its structure (Figure 7) is composed of a flat, aromatic chromophore, 2-amino-4,5-dimethyl-3-phenoxazone-1,8-dicarboxylic acid, and two identical cyclic pentapeptide lactones. The amino acid sequence of the attached pentapeptide is:



where Thr = threonine, Val = valine, Pro = proline, Sar = sarcosine, MeVal: N-methylvaline, L and D refer to the stereochemistry of the amino acid residue, threonine is bonded through an amide bond with the

chromophore, and the lactone linkage connects the carboxy terminus of the methylvaline residue with the hydroxyl function of the threonine. This structure was elucidated by chemical degradation and verified by synthesis. (Reviews 73,74).

Actinomycin D exhibits some antibacterial activity, especially against Gram (+) bacteria such as B.subtilis. Replication of double stranded DNA viruses is also inhibited by actinomycin D, though RNA viruses are unaffected.<sup>75</sup> Clinically this antibiotic was developed by Merck Sharp and Dohme as dactinomycin (Cosmegen R) for use against neoplasia in man. Cancers for which actinomycin D has shown effectiveness against include nephroblastoma (like Wilms tumor), Ewing's sarcoma, rhabdomyosarcoma; methotrexate-resistant choriocarcinoma, malignant melanoma, and others.<sup>76</sup> Limiting toxicity is usually bone marrow depression. This biological activity of actinomycin D is believed to stem from its ability to selectively inhibit DNA-directed RNA synthesis, most likely achieved through the formation of long-lived blocks to RNA polymerase progression along the DNA template.<sup>77</sup>

Spectrophotometric studies,<sup>29,78</sup> of equilibrium binding to both natural and homopolymer nucleic acids has indicated binding constants on the order of  $0.6-3.3 \times 10^6 \text{ M}^{-1}$  at 100 to 200 mM Na<sup>+</sup> with a binding site size of 4.5-6 base pairs. Sequence specificity is for nucleotides containing a 2-amino functionality such as guanine and diaminopurine though there are exceptions.<sup>50</sup> The alternation of purine and pyrimidine nucleotides also appears important, as shown in the ordered series of trinucleotide-repeating homopolymers exhibiting actinomycin binding: 5' GC > GGG > GT, GTT > GA, GAA, GTA > GAT 3'. There is a conformational

aspect to this binding, with little to no interaction observed with A-form nucleic acids such as RNA.<sup>75</sup> The kinetics of association and dissociation of actinomycin to DNA are quite slow,  $k_{\text{assoc}} = 10^{-4} \text{ M}^{-1} \text{ sec}^{-1}$  and  $k_{\text{dissoc}} = 10^{-3} \text{ sec}^{-1}$ .<sup>78</sup> A change in the conformation of the peptide rings bound to DNA is thought to be the rate-limiting step.<sup>79</sup>

Actinomycin D was thought to bind DNA by intercalation with the cyclic pentapeptides hydrogen bonding in the minor groove. The intercalative mode of binding was verified by changes in the superhelicity of  $\phi$ X174 RF DNA (unwinding angle,  $260^\circ$ ) as determined by analytical ultracentrifugation.<sup>65</sup> Additional structural information concerning the actinomycin D:DNA complex was obtained by X-ray crystallography. A 1:2 antibiotic/deoxyguanosine complex was investigated to a standard deviation in bond lengths of 0.03 Å.<sup>80</sup> This complex exhibited 2-fold symmetry, with the guanines located on either side of the phenoxazone chromophore yet on the same side of the peptide rings. CPK and computer modeling studies, superimposing the crystal structure onto a simulated hexanucleotide 5'-ATGCAT, extend the results to DNA binding.<sup>81</sup> Intercalation is confirmed, with the cyclic pentapeptides located in the minor groove. This complex is stabilized by numerous hydrogen bonds and van der Waals interactions, most important of these being the strong hydrogen bond connecting the 2-amino group of guanine with the carbonyl oxygen of L-threonine. X-ray crystal studies on a 1:2 antibiotic/deoxyguanylyl-3',5'-deoxycytidine complex demonstrate an unusual pseudo-intercalated structure which may indicate the possibility of interhelical crosslinks upon actinomycin binding.<sup>82</sup> Further evidence against actinomycin binding to RNA is shown, this

involving the steric hindrances between the N-2 amino group of the phenoxazone ring and the O-2' hydroxyl group of ribose sugar.

NMR spectroscopy, both  $^1\text{H}$  and  $^{31}\text{P}$  has provided information on the interaction of actinomycin with deoxynucleotides,<sup>83</sup> dinucleotides, oligonucleotides,<sup>84</sup> and the self complementary dodecamer.<sup>85</sup> From studies on complexes between mono- and dinucleotides with actinomycin it was shown that the benzenoid portion of the phenoxazone ring binds either guanine or adenine equally well, while the quinoid portion prefers guanine. This work emphasizes the importance of stacking forces in the recognition of certain sequences and the stabilization of the antibiotic/DNA complex. With the self complementary dodecamer, actinomycin was shown to intercalate between the 5'GC-3' base pairs and was still able to accommodate simultaneous groove binding by the antibiotic netropsin, as demonstrated earlier by optical spectroscopic means.<sup>49</sup>

#### **Netropsin and Distamycin**

Netropsin and distamycin A are related basic oligopeptide antibiotics isolated from Streptomyces netropsis and distallicus, respectively (Figure 7).<sup>86,87</sup> Netropsin consists of two 4-amino-2-carboxylic acid-N-methylpyrrole units linked by amide bonds with a propionamide side chain on the carboxyl terminus and a guanidinoacetamido side chain on the amino terminus. Distamycin has instead three N-methylpyrrole units and a formyl side chain on the amino terminus. Both chemical structures were determined by chemical means;<sup>88,89</sup> distamycin A's structure has been confirmed by total synthesis.<sup>90</sup> An x-ray crystal structure exists for the sulfate salt of

netropsin.<sup>91</sup> The majority of the molecule is essentially flat, with a pronounced curvature in the pyrrole/peptide backbone. Amide groups are on the concave side; carbonyl and methyl, on the convex.

Netropsin inhibits the growth of several bacterial species in vitro, but demonstrates little effect in vivo.<sup>92</sup> Netropsin has also been found to exhibit a significant therapeutic effect against various DNA virus infections, but no effect against RNA viruses. Distamycin A has antifungal, antimitotic, and anti(DNA)viral activities.<sup>92</sup> Clinically it is applied as a topical ointment in the treatment of chickenpox, herpes zoster, and eruptions resulting from smallpox vaccinations. These antibiotics derive their activities by interfering with the initiation of RNA synthesis, perhaps by selectively binding to the specific promoter sequences on the DNA template. This effectiveness is proportional to the number of N-methylpyrrole units present, within the limits being 2-5.

Both antibiotics were found to have bathochromatic shifts in their absorption spectra upon interaction with double-stranded DNA, but not with single-stranded DNA, or RNA.<sup>92</sup> Cotton effects were observed in the circular dichroism spectra, these being proportional to the number of pyrrole units present.<sup>93</sup> Both antibiotics increase the thermal denaturation temperature of DNA.<sup>94</sup> Hydrodynamically, netropsin initially increases the viscosity of DNA while distamycin decreases same.<sup>95</sup> Sequence specificity appears to be for A+T rich DNAs,<sup>49</sup> with order of preference being:<sup>96</sup> 5'-d(A-A-A-A), d(A-A-T-T) > d(A-T-A-T) >> d(A-C-A-C), d(G-C-G-C)-3'. Binding constants for distamycin have been

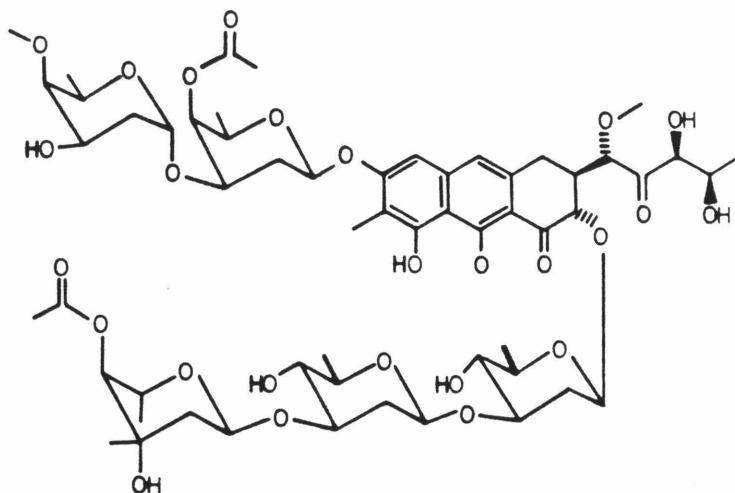
obtained from sedimentation data. For the weak binding process with a site size of 3 base pairs,  $K = 0.5 - 1.2 \times 10^6 \text{ M}^{-1}$ . For the strong binding process 1 distamycin:8 base pairs,  $K = 2.4 \times 10^9 \text{ M}^{-1}$ .<sup>94</sup> Binding site size determinations by a number of means shows distamycin to bind to 6 base pairs, while netropsin covers 4-5 bp.<sup>86</sup> DNA conformation plays a major role in the binding of these antibiotics.<sup>87</sup> Both antibiotics bind only to B form DNAs. This binding has been found to be nonintercalative.<sup>65,97</sup> Binding is in the minor groove, as determined by methylation and modified DNA studies.<sup>49,98</sup>

Structural studies indicate that these N-methylpyrrole oligopeptide antibiotics bind in the minor groove of A+T rich DNA with the amide nitrogens involved in hydrogen bond interactions with the O(2) atoms of thymine or N(3) atoms of adenine.<sup>99</sup> Electrostatic interactions would take place between the positively charged amidine and guanidine residues of the antibiotics and the negatively charged phosphates on the DNA. Steric interactions between the N(2) of guanine and/or DNA conformational changes caused by G·C base pairs would prevent antibiotic binding to G+C rich regions of DNA. Such a model has been confirmed by NOE (nuclear Overhauser effect) NMR experiments.<sup>30</sup> Currently, a 1.7 Å netropsin:DNA dodecamer x-ray crystal structure is being determined.<sup>100</sup>

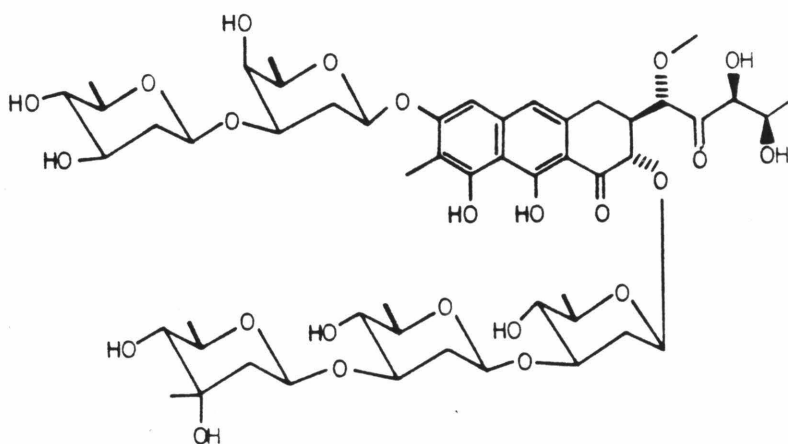
#### **Chromomycin, Mithramycin, and Olivomycin**

Chromomycin A<sub>3</sub>, mithramycin, and olivomycin are three similar antibiotics of the aureolic acid group, first isolated in Japan, USA, and USSR, respectively. Various Streptomyces species have served as the sources of the yellow, crystalline compounds. All have structures centered on a 3(3,4-dihydroxy-1-methoxy-2-oxopentyl)-3,4-dihydro-

Chromomycin A<sub>3</sub>



Mithramycin



Olivomycin A

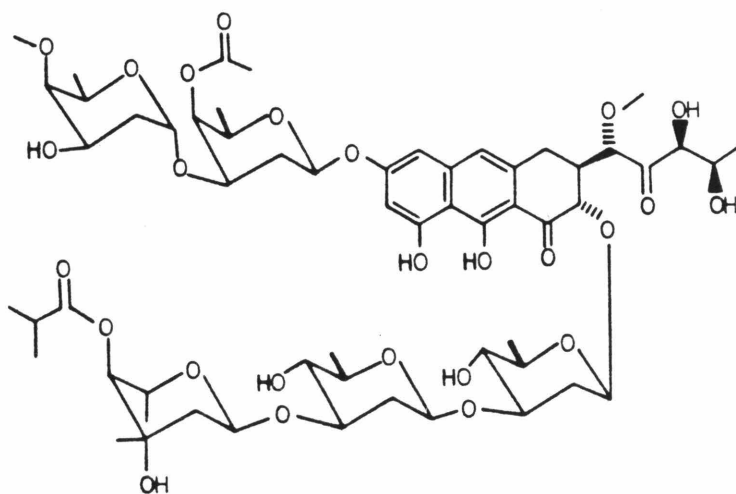


**Figure 8**

Structures of aureolic acid-like antibiotics: chromomycin A<sub>3</sub>, mithramycin, and olivomycin.

8,9-dihydroxyl-1(2H)- anthracene chromophore with a possible methyl substituent at the 7 position (chromomycin and mithramycin); a disaccharide at the 6 position and a trisaccharide at the 2 position. The types of sugars present varies among the different antibiotics. The structures of these three antibiotics are shown (Figure 8). Structure elucidation was carried out by degradative studies, with the structures of the sugars being verified by synthesis (Reviews 101,102). The proper assignment of the interglycosidic linkages in the saccharides has been performed by  $^1\text{H}$  and  $^{13}\text{C}$  NMR.<sup>103-105</sup>

These aureolic acid antibiotics have been shown to strongly inhibit many Gram(+) bacteria and DNA viruses, while having little effect on Gram(-) bacteria and RNA viruses.<sup>101,106</sup> Mammalian cells, both from normal and tumor sources, are often very sensitive to this class of antibiotics. Clinically these antibiotics have been applied effectively against testicular embryonal cell carcinoma and choriocarcinoma.<sup>106</sup> Toxic effects include hepatotoxicity, hypocalcemia, and hemorrhagic syndrome, with the degree of severity being mithramycin > chromomycin A<sub>3</sub> > olivomycin. Cellular morphological changes include nucleolar segregations and condensations with mitosis interrupted in metaphase. These *in vivo* effects are thought to be caused by the formation of kinetic blockades to the propagation of both RNA and DNA polymerases along an affected DNA template.<sup>102</sup>

The interaction between nucleic acids and each of the antibiotics chromomycin A<sub>3</sub>, mithramycin, and olivomycin is similar but not well characterized.<sup>102</sup> They require a stoichiometric amount of  $\text{Mg}^{2+}$  for binding to double-stranded DNAs. No interaction is seen with

single-stranded DNAs or RNA. Binding constants of  $1.0-2.0 \times 10^5 \text{ M}^{-1}$  have been found at 100 to 200 mM  $\text{Na}^+$ , with limiting site sizes of 4-5 base pairs.<sup>107,108</sup> Kinetics of this binding interaction are slow  $\tau_{\text{assoc}1/2} \sim 30 \text{ sec}$  and  $\tau_{\text{dissoc}1/2} \sim 6000 \text{ sec}$ , with rates of dissociation inversely proportional to number of sugar residues present in the side chains.<sup>107</sup> Sequence specificity is for the 2-amino functionality of purines and is an inherent characteristic of the chromophore. These antibiotics are believed to bind in the minor groove of double-stranded DNA, but not thorough intercalation.<sup>65</sup>

### **Echinomycin**

Echinomycin (Quinomycin A, levomycin, actinoleukin, antibiotic X-948) is a white crystalline antibiotic isolated from Streptomyces aureus and other similar species.<sup>109</sup> Its structure consists of two quinoxaline 2-carboxylic acid chromophores linked to a thioacetal cross-bridged cyclic octapeptide dilactone (Figure 9). This revised structure was determined by NMR and gives echinomycin a pseudo two-fold rotational axis of symmetry.<sup>110,111</sup> Echinomycin exhibits wide activities against Gram(+) bacterias, mycoplasma, viruses and various tumors.<sup>109</sup> Cytotoxic effect is believed to be nuclear in nature, exhibiting dispersion of the nucleoli and chromatin aggregation in cell culture. The molecular basis of drug action follows from the inhibition of RNA synthesis from double-stranded DNA templates.

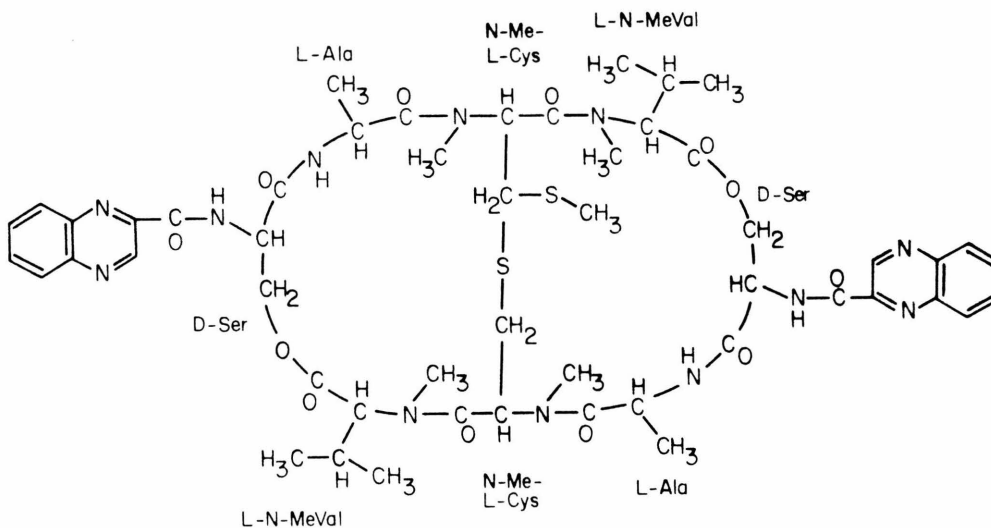


**Figure 9**

Structure of echinomycin according to Dell et al.

With the development of solvent partition methods, echinomycin:DNA interactions could be studied by physical methods in aqueous solution.<sup>112</sup> Echinomycin was the first bisintercalator characterized.<sup>113</sup> It binds to various double-stranded DNAs with a binding constant ranging from  $0.3$  to  $3.1 \times 10^6 \text{ M}^{-1}$  at  $10$  to  $20 \text{ mM Na}^+$ .<sup>114</sup> Binding is ionic strength dependent, decreasing by a factor of  $4$  upon a  $10$ -fold increase in salt concentration. The binding site size is approximately  $4$  base pairs. Sequence specificity is for G+C rich DNAs with an order of preference on homopolymers being:  $dG \cdot dC > d(G-C) > d(A-T) \gg dA \cdot dT$ . The  $\alpha$  value for echinomycin is  $9.01$ , indicative of a moderate preference for binding sites containing three G·C base pairs. The integrity of the thioacetal cross-bridge and the lactone linkages is

essential for strong DNA binding.<sup>115</sup> The kinetics of dissociation of the echinomycin:DNA complex was shown to be composed of three different dissociation times, each believed to correspond to a particular class of binding sites.<sup>116</sup> The slowest dissociation rates are seen for G+C rich sites with time constants on the order of 140-300 sec. Dissociation rates increase with increasing ionic strength.

The conformation of echinomycin has been investigated both by  $^1\text{H}$  and  $^{13}\text{C}$  NMR<sup>117</sup> and by energy calculations.<sup>118</sup> From this it was determined that echinomycin assumes a rigid octapeptide conformation with alternating peptide carbonyl groups above and below the plane of the ring, with the two chromophores projecting out of one side of the ring and the thioacetal cross-bridge projecting the other way. This would allow a possible hydrogen bond to form between the alanine carbonyl groups and the 2-amino group of guanine. A crystal structure has been determined for the similar quinoxaline antibiotic Tandem,<sup>124</sup> though it would be hard to extrapolate from this case to the echinomycin:DNA complex.

### **Anthracyclines**

Adriamycin (**adr**, Figure 10) is an antitumor antibiotic.<sup>120,121</sup> It binds to DNA by intercalation together with an electrostatic component.<sup>122</sup> Binding constant for calf thymus DNA at 100 mM  $\text{Na}^+$  is  $3.67 \times 10^6 \text{ M}^{-1}$  with a binding site size of 3 base pairs.<sup>123</sup> There appears to be an absolute G or C nucleotide requirement in the binding site.<sup>124</sup> Nogalamycin (**nog**, Figure 10) is also an antitumor antibiotic.<sup>125</sup> It is believed to only partially intercalate into double stranded DNA, together with some electrostatic interaction.<sup>65,126</sup> Binding constant of

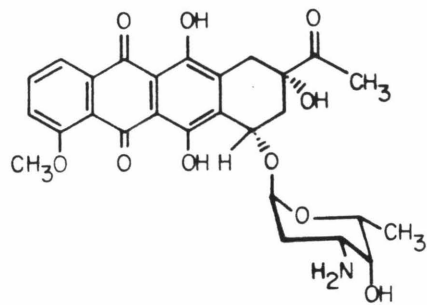
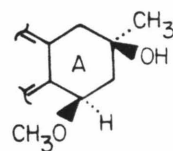
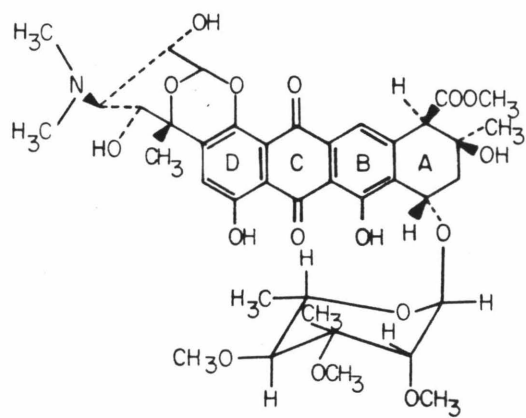


Figure 10

dau



ngr

nog

$10^6 \text{ M}^{-1}$  on calf thymus DNA at  $\sim 100 \text{ mM}$  salt has been shown.<sup>126</sup> Binding site size is from 3-5 base pairs.<sup>126,127</sup> Sequence specificity is for alternating AT regions.<sup>128</sup> 7-Con-0-methylnogarol (**ngr**, Figure 10) is an antitumor antibiotic structurally similar to **nog** but only weakly interacts with DNA.<sup>129</sup>

### **Quinoxalines**

Triostin A (**tri**, Figure 11) is an antibiotic like echinomycin but contains a disulfide instead of a thioacetal cross-bridge.<sup>109</sup> **Tri** is a bisintercalator with its cyclic octapeptide backbone located in the minor groove of DNA.<sup>130</sup> Binding constant is  $7.0 \times 10^5 \text{ M}^{-1}$  on calf thymus DNA at  $10 \text{ mM Na}^+$ . Binding site size is 4 base pairs. Specificity is a slight G-C preference with  $\alpha = 2.32$ , indicative of one G-C base pair per binding site. Tandem (**tan**, Figure 11) is structurally identical to **tri** except for the absence of the four N-methyl groups on the cyclic peptide backbone.<sup>115</sup> Binding is bisintercalative with a constant of  $7.64 \times 10^4 \text{ M}^{-1}$  on calf thymus DNA at  $10 \text{ mM Na}^+$ . Binding increases 200 fold for a dA-dT homopolymer. Binding site size is 4 base pairs, with a strong A-T preference ( $\alpha = 0.105 = 3 \text{ A}\cdot\text{T}$  base pairs in binding site). [Ala<sup>3</sup>, Ala<sup>7</sup>] Tandem, known as AY-285 (**285**, Figure 11) is a tandem analog lacking the disulfide cross-bridge. It shows only weak ( $< 10^3 \text{ M}^{-1}$ ) binding to DNA.<sup>131</sup> [L-Ser<sup>1</sup>, L-Ser<sup>5</sup>] Tandem, otherwise known as Elserta or AY-206 (**206**, Figure 11) is another tandem analog which shows weak binding.<sup>115</sup>

### **Tilerones**

The tilerones are a series of antiviral drugs which are capable of inducing interferon *in vivo*.<sup>132</sup> They bind to DNA by sideways

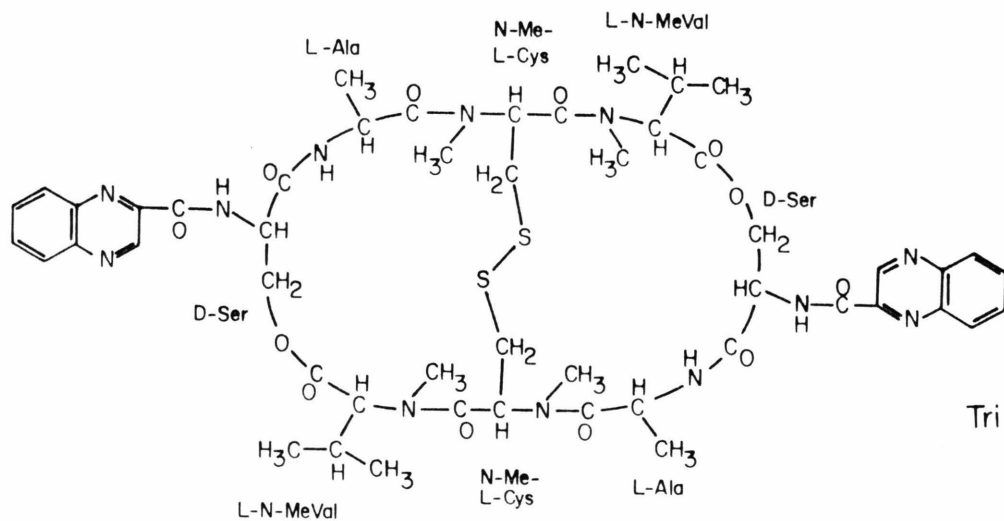
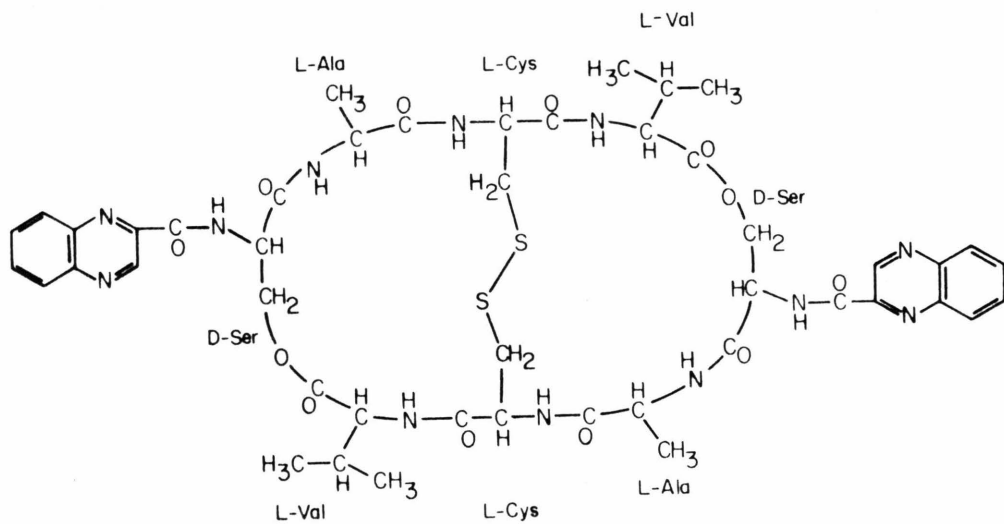
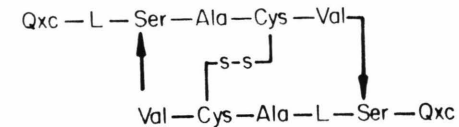
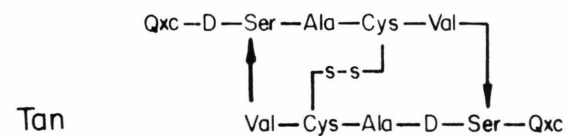
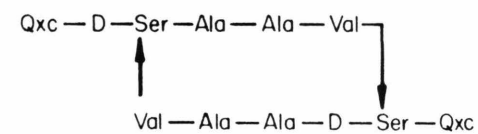


Figure 11



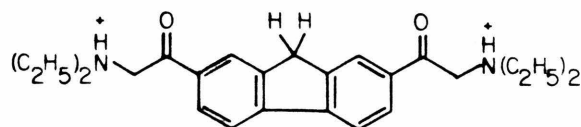
206



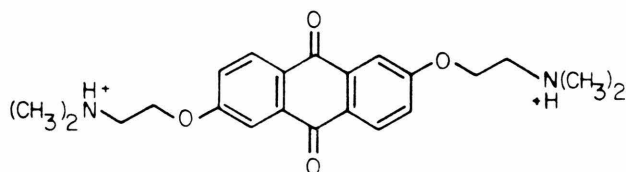
285

intercalation, with one side chain in the minor groove and the other in the major.<sup>133,134</sup> Tilerones show a strong A+T preference.<sup>132</sup> Three that were investigated are analog R11,022DA 2,7-bis(diethylaminoacetyl)-fluorene·2HCl (**002**); analog R10,043DA 2,6-bis[2(dimethylamino)ethoxy]anthraquinene·2HCl (**043**); and analog R10,874DA 3,6-bis[2-(dimethylamino)ethoxy]-9H-xanthen-9-one·2HCl (**874**). These structures are shown in Figure 12.

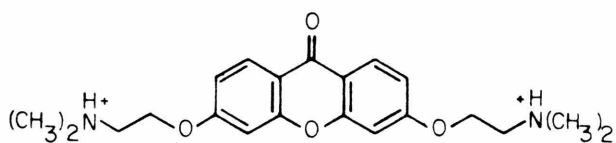
Figure 12



002



043



847

### Miscellaneous

Berenil (**ber**, Figure 13) is an anti-trypanocidal and -babescidal antibiotic.<sup>135</sup> It binds to DNA across the minor groove and shows a slight A·T preference.<sup>86,136</sup> Binding constant is  $1 \times 10^6 \text{ M}^{-1}$  {100 mM  $\text{Na}^+$ , calf thymus DNA} and binding site size is 4 base pairs.<sup>65,136</sup>

N-acetylbleomycin (**ableo**, Figure 13) is an inactive analog of bleomycin. DNA binding is both intercalative and electrostatic, with binding constant of  $1.2 \times 10^5 \text{ M}^{-1}$  and binding site size of 4-5 base pairs.<sup>137-139</sup> Binding specificity of **ableo** has not been assigned, though bleomycin cleaves at pyrimidines 3' to a guanine (5'-Gpyr-3').<sup>140</sup>

Bismethidiumspemine (**BMSp**, Figure 13) is a synthetic bisintercalator which also interacts electrostatically with DNA.<sup>141</sup> Binding constant is  $> 4 \times 10^9$  at 75 mM Na<sup>+</sup> on calf thymus DNA. Binding site size is 4 base pairs. A preference for poly(dC-dC) and polyA-dT is noted.<sup>142</sup>

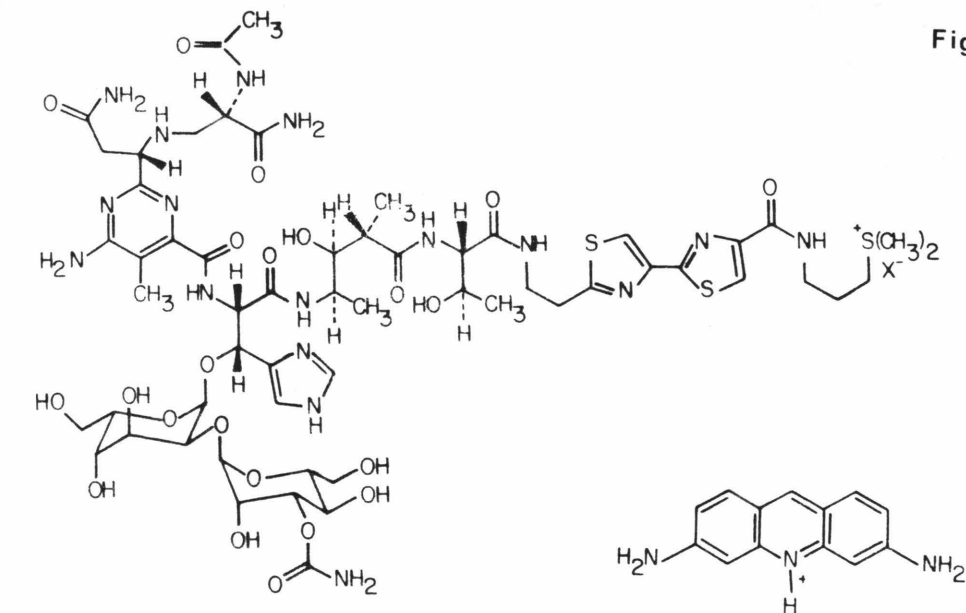
Irehdiammine A (**ire**, Figure 13) is a steroidal alkaloid which binds to DNA electrostatically.<sup>143</sup> Binding site occupied 2 base pairs.<sup>144</sup> **Ire** binding is thought to stabilize  $\beta$ -kinked DNA.<sup>145</sup>

Methyl green (**mg**, Figure 13) is an organic dye used as a biological stain.<sup>146</sup> **MG** binds to DNA electrostatically across its minor groove.<sup>147</sup> Binding constant is  $3.1 \times 10^3 \text{ M}^{-1}$  ( $\sim 100 \text{ mM Na}^+$ , calf thymus DNA) with a binding site size of 2 base pairs, preferably A-T.<sup>148,149</sup>

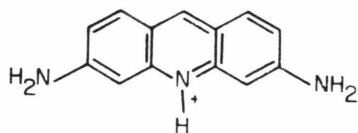
Proflavin (**pro**, Figure 13) is a DNA intercalator<sup>14</sup> which exhibits antibacterial and antimalarial properties.<sup>150</sup> Binding constant is  $1.3 \times 10^6 \text{ M}^{-1}$  for calf thymus DNA at  $\sim 100 \text{ mM Na}^+$ .<sup>151</sup> Binding site size is 2 base pairs. **Pro** shows no binding specificity.<sup>152</sup>

Streptomycin (**str**, Figure 13) is a polysaccharide antibiotic<sup>153</sup> which has been used as a DNA precipitating agent.<sup>154</sup> Binding is weak and electrostatic.<sup>65,155</sup>

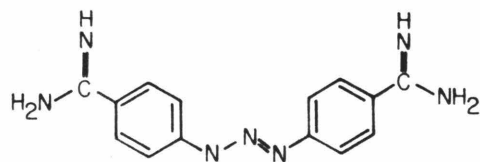
Figure 13



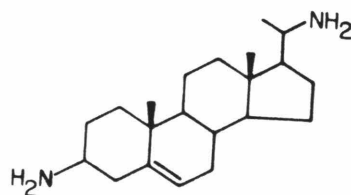
ableo



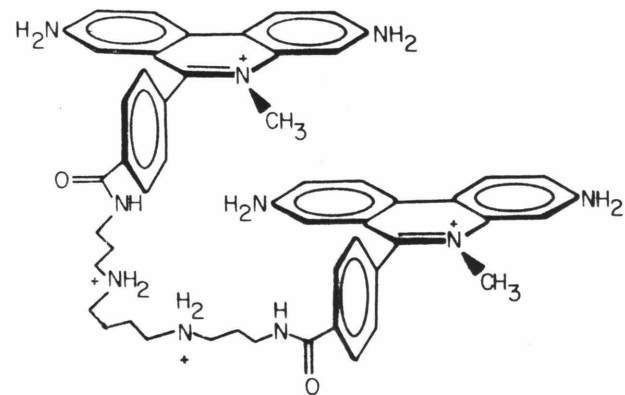
Pro



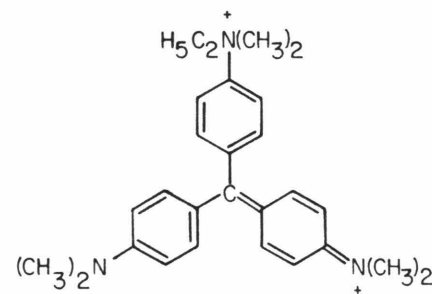
ber



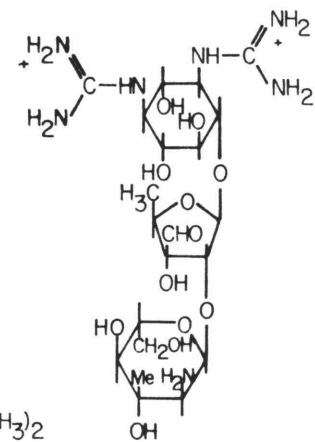
ire



BMSp



mg



str

### **Footprinting Small Molecules by Alternative Methods**

With the availability of efficient DNA cleavers whose interactions may be perturbed by the presence of competitively binding molecules, it should be possible to directly determine the preferred binding sites of small molecules on natural DNAs by a variety of footprinting methods.<sup>156</sup> Prior to our original footprinting work the only direct sequence determinations were performed by inhibiting exonuclease III digestions at specific sites of altered DNA structure by covalently bound trans- and cis-dichlorodiammine-platinum (II)<sup>157,158</sup> and cyclobutane pyrimidine dimers.<sup>158</sup> Inhibition of bleomycin cleavage by the competitive simultaneous binding of small molecule actinomycin D, distamycin A, and ethidium has been performed, but its resolving capacity is limited by the sequence specificity of bleomycin cleavage.<sup>159</sup> Selective binding of actinomycin D and distamycin A have been investigated by inhibition of *E. coli* DNA polymerase I mediated nick translation.<sup>160</sup> Inhibition of polymerase action has obvious biological relevance, and this method allows determination of sites where these compounds may be evincing their biological activities. However this method is limited in determining the exact binding locations and site sizes for individual small molecules, given that its mode for responding to small molecule interference is not entirely understood. Restriction endonucleases have also been employed to investigate small molecule:DNA interactions.<sup>161-163</sup> Due to their high level of cleavage specificity, the number of sites probed per DNA sequence is not very large. DNase I footprinting has been performed by another group of investigators on the antibiotics actinomycin D and netropsin, proving complementary results as our work.<sup>164</sup>

## RESULTS AND DISCUSSION

### Specificity of MPE-Fe(II) Cleavage

MPE-Fe(II) mediated DNA strand scissions are presumed to follow from oxidative cleavage of the deoxyribose ring by a diffusible species in a mechanism analogous to metal-mediated Haber-Weiss reactions.<sup>165,166</sup> If this reaction proceeds through initial abstraction of the 4' hydrogen by  $\cdot\text{OH}$ , as in the case of bleomycin-mediated DNA cleavage,<sup>167</sup> no base specificity should be observed. Preliminary studies concurred with this expectation, demonstrating the production of random breaks in a 3' end labeled 382 bp DNA restriction fragment.<sup>51</sup> Upon more extensive studies a slight amount of sequence specificity, manifesting itself in the appearance of nonuniformity in autoradiogram band intensities, was observed in the MPE-Fe(II) cleavage control lanes for certain DNA restriction fragments. This nonuniformity presents itself as regions containing series of either lightened or darkened band intensities within an otherwise uniform cleavage pattern. Such specificity differs from either the base specific pattern exhibited by the Maxam-Gilbert G reaction,<sup>33</sup> or the variable intensity cleavage pattern seen for DNase I.<sup>41</sup>

To determine the sequence specificity of the MPE cleavage reaction, MPE-Fe(II) cleavage control lanes for the DNA restriction fragments on which the binding specificity of echinomycin was investigated have been analyzed by densitometry. The resulting cleavage histograms are shown in Figure 14a,b. A table listing the nucleotide sequences of those sites exhibiting either enhanced or diminished MPE cleavage is shown (Table II). In all 13 sites of altered cleavage

**Figure 14**

The specificity of MPE cleavage. Histograms correspond to sites of cleavage inhibition; arrows correspond to sites of cleavage enhancement. The height of the histograms or length of the arrows correspond to the amounts of cleavage inhibition or enhancement, respectively. Notice the relative lack of sequence specificity on the first three sequences when compared with the last two. These latter sequences contain large A+T rich regions, sometimes flanked by G+C rich regions. Also notice the general asymmetry in both the inhibited and enhanced cleavage sites. Both exhibit 3' overhangs. These data are obtained from the MPE cleavage control lanes, Figures 40 (274/278), 39 (378,382), 41 (117 & 168) and 42 (167, 517).

↓ ↓ ↓ ↓ ↓

5' CATTAGGCACCCCAGGCTTTACACTTTATGCTTCCGGCTC  
 117 bp 3' GTAATCCGTGGGGTCCGAAATGTGAAATACGAAGGCCGAG

↑ ↑ ↑ ↑

GTATAATGTGTGGAATTGTGAGCGGATAACAATTTACACA 3' 168 bp  
 CATATTACACACCTTAACACTCGCCTATTGTTAAAGTGTGT 5'

274-278

5' ATCACCGCGCCACAGGTGCGGTTGCTGGCGCCTATATCGCCGACATCACCGATGGGGAAGATCGGGCTC  
 .420 .440 .460

3' TAGTGGCCGCGGTGTCCACGCCAACGACCGCGGATATAGCGGCTGTAGTGGCTACCCCTTCTAGCCCGAG

378-382

5' TCGCGTAGTCGATAGTGGCTCCAAGTAGCGAAGCGAGCAGGACTGGGCGGCGGC  
 .340 .320 .300

3' AGCGCATCAGCTATCACCGAGGTTTCATCGCTTCGCTCGTCTGACCCGCGCGCG



Table II - Altered Cleavage Sites for MPE·Fe(II)

Fragment Length (bp)	Figure Number Containing		Nucleotide Sequence of Sites Exhibiting Cleavage:	
	Cleavage Histogram	Autoradiogram	Enhancement	Diminution
117 & 168 (pLJ 3)	19a	46 (lanes 2,7)	5'-(CC)CAG(GC)-3'	--
167 (pBR 322)	19b	47 (lanes 13,14)	(TG)CGG(TA)	(CT)TTA(AT) (GT)TTA(TC) (TT)AAATT(GC)
274-278	19a	45 (lanes 3,4)	--	(GA)A (GA)
378-382	19a	44 (lanes 2,12)	--	--
517	19b	47 (lanes 5,6)	(CA)GGT(GG) (CG)GGG(AA)	(AT)TTT(TA) (TT)AAT(GT) (AT)AAT(AA) (GT)TTC(TT) (AC)TT (TT)

intensity, 4 enhanced and 9 diminished, are tabulated. The average length of these sites is 2.9 base pairs, with extremes ranging from 1-5 base pairs. The enhanced sites are composed of 83% G·C base pairs, while the diminished cleavage sites are 96% A·T. The nucleotides surrounding these sites are also G+C and A+T rich, respectively. This might be expected from the slight G+C binding preference of the methidium chromophore.<sup>168</sup>

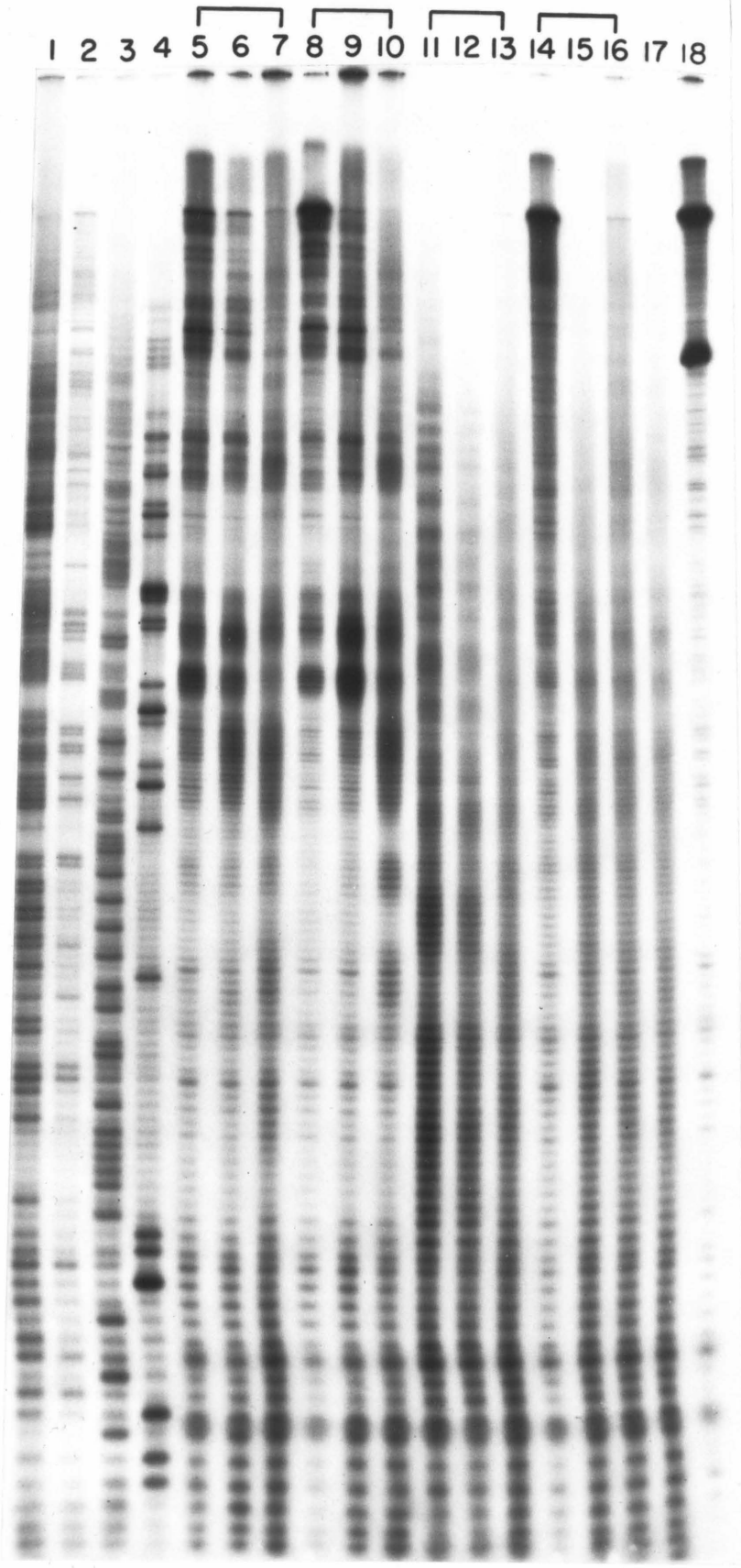
### **MPE Cleavage Inhibition Used to Determine Small Molecule Preferred Binding Sites<sup>169</sup>**

Given that MPE·Fe(II) is a relatively nonsequence-specific DNA cleaving agent, MPE·Fe(II) mimics the behavior of a DNase and, because of its smaller size, proves a useful tool for probing the locations and extent of binding sites of small molecules on naturally occurring, double stranded, heterogeneous DNA. For an investigation of sequence-specific inhibition of DNA strand cleavage (footprinting) by the antibiotics daunomycin, actinomycin D, distamycin A, and netropsin, a naturally occurring DNA substrate of known sequence was prepared. A 517 base pair Rsa I-Eco RI restriction fragment from the plasmid pBR-322 (nucleotides 3847-4363) was chosen. The Eco RI site was 3' end labeled with <sup>32</sup>P. MPE·Fe(II)/dithiothreitol was allowed to react with the 517 base pair fragment alone and with the 517 base pair fragment pre-equilibrated with each of the four inhibiting drugs. Cleavage by MPE·Fe(II) was stopped after 10 min by freezing, lyophilization, and resuspension in a formamide buffer. The end-labeled [<sup>32</sup>P]DNA products were analyzed by denaturing 8% polyacrylamide/50% urea gel electrophoresis capable of resolving DNA fragments differing in length by one

**Figure 15**

**Footprinting actinomycin D, distamycin A, daunomycin and netropsin.**

Autoradiogram of 3' end labeled 517 bp DNA fragment:  
Lanes 1-4 were the Maxam-Gilbert C+T, C, A>C, and G specific reactions, respectively. Lane 18 contained the intact buffered DNA. All other lanes contained 10 mM Tris·Cl [pH 7.4], 50 mM NaCl, 100  $\mu$ M base pairs DNA, 4 mM DTT, 10  $\mu$ M MPE and 10  $\mu$ M Fe(II). Lanes 5-7 contained **net** at 230  $\mu$ M, 23  $\mu$ M, and 2.3  $\mu$ M, respectively. Lanes 8-10 contained **dis** at 310  $\mu$ M, and 31  $\mu$ M and 3.1 M, respectively. Lanes 11-13 contained **act** at 325  $\mu$ M, 32.5  $\mu$ M, and 3.25  $\mu$ M respectively. Lanes 14-16 contained **dau** at 150  $\mu$ M, 15  $\mu$ M, and 1.5  $\mu$ M, respectively. Lane 17 was the MPE·Fe(II) cleavage control.



nucleotide. The autoradiogram data are shown in Figure 15.

**Control.** Two control experiments in the absence of inhibiting drugs were carried out. The first (Figure 15, lane 18) was the buffered intact DNA (100  $\mu$ M in base pairs) in the presence of 10  $\mu$ M Fe(II) and 4 mM dithiothreitol--concentrations used in all subsequent cleavage-inhibition reactions. The 517 nucleotide-long DNA remained intact, although trace quantities of nicked DNA could be seen that later were shown to result from nonspecific endonuclease activity. The two bands at the top of control lane 18 are presumably the result of incomplete denaturation of the 517 base pair fragment. The second control (Figure 15, lane 17) depicted the relatively uniform cleavage pattern generated by MPE (10  $\mu$ M) in the presence of Fe(II) (10  $\mu$ M) and dithiothreitol (4 mM). This provided the baseline by which other cleavage patterns were then compared. We found it convenient to analyze the data by densitometry (Figure 16, lane 17).

**Daunomycin.** No pattern was observed with daunomycin inhibition of MPE•Fe(II) cleavage. Samples with increasing concentrations of daunomycin (Figure 15, lanes 16-14) were allowed to incubate with the 517 base pair DNA fragment. Treatment with MPE•Fe(II)/dithiothreitol afforded a uniform cleavage pattern not too different from that of the MPE•Fe(II) control lane. Increasing amounts of daunomycin increased the average length of the cleaved DNA fragment. The highest daunomycin concentration is shown in lane 14, where much of the 517 base pair fragment remained intact.

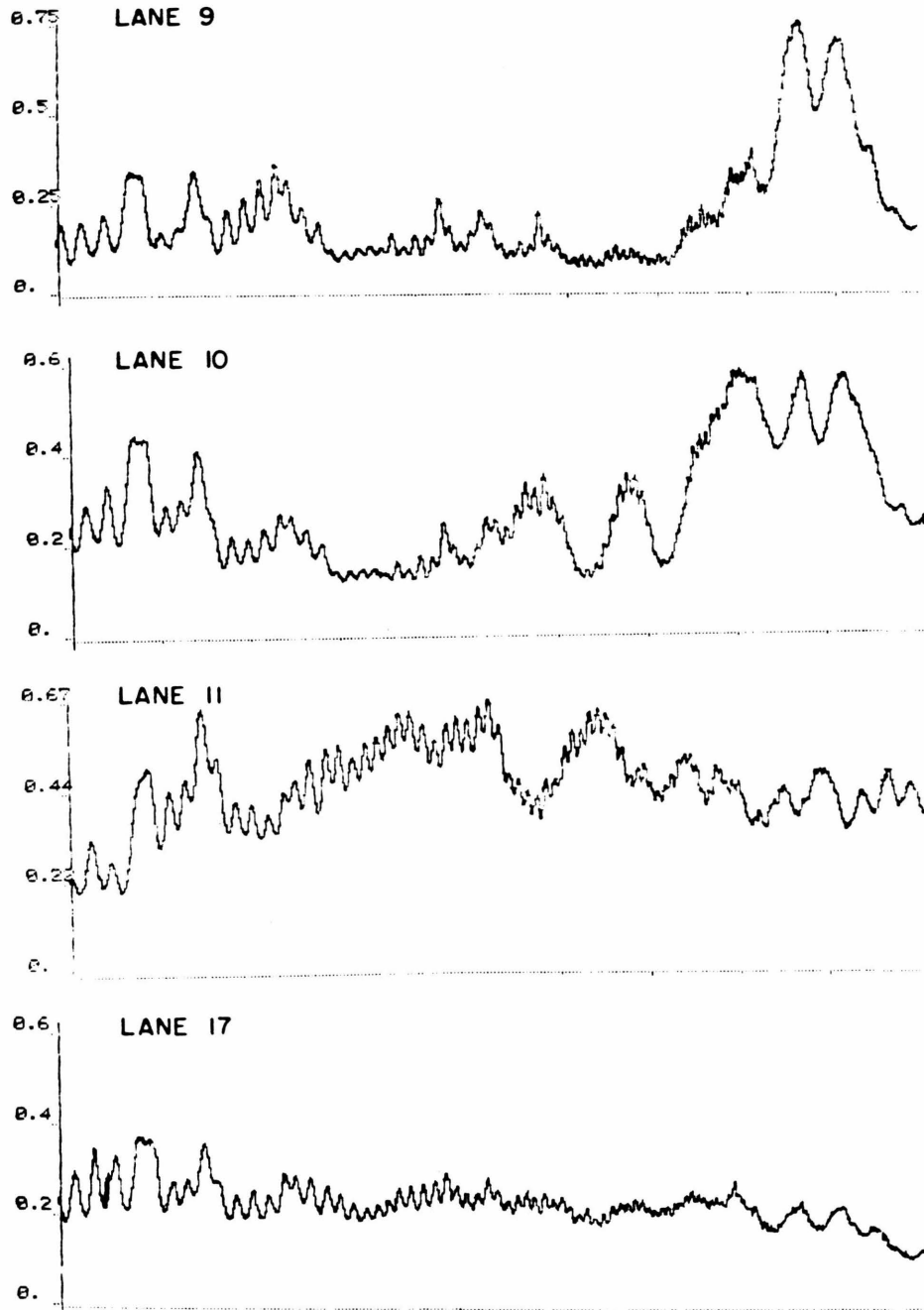


**Figure 16**

Densitometer scan of autoradiogram (Figure 15). Horizontal axis is distance. Reading left to right corresponds to the bottom to middle of autoradiogram. Vertical axis is absorbance. Valleys are small molecule protected regions from  $MPE \cdot Fe(II)$  cleavage.

**Actinomycin D.** Actinomycin D provided the first evidence for the feasibility of the MPE•Fe(II) inhibition pattern procedure. A series of bands or regions of alternating high and low density on the autoradiogram were observed when MPE•Fe(II)/dithiothreitol cleaved DNA in the presence of actinomycin (Figure 15, lanes 13-11). The highest concentration of actinomycin D showed the sharpest inhibition patterns (lane 11). The regions of low density, which indicate reduced cleavage by MPE•Fe(II), appeared to be 4-16 nucleotides in length and centered around at least one or more G•C base pairs. The densitometer trace (Figure 16, lane 11) allowed a measure of the actinomycin blocking of MPE•Fe(II) DNA cleavage on a 103-nucleotide section of the 517 base pair restriction fragment, illustrated as protected regions on the sequence in Figure 17, lane 11.

**Distamycin A.** Lower concentrations of distamycin A were sufficient to produce well-resolved inhibition patterns compared to the case of actinomycin D. Certain A+T rich regions that suffered efficient MPE•Fe(II) cleavage in the presence of actinomycin were protected by distamycin (Figure 15, light regions on gel lanes 10-8). Inspection of gel lanes 10 and 11 (distamycin and actinomycin, respectively) reveals complementary regions (G+C vs. A+T rich) resulting from different protection by the two drugs. We were able to observe the effect of increasing concentration on site selection by distamycin A. At low distamycin concentrations, we observed a series of inhibition gaps 4-16 nucleotides in length -- regions rich in A•T base pairs with unprotected spacer regions between them (see Figure 17, lane 10). As the distamycin concentration was increased, the flanking spacer regions



**Figure 17.**

Illustration of small molecule protected regions (black areas) from MPE-Fe(II) cleavage on 103 base pairs of the lower, 3' labeled strand of the 517 bp DNA fragment. The sequence from left to right corresponds to the bottom to middle of the gel autoradiogram in Figure 15, lane 11 (act at 325  $\mu$ M) and lanes 10 and 9 (dis at 3.1 and 31  $\mu$ M, respectively.)

rich in A+T coalesced into one long A+T rich protected region (lane 11). However, certain sequences containing four or more contiguous G·C base pairs remained unprotected even at the highest concentrations of distamycin.

**Netropsin.** Netropsin, a basic oligopeptide similar in structure to distamycin A, appeared to show the identical inhibition patterns of distamycin A (Figure 15, lanes 7-5). Not only were the locations and lengths of the various protected regions duplicated, but also the identical coalescence of protected A+T rich regions at increasing concentrations of netropsin was observed.

**Opposite Strand Analyses Afford More Precise Localization of Small Molecule Binding Sites.<sup>170</sup>**

With the application of a complementary-strand analysis of a small molecule binding sites on DNA, it becomes possible to more precisely delineate their actual sizes and locations. Given the strand asymmetry of MPE cleavage as apparent in the enhanced and diminished cleavage site earlier described, together with CPK model building studies of MPE·DNA interactions, a shift of at least 1 base pair to the 3' side of the actual binding site would be expected in the location of the footprint. This hypothesis, referred to as the asymmetric model, was incorporated in the determination of small molecule binding sites (Figure 18).

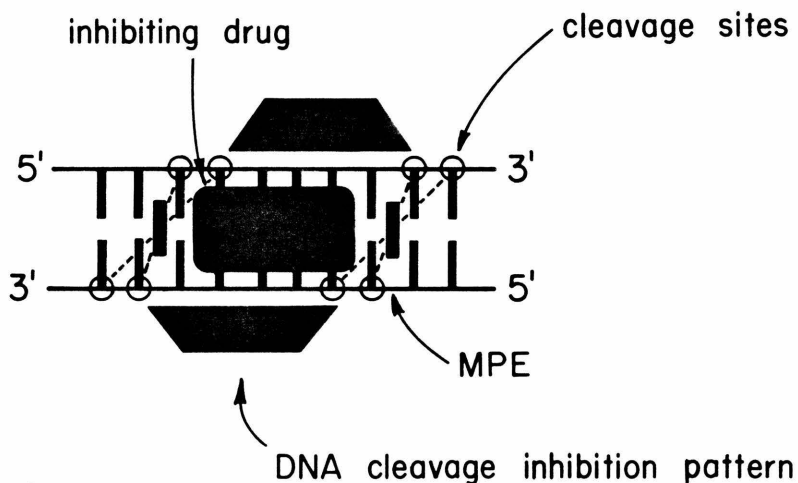


**Figure 18**

The asymmetric model for footprinting by MPE. Inhibiting ligand bound in the minor groove of double-helical DNA limits the possible locations where MPE may intercalate. Given the inherent asymmetry associated with right-handed DNA, certain sites are most accessible to  $\cdot\text{OH}$ -mediated cleavage. Therefore a shift towards the DNA 3' end will be observed on each strand for the footprint relative to the actual location of the bound inhibiting ligand.

For an investigation of the sequence-specific DNA cleavage inhibition by actinomycin and distamycin with  $\text{MPE}\cdot\text{Fe}(\text{II})$ , two DNA substrates were prepared. The 117-bp and 168-bp restriction fragments,

each containing the lactose operon promoter-operator region, were prepared with the 3' ends labeled with  $^{32}\text{P}$  on complementary strands.  $\text{MPE}\cdot\text{Fe(II)}/\text{DTT}$  was allowed to react with the 117-bp or 168 bp fragments alone (Figure 19) and with the 117-bp or 168 bp fragments preequilibrated with either actinomycin or distamycin (Figure 20). Partial cleavage by  $\text{MPE}\cdot\text{Fe(II)}$  was stopped after 15 minutes by freezing, lyophilization, and resuspension in formamide buffer. The  $^{32}\text{P}$ -end-labeled DNA products were analyzed by denaturing 8% polyacrylamide/50% urea gel electrophoresis, which is capable of resolving DNA fragments differing in length by one nucleotide. The autoradiographic data are shown in Figures 19 and 20.

**Controls.** Several control experiments in the absence of inhibiting drugs were carried out. Lanes 1 and 18 of Figure 19 are the buffered, intact 117-bp and 168-bp DNA fragments (200  $\mu\text{M}$  in base pairs). The two bands at the top of these control lanes presumably arise from incomplete denaturation. Lanes 2-5 (117-bp fragment) and 14-17 (168-bp fragment) of Figure 19 contain 200  $\mu\text{M}$  DNA, 50  $\mu\text{M}$   $\text{Fe(II)}$ , 4.6 mM DTT, 5-40  $\mu\text{M}$  MPE. Lanes 2-5 and 14-17 depict the relatively uniform cleavage pattern generated by MPE over a broad concentration range. This provides the baseline by which other cleavage patterns are compared. Lanes 6-13 are the products of the Maxam-Gilbert sequencing reactions and are used as markers for base identification.

Lanes 1 and 24 of Figure 20 are the buffered, intact 117-bp and 168-bp DNA fragments, respectively (100  $\mu\text{M}$  in base pairs). Lanes 2 (117-bp fragment) and 23 (168-bp fragment) are controls containing 100  $\mu\text{M}$  DNA, 10  $\mu\text{M}$   $\text{MPE}\cdot\text{Fe(II)}$ , and 4 mM DTT, indicating a uniform cleavage

**Figure 19**  
**Efficiencies and sequence specificities of MPE·Fe(II)**  
**mediated DNA cleavage.**

Autoradiogram of 3' end labeled 117 bp and 168 bp DNA fragments: Lanes 1-9 contained 117 bp, and lanes 10-18 contained 168 bp DNA. Lanes 6-9 and is descending order lanes 13-10 were the Maxam-Gilbert C+T, C, A>C, and G reactions, respectively. Lanes 1 and 18 contained the intact DNA fragments. All non-Maxam-Gilbert lanes contained 10 mM Tris·Cl [pH 7.4], 50 mM NaCl, 200  $\mu$ M base pairs DNA, 4.6 mM DTT, and 50  $\mu$ M Fe(II). Lanes 1-5, corresponding to lanes 18,14,17,16,15 in this order, contained 0,5,10,20, and 40  $\mu$ M MPE, respectively.

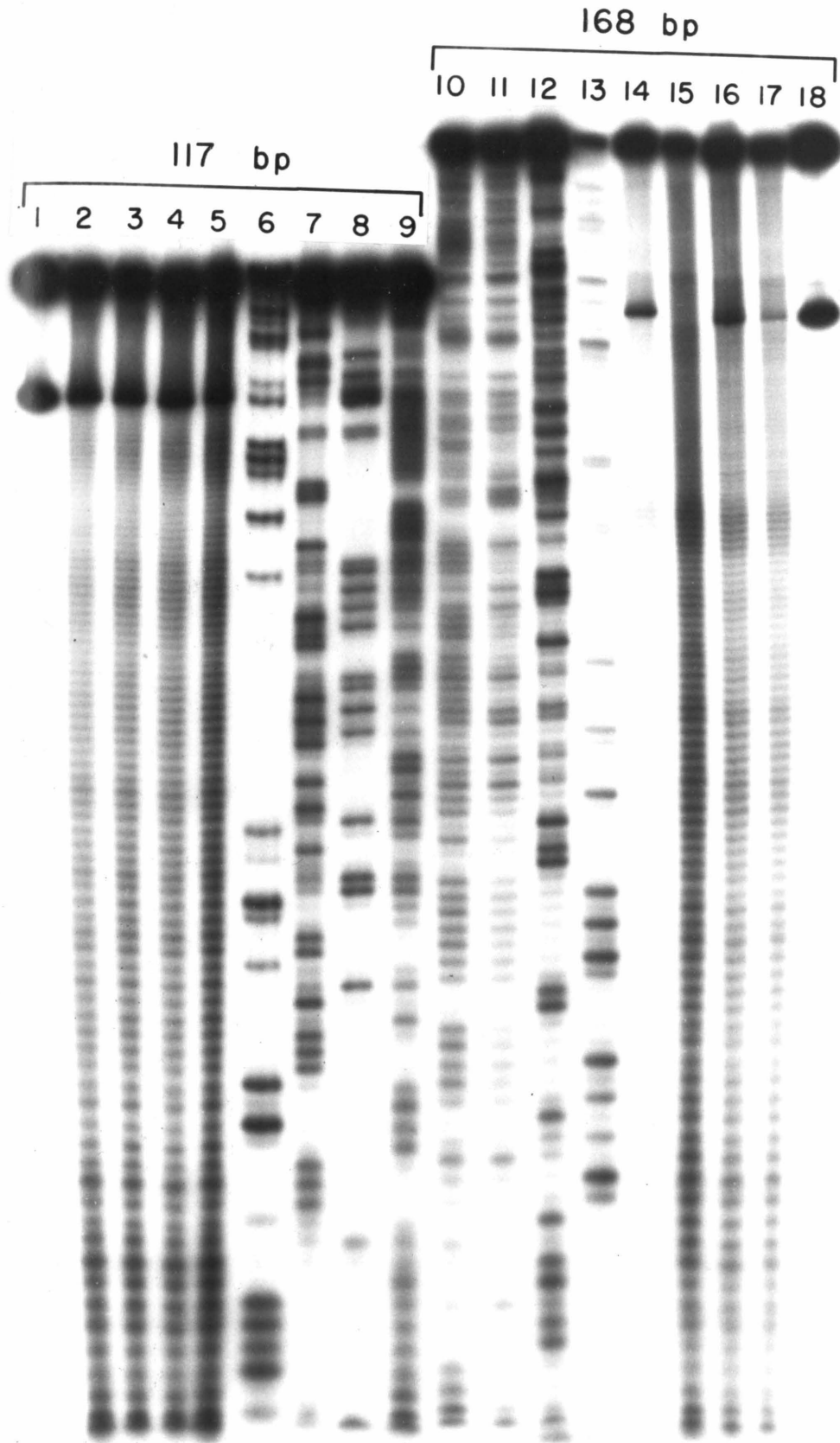
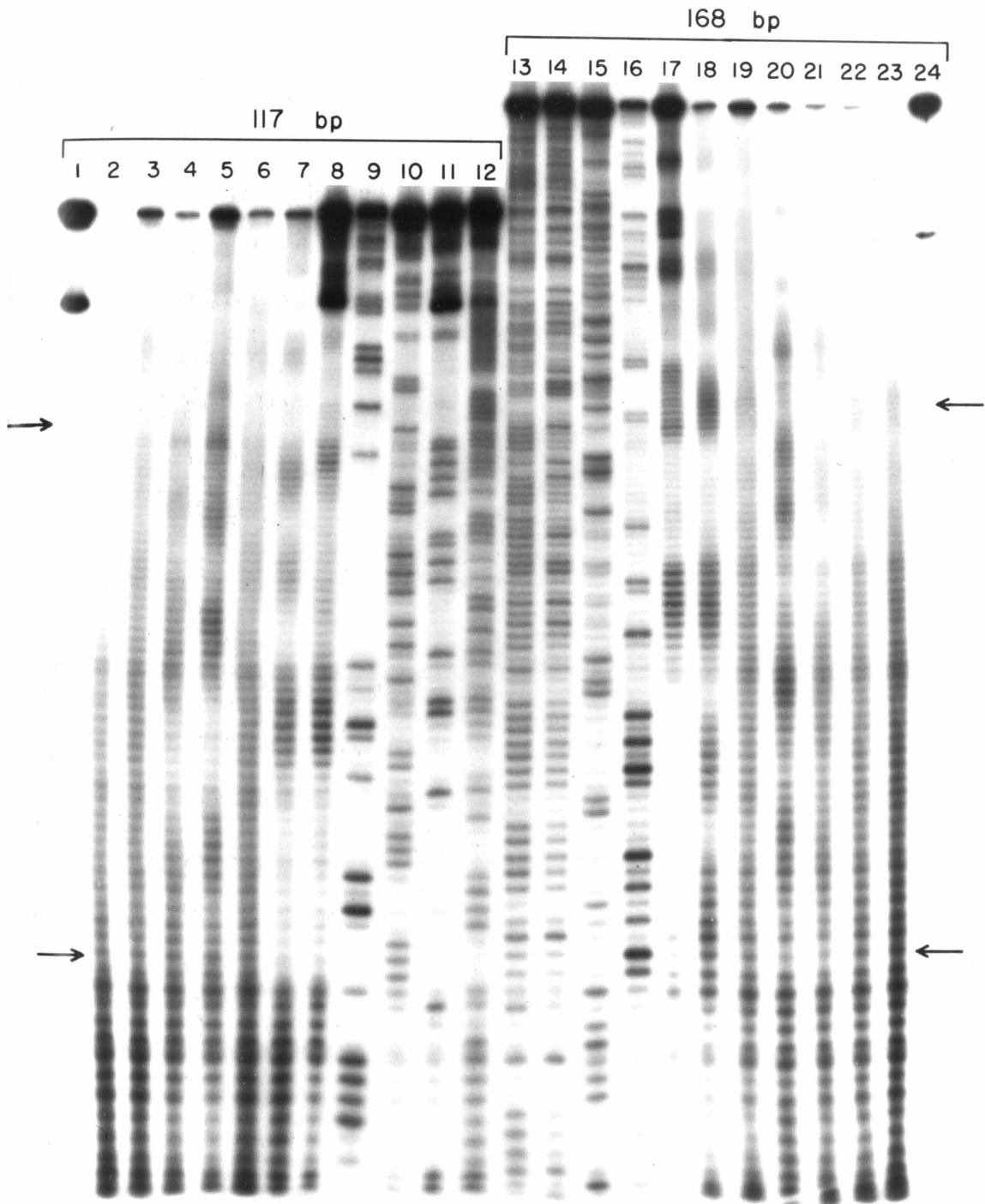


**Figure 20**

**Complementary-strand analyses of actinomycin and distamycin binding sites.**

Autoradiogram of 3' end labeled 117 bp and 168 bp DNA fragments: Lanes 1-12 contained 117 bp, and lanes 13-24 contained 168 bp DNA. Lanes 9-12 and in descending order 16-13 were the Maxam-Gilbert C+T, C, A+C, and G specific reactions, respectively. Lanes 1 and 24 were the intact buffered DNA fragments. Lanes 2-8 and in descending order 23-17 contained 10 mM Tris·Cl [pH 7.4], 50 mM NaCl, 100  $\mu$ M base pairs DNA, 4 mM DTT, 10  $\mu$ M Fe(II), and 10  $\mu$ M MPE. Lanes 3-5 and in descending order 22-20 contained **act** at 1, 10, and 100  $\mu$ M, respectively. Lanes 6-8 and in descending order 19-17 contained **dis** at 1, 10, and 100  $\mu$ M, respectively. Lanes 2 and 23 were the MPE·Fe(II) cleavage controls.



pattern.

**Actinomycin.** Different concentrations of actinomycin (1  $\mu$ M, 10  $\mu$ M, and 100  $\mu$ M) were allowed to equilibrate with the 117-bp and 168 bp DNA fragments (100  $\mu$ M bp). To this was added 10  $\mu$ M MPE•Fe(II) and 4 mM DTT (final concentrations). A series of bands or regions of alternating high and low density on the autoradiogram are observed when MPE•Fe(II)/DTT cleaves DNA in the presence of actinomycin. The highest concentration of actinomycin D (100  $\mu$ M) shows the sharpest footprinting patterns (Figure 20, lanes 5 and 20). The densitometer trace allows a measure of the actinomycin blocking of MPE•Fe(II) DNA cleavage on a 50 bp section of the 117 bp and 168 bp restriction fragments (Figure 21), which are illustrated as protected regions on opposite strands in Figure 22.

It may be observed that these actinomycin footprints are asymmetric, with a 3' overhang extending from 1-3 base pairs. Utilizing the asymmetric model, the preferred binding sites have been determined (Figure 23). Given that the 50 bp sequence analyzed is 44% G+C and 56% A+T, those 22 base pairs protected by actinomycin are 68% G+C in composition. The minimum protected region observed is the 3-bp sequence, 5'-GTG-3'. Larger footprints may be composed of multiple or overlapping binding sites.

**Distamycin.** Different concentrations of distamycin (1  $\mu$ M, 10  $\mu$ M, and 100  $\mu$ M) were allowed to equilibrate with the 117 bp and 168 bp DNA fragments (100  $\mu$ M bp). To this was added 10  $\mu$ M MPE•Fe(II) and 4 mM DTT (final concentrations). Lower concentrations of distamycin (10  $\mu$ M) were sufficient to produce footprints that are well resolved compared

**Figure 21**

Densitometer scans of the (A) 117 bp and (B) 168 bp DNA fragments. Reading left to right on the scan equates to reading from lower arrow to upper arrow on the gel autoradiogram (Figure 20). These scans correspond to (from top to bottom): (A) lane 5, 100  $\mu$ M **act**; lane 7, 10  $\mu$ M **dis**; lane 1, MPE·Fe(II) control; (B) lane 20, 100  $\mu$ M **act**; lane 18, 10  $\mu$ M **dis**; lane 23, MPE·Fe(II) control.

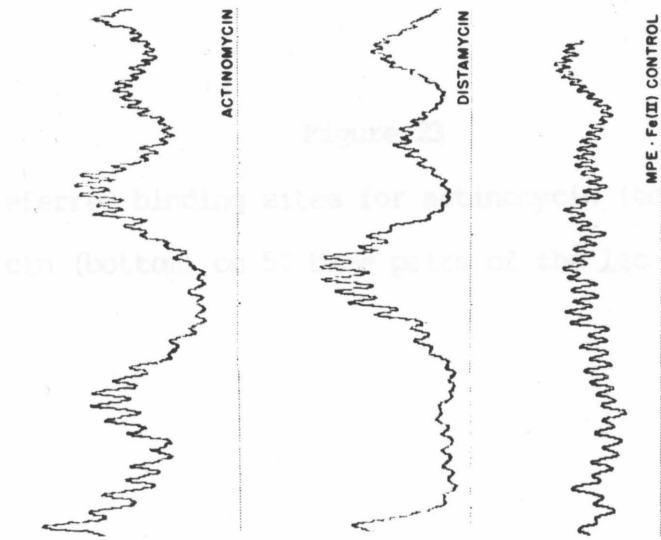
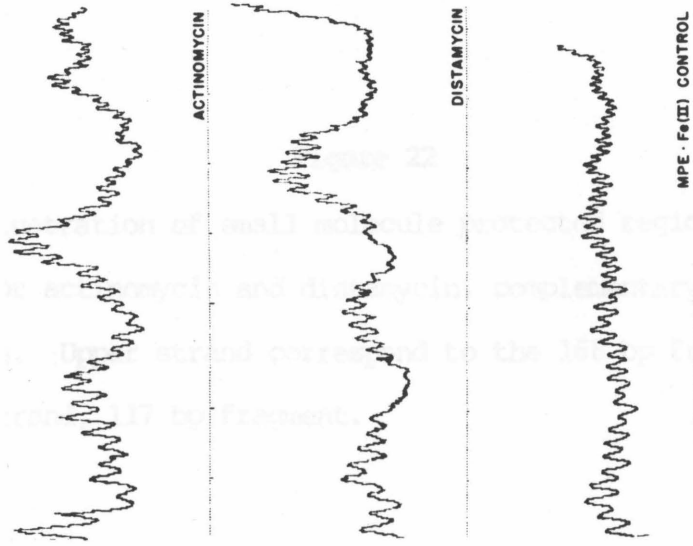


**Figure 22**

Illustration of small molecule protected regions (black area) for actinomycin and distamycin, complementary strand analyses. Upper strand correspond to the 168 bp fragment; lower strand, 117 bp fragment.

**Figure 23**

Preferred binding sites for actinomycin (top) and distamycin (bottom) on 50 base pairs of the lac operon.

**Act**

5' CTTTACACTTTATGCTTCCGGCTCGTATAAATGTGTGGAATTGTGAGCGGA 3'  
\*3' GAAATGTGAAATACGAAGGCCGAGCATATTACACACCTTAACACTCGCCT 5'

**Dis**

5' CTTTACACTTTATGCTTCCGGCTCGTATAAATGTGTGGAATTGTGAGCGGA 3'  
\*3' GAAATGTGAAATACGAAGGCCGAGCATATTACACACCTTAACACTCGCCT 5'

100  $\mu$ M actinomycin

5' CTTTACAC TTTATGCTTCCGGC TCGTATAATG TGTGG AATTG TGAGC GGA 3' 168 bp  
117 bp 3' GAAATGTG AAATACGAAGGCCG AGCATATTAC ACACC TTAAC ACTCG CCT 5'

10  $\mu$ M distamycin

5' CTTTACACTTTATGCT TCCGGCTCGT ATAAT GTGTGG AATT GTGAGCGGA 3' 168 bp  
117 bp 3' GAAATGTGAAATACGA AGGCCGAGCA TATTACACACC TTAA CACTCGCCT 5'

with the case of actinomycin. Certain dA·dT rich regions that suffered efficient MPE·Fe(II) cleavage in the presence of actinomycin are now protected by distamycin. Inspection of gel-lanes 5 and 7 of Figure 20 (actinomycin and distamycin, respectively) reveals complementary regions (dG·dC vs. dA·dT rich), resulting from different protection by the two drugs. Measurement of the distamycin blocking of MPE·Fe(II) cleavage is performed by densitometry (Figure 21), which is illustrated as protected region on opposite strands of the 50 bp section (Figure 22).

Again a similar degree of 3' overhang in the distamycin footprints is observed. Interpretation of the preferred binding sites (Figure 23) shows three sites ranging from 4-15 bp at a dis/bp ratio of 1:10. These sites total 24 base pairs, and are predominantly (83%) A+T in composition.

#### **MPE·Fe(II) Footprinting of Chromomycin A<sub>3</sub>, Mithramycin, and Olivomycin<sup>171</sup>**

Chromomycin, mithramycin, and olivomycin are a series of antibiotics which bind to DNA with a specificity for guanine and a stoichiometric Mg<sup>2+</sup> requirement.<sup>102,107</sup> Binding affinities and kinetics are similar to those of actinomycin, though intercalation is considered unlikely.<sup>65,107</sup> Since little else is known about their interaction with DNA, these antibiotics provided useful subjects for MPE footprinting analyses.

For an investigation of the DNA cleavage inhibition patterns produced by partial digestion of DNA restriction fragments protected by chromomycin, mithramycin, and olivomycin, two DNA substrates containing regions of identical sequence were studied. Two DNA restriction

fragments, 117 and 168 base pairs in length, each containing the lactose operon promoter-operator region were prepared with complementary strands labeled with  $^{32}\text{P}$  at the 3' end.  $\text{MPE}\cdot\text{Fe}(\text{II})$  was allowed to partially cleave the 117 and 168 base pairs fragments alone and the 117 and 168 base pair fragments preequilibrated with either chromomycin, mithramycin or olivomycin together with a twice stoichiometric amount of  $\text{Mg}^{2+}$ . Partial cleavage by  $\text{MPE}\cdot\text{Fe}(\text{II})$  was stopped after 15 min by freezing, lyophilization, and resuspension in formamide buffer. The  $^{32}\text{P}$  end-labeled DNA products were analyzed by 8% polyacrylamide/50% urea denaturing gel electrophoresis capable of resolving DNA fragments differing in length by one nucleotide. The autoradiogram data are shown in Figures 24 and 25.

**Controls.** Experiments in the absence of inhibiting drugs were carried out. Lanes 1 and 13 (Figure 24) are the buffered intact 117 and 168 base pair DNA fragments (100  $\mu\text{M}$  in base pairs), respectively. The two bands at the top of control lanes 1 and 13 presumably arise from incomplete denaturation. Lanes 2 (117 base pair DNA fragment) and 14 (168 base pair DNA fragment) are controls containing 100  $\mu\text{M}$  DNA, 10  $\mu\text{M}$   $\text{MPE}\cdot\text{Fe}(\text{II})$ , and 4 mM dithiothreitol (DTT), demonstrating the relatively uniform cleavage pattern generated by  $\text{MPE}\cdot\text{Fe}(\text{II})$ . Lanes 2 and 14 provide the base line by which other DNA cleavage patterns in the presence of drugs are compared. As shown in Figure 25, lanes 2,4,6, and 8, a range of concentrations of  $\text{Mg}^{2+}$  (1  $\mu\text{M}$  - 1 mM) was found not to effect the low sequence-specific cleavage of DNA by  $\text{MPE}\cdot\text{Fe}(\text{II})$ . Lanes 12 and 24 are the products of the Maxam-Gilbert sequencing reactions for G and are used as markers for base identifications.

**Figure 24**

**Complementary-strand analyses of chromomycin A<sub>3</sub>-  
mithramycin- and olivomycin-binding sites.**

Autoradiogram of 3' end labeled 117 bp and 168 bp DNA fragments: Lanes 1-12 contained 117 bp, and lanes 13-24 contained 168 bp DNA. Lanes 12 and 24 were the Maxam-Gilbert G reaction on the 117 and 168 bp fragments, respectively. Lanes 1 and 3 were the intact buffered DNAs. Lanes 2-11 and 14-23 contained 10 mM Tris·Cl [pH 7.4], 50 mM NaCl, 1.1 mM NH<sub>4</sub>OAc, 0.18 mM EDTA, 100 μM base pairs DNA, 4 mM DTT, and 10 μM MPE·Fe(II). Lanes 3-5 and 15-17 contained 6.3, 25 and 100 μM **chr**, respectively. Lanes 6-8 and 18-20 contained 6.3, 25, and 100 μM **mit**, respectively. Lanes 9-11 and 21-23 contained 6.3, 25 and 100 μM **olv**, respectively. Each reaction containing **chr**, **mit**, or **olv** also contained a two-fold molar excess of Mg<sup>2+</sup>. Lanes 2 and 14 were the MPE·Fe(II) cleavage controls.

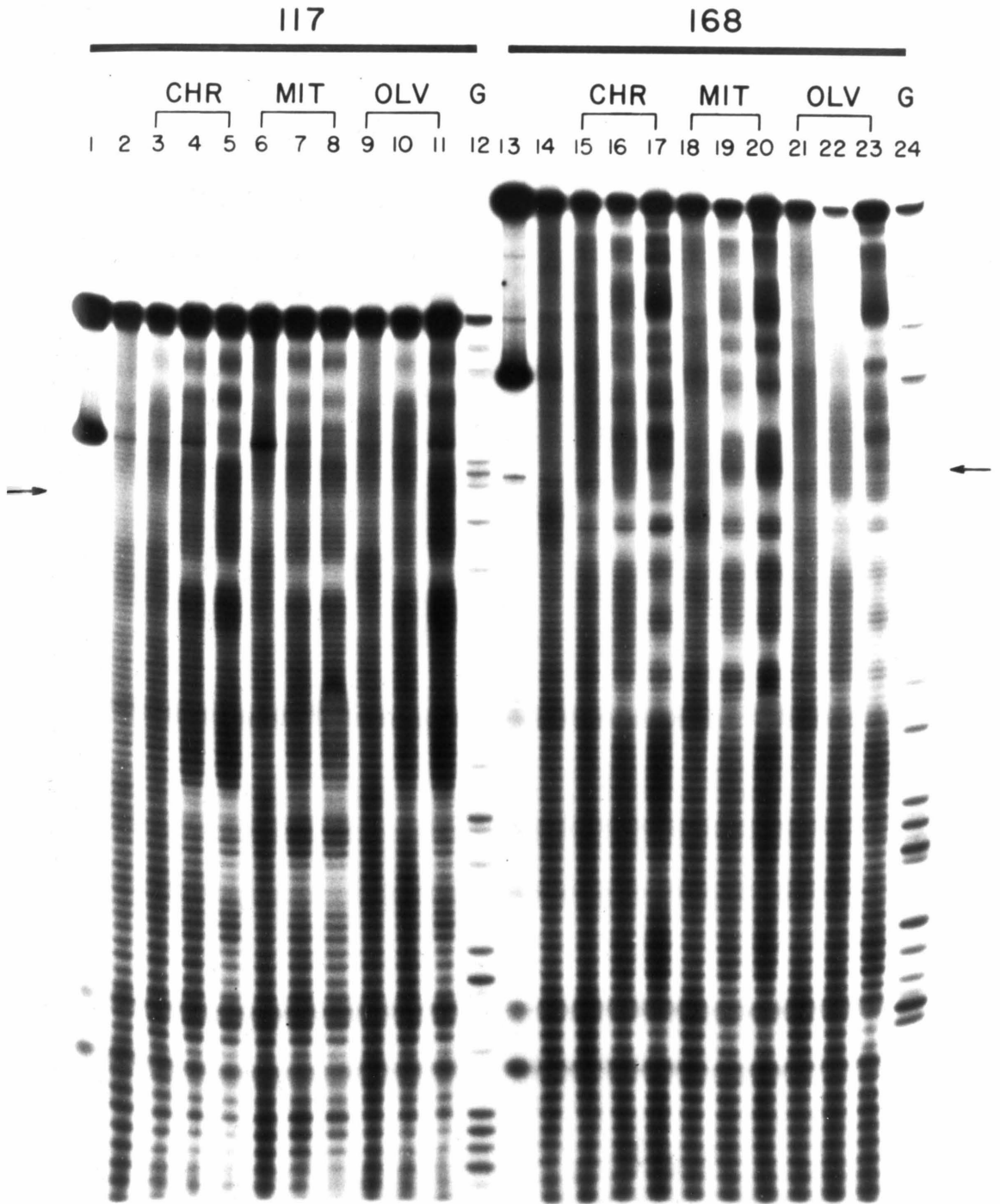
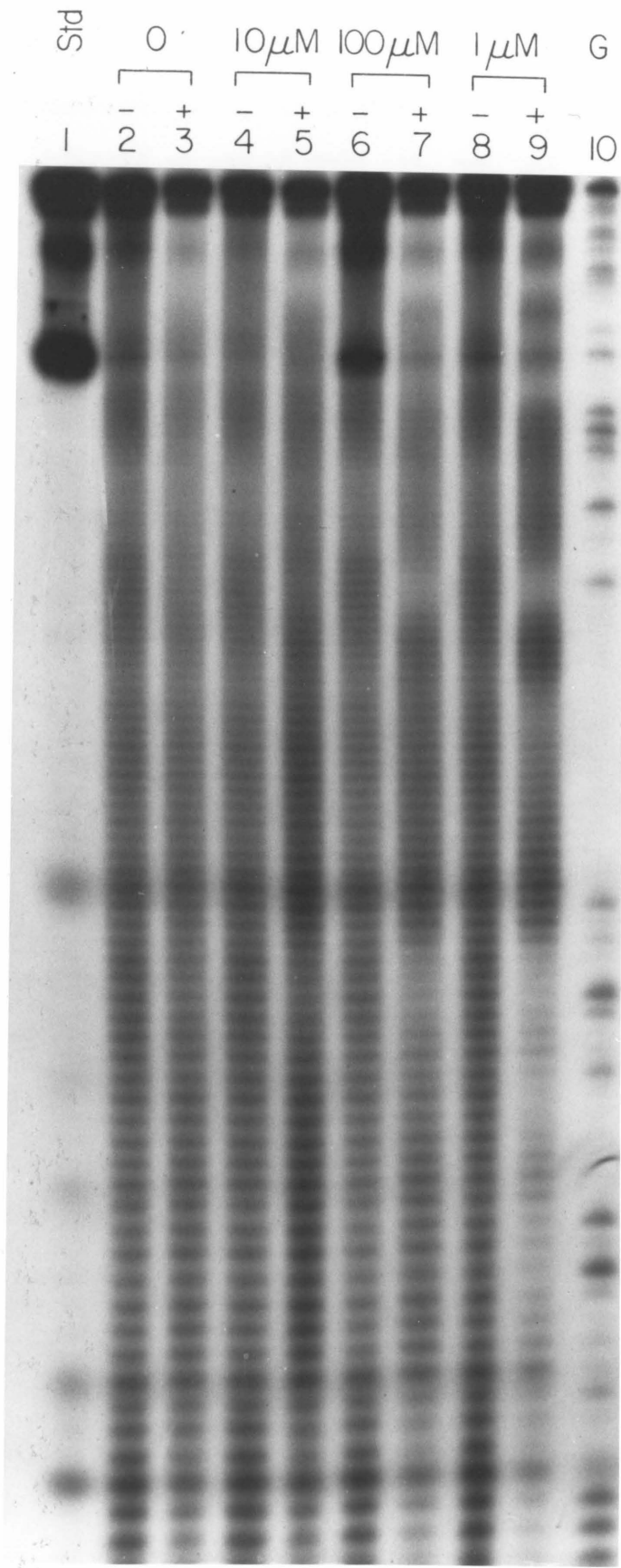


**Figure 25**

**Magnesium ion dependence for chromomycin footprinting.**

Autoradiogram of 3' end labeled 117 bp DNA fragment:  
Lane 10 was the Maxam-Gilbert G reaction. Lane 1 was the intact buffered DNA. Lanes 2-9 contained 10 mM Tris·Cl [pH 7.4], 50 mM NaCl, 100  $\mu$ M base pairs DNA, 4 mM DTT, and 10  $\mu$ M MPE·Fe(II). Plus (+) lanes contained 100 nM chr; minus (-) do not. Lanes 2 and 3 had no  $Mg^{2+}$ ; lanes 4 and 5, 10  $\mu$ M  $Mg^{2+}$ ; lanes 6 and 7, 100  $\mu$ M  $Mg^{2+}$ ; and lanes 8 and 9 had 1 mM  $Mg^{2+}$  present.



**Chromomycin, Mithramycin, and Olivomycin** (structures, see Figure 8). Different concentrations of chromomycin (6.25, 25, and 100  $\mu$ M) in the presence of a 2-fold excess of  $Mg^{2+}$  (13, 50, and 200  $\mu$ M, respectively) were allowed to equilibrate with the 117 and 168 base pair DNA fragments (100  $\mu$ M in base pairs). To these were added at a final concentration 10  $\mu$ M MPE $\cdot$ Fe(II) and 4 mM dithiothreitol. From the DNA cleavage inhibition patterns observed in the gel autoradiogram (Figure 24, lanes 3-5, 15-17), the preferred binding sites for chromomycin/ $Mg^{2+}$  appear to be a minimum of three base pairs in size containing at least two contiguous  $\alpha C \cdot \alpha G$  base pairs. Similar results were found with mithramycin/ $Mg^{2+}$  and olivomycin/ $Mg^{2+}$ . We found that at least 1 equiv. of  $Mg^{2+}$  was required for a well-defined DNA cleavage inhibition pattern. (Figure 25, lanes 3,5,7, and 9) The densitometer trace of the DNA cleavage inhibition pattern on the autoradiogram for the three drugs at the highest concentration (lanes 5,8,11,17,20, and 23) indicates that many but not all binding sites are identical for the three antibiotics (Figure 26). Most striking is the near identity of the chromomycin and olivomycin densitometer traces. The structural feature common to chromomycin and olivomycin is the five sugar moieties. They differ by a methyl group in the aglycon. Mithramycin bears different hexopyranoses. An illustration of the opposite strand footprints and interpreted binding sites for chromomycin, mithramycin, and olivomycin is shown in Figures 27-29.

The number of sites protected from MPE $\cdot$ Fe(II) cleavage increases as the concentration of drugs with  $Mg^{2+}$  is raised. This allows a determination of the relative binding affinities for multiple sites on

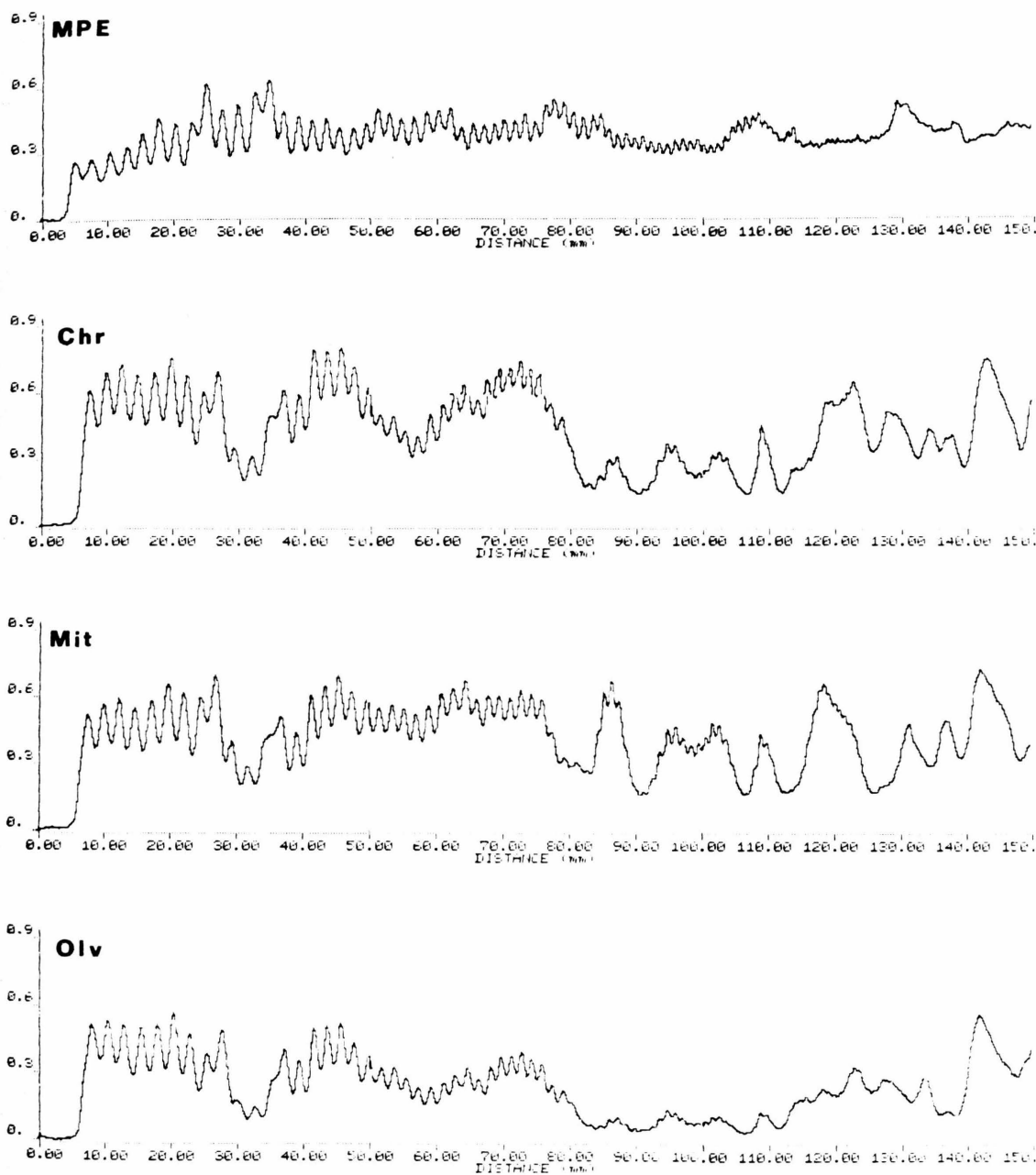


**Figure 26**

Densitometer scan. Left to right corresponds to the bottom to the arrow of the gel autoradiogram shown in Figure 24. Lanes are: (14) MPE•Fe(II) control, (17) 100  $\mu$ M chromomycin, (20) 100  $\mu$ M mithramycin, (23) 100  $\mu$ M olivomycin.

**Figures 27-29**

Illustrations of antibiotic-protected regions (black histograms) from MPE cleavage on 70 base pairs of the lac operon. Arrows indicate the bottom of the gel autoradiogram for each strand. Height of histogram proportional to the amount of cleavage inhibition. Interpretation of footprints is shown on the lower most sequence. Boxed preferred binding sites are ranked according to their order of appearance 1 > 2 > 3. Figure 27 depicts chromomycin; Figure 28, mithramycin, Figure 29, olivomycin.

6.3  $\mu\text{m}$  Chromomycin A<sub>3</sub>



25  $\mu\text{m}$  Chromomycin A<sub>3</sub>



100  $\mu\text{m}$  Chromomycin A<sub>3</sub>



6.3  $\mu$ m Mithramycin

GGCACCCCAGGCTTTACACTTTATGCTTCCGGCTCGTATAATGTGTGGAATTGTGAGCGGATAACAATTT 168 bp  
117 bp CCGTGGGGTCCGAAATGTGAAATACGAAGGCCGAGCATATTACACACCTTAACACTCGCCTATTGTTAAA

25  $\mu$ m Mithramycin

GGCACCCCAGGCTTTACACTTTATGCTTCCGGCTCGTATAATGTGTGGAATTGTGAGCGGATAACAATTT 168 bp  
117 bp CCGTGGGGTCCGAAATGTGAAATACGAAGGCCGAGCATATTACACACCTTAACACTCGCCTATTGTTAAA

100  $\mu$ m Mithramycin

GGCACCCCAGGCTTTACACTTTATGCTTCCGGCTCGTATAATGTGTGGAATTGTGAGCGGATAACAATTT 168 bp  
117 bp CCGTGGGGTCCGAAATGTGAAATACGAAGGCCGAGCATATTACACACCTTAACACTCGCCTATTGTTAAA

GGC ACC CCAG GCT TTACACTTTAT GCT TCCG GCT CGTATAATGTGTGGAATTGTGAG CGG ATAACAATTT 168 bp  
117 bp CCG TGG GGT CCGA AATGTGAAATA CGA AGGC CGA GCATATTACACACCTTAACACTC GCC TATTGTTAAA

6.3  $\mu$ m Olivomycin

GGCACCCCAGGCTTTACACTTTATGCTTCCGGCTCGTATAATGTGTGGAATTGTGAGCGGATAACAATTT 168 bp  
117 bp CCGTGGGGTCCGAAATGTGAAATACGAAGGCCGAGCATATTACACACCTTAACACTCGCCTATTGTTAAA

25  $\mu$ m Olivomycin

GGCACCCCAGGCTTTACACTTTATGCTTCCGGCTCGTATAATGTGTGGAATTGTGAGCGGATAACAATTT 168 bp  
117 bp CCGTGGGGTCCGAAATGTGAAATACGAAGGCCGAGCATATTACACACCTTAACACTCGCCTATTGTTAAA

100  $\mu$ m Olivomycin

GGCACCCCAGGCTTTACACTTTATGCTTCCGGCTCGTATAATGTGTGGAATTGTGAGCGGATAACAATTT 168 bp  
117 bp CCGTGGGGTCCGAAATGTGAAATACGAAGGCCGAGCATATTACACACCTTAACACTCGCCTATTGTTAAA

1 2 3 3 2 3 3 2  
GGCACCCCAAGCTTTACACTTTATGCTTCCGGCTCGTATAATGTGTGGAATTGTGAGCGGATAACAATTT 168 bp  
117 bp CCGTGGGGTCCGAAATGTGAAATACGAAGGCCGAGCATATTACACACCTTAACACTCGCCTATTGTTAAA

the heterogeneous DNA. The chromomycin footprints as a function of increasing concentration are shown in Figure 27. For chromomycin/Mg<sup>2+</sup>, the preferred sites on the 70 base pairs of DNA examined are (in decreasing affinity) 3'-GGG, CGA >> CCG, GCC >> CGA, CCT > GTG-5'.

For mithramycin/Mg<sup>2+</sup>, the preferred sites are 3'-CGA >> GCC, TGG, CGA-5' (Figure 28); while for olivomycin/Mg<sup>2+</sup>, the preferred sites are 3'-GGG >> CCG, GCC >> CGA, CCT > TGA, ACA (Figure 29). It may be noted that identical nucleotide triplets, 3'-CGA-5' in both chromomycin and mithramycin results, appear multiple times with different affinities, depending on their location in the 70 bp sequence. While there exists a similarity in both the locations and number of preferred binding sites for the three antibiotics at high concentration (100 μM), the order in which these binding sites appear differs depending on the antibiotic. For example, the very weak chromomycin binding site 3'-CGA-5' is a strong binding site for mithramycin. In all cases, the preferred binding sites for these antibiotics tended to be 3 bp in length and contained two or more guanine bases.

#### **Comparison of MPE·Fe(II) and DNase I Footprinting<sup>172</sup>**

As described earlier in the introductory portion of this thesis, concurrent work performed by Lane et al. has demonstrated the feasibility of determining the sequence specificity of actinomycin and netropsin binding to heterogeneous DNA by DNase I footprinting.<sup>164</sup> Though MPE and DNase both cleave DNA they differ with regard to size, mechanism of cleavage, and level of sequence neutrality. It could then be anticipated that they should respond differently to the presence of a bound small molecule and report different footprinting patterns. An

**Figure 30**

**A comparison of MPE- and DNase I-generated footprinting patterns for the antibiotics actinomycin, chromomycin and distamycin.**

Autoradiogram of the 3' end labeled 382 bp DNA fragment: Lane 1 contained the intact DNA. Lane 16 was the Maxam-Gilbert G lane. All other even-numbered lanes (2,4,6,8,10,12,14) contained 10 mM Tris·Cl [pH 7.4], 50 mM NaCl, 200  $\mu$ M base pairs DNA, 4 mM DTT and 10  $\mu$ M MPE·Fe(II) with final concentrations in a 10  $\mu$ l reaction volume. All other odd-numbered lanes (3,5,7,9,13,15) contained 10 mM Tris·Cl [pH 7.9], 10 mM KCl, 10 mM MgCl<sub>2</sub>, 5 mM CaCl<sub>2</sub>, 200  $\mu$ M base pairs DNA, 0.1 mM DTT, and 0.5  $\mu$ g/ml DNase I final concentrations in an 10  $\mu$ l reaction volume. Inhibiting drugs in these reactions are: lanes 4 and 5, 12.5  $\mu$ M **act**; lanes 6 and 7, 50  $\mu$ M **act**; lanes 8 and 9, 12.5  $\mu$ M **chr** and 25  $\mu$ M Mg<sup>2+</sup>; lanes 10 and 11, 50  $\mu$ M **chr** and 100  $\mu$ M Mg<sup>2+</sup>; lanes 12 and 13 12.5  $\mu$ M **dis**; ;lanes 14 and 15, 50  $\mu$ M **dis**.

DNA STD  
MPE·Fe(II)  
DNase I

ACT      CHR      DIST      G

1 2 3 4 5 6 7 8 9 10 11 12 13 14 15 16

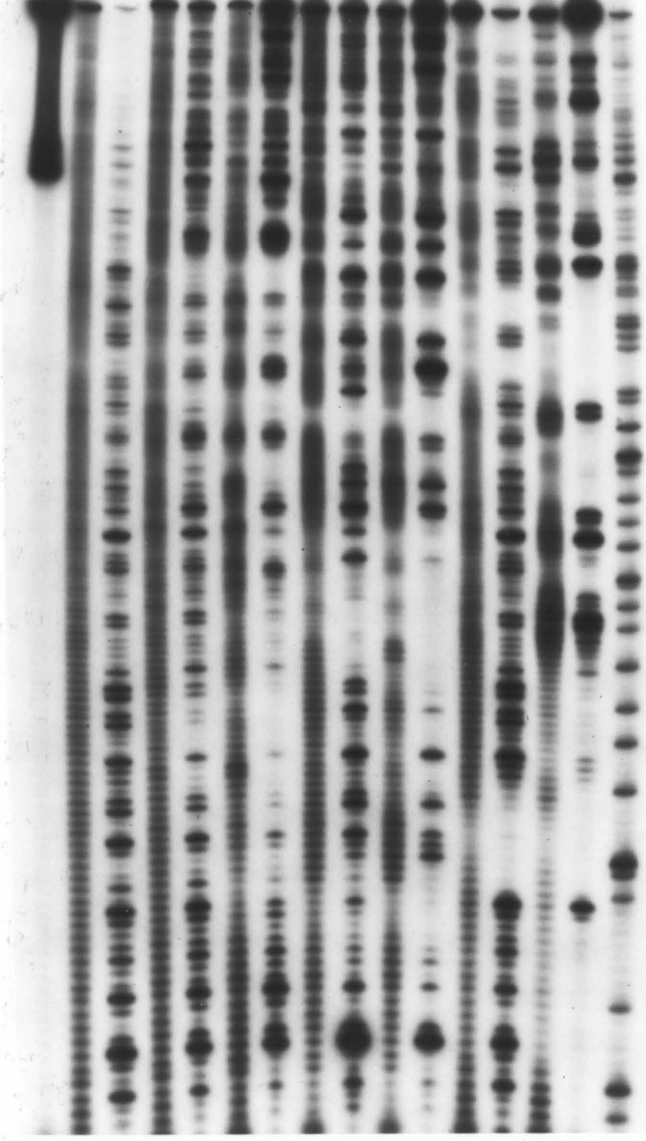


**Figure 31**

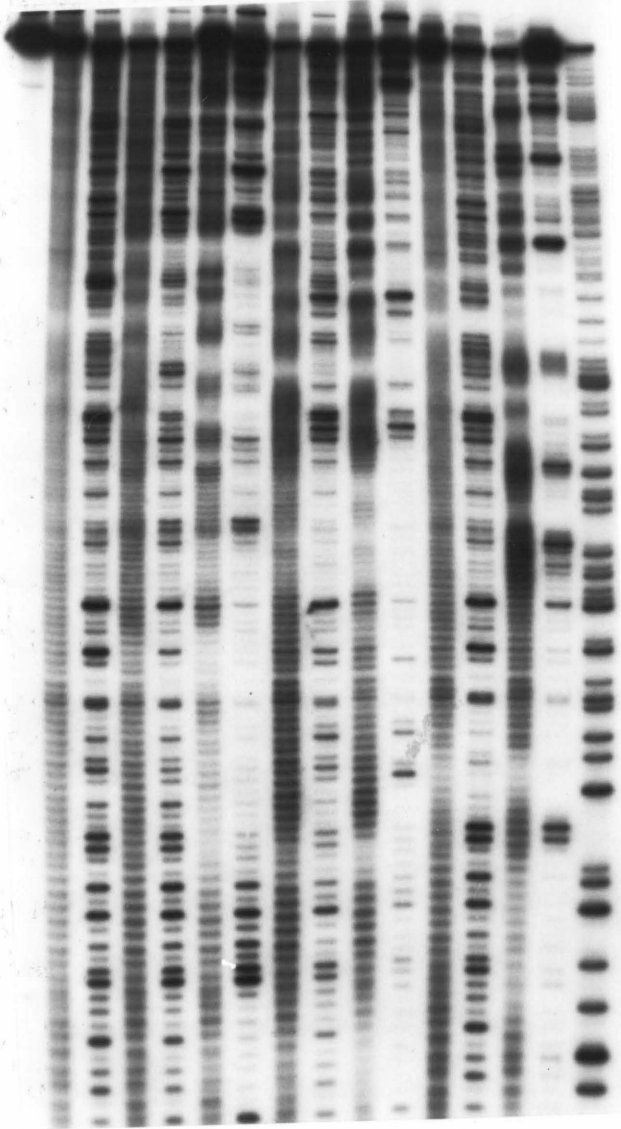
**A comparison of MPE- and DNase-I generated footprinting patterns for the antibiotics actinomycin, chromomycin, and distamycin**

Autoradiogram of the 5' end labeled 378 bp DNA fragment: Lane 1 contained the intact DNA. Lane 16 was the Maxam-Gilbert G lane. All other even-numbered lanes (2,4,6,8,10,12,14) contained 10 mM Tris·Cl [pH 7.4], 50 mM NaCl, 400  $\mu$ M base pairs DNA, 4 mM DTT, and 10  $\mu$ M MPE·Fe(II). All other odd-numbered lanes (3,5,7,9,11,13,15) contained 10 mM Tris·Cl [pH 7.9], 10 mM KCl, 10 mM MgCl<sub>2</sub>, 5 mM CaCl<sub>2</sub>, 400  $\mu$ M base pairs DNA, 0.1 mM DTT, and 02.  $\mu$ g/ml DNase I. Inhibiting drugs in these reactions were: lanes 4 and 5, 25  $\mu$ M **act**; lanes 6 and 7, 100  $\mu$ M **act**; lanes 8 and 9, 25  $\mu$ M **chr**, and 50  $\mu$ M Mg<sup>2+</sup>; lanes 10 and 11, 100  $\mu$ M **chr** at 200  $\mu$ M Mg<sup>2+</sup>; lanes 12 and 13, 25  $\mu$ M **dis**; lanes 14 and 15, 100  $\mu$ M **dis**.

DNA STD  
MPE·Fe(II)  
DNase I

ACT      CHR      DIST    G

1 2 3 4 5 6 7 8 9 10 11 12 13 14 15 16



understanding of this difference in patterns was obtained through a parallel comparison of the two footprinting techniques on a series of small molecules, actinomycin, chromomycin, and distamycin, and the regulatory protein *lac* repressor.

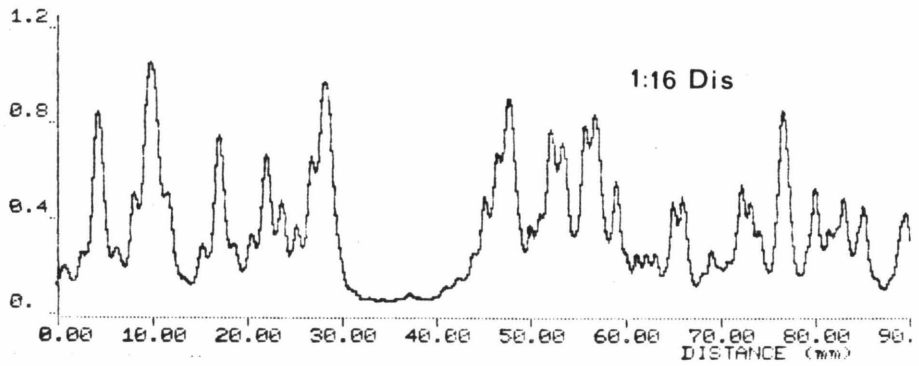
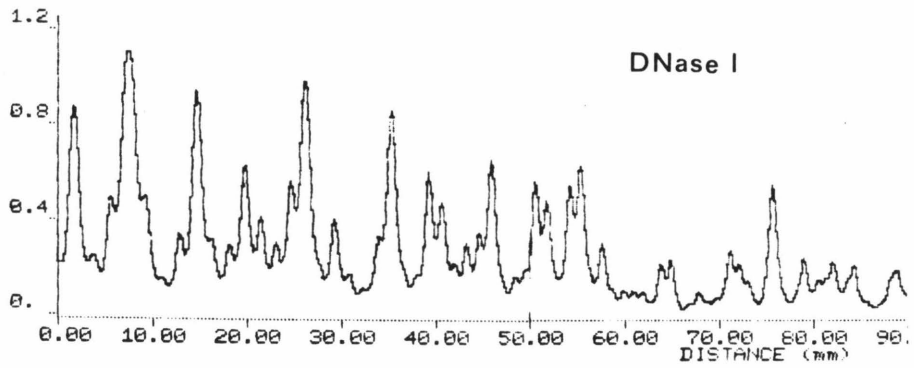
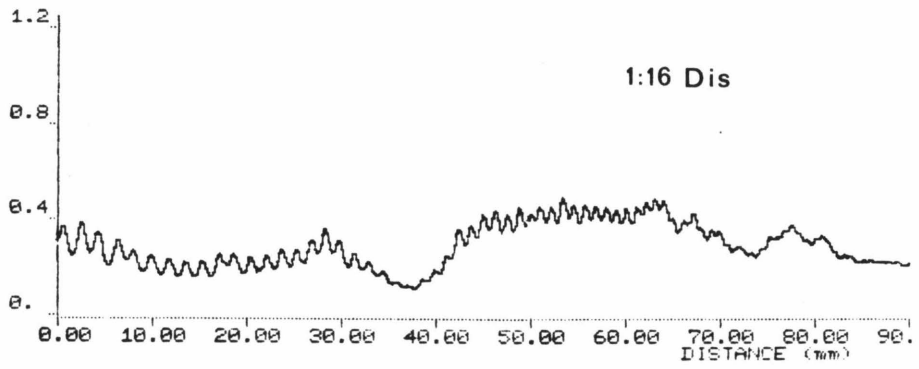
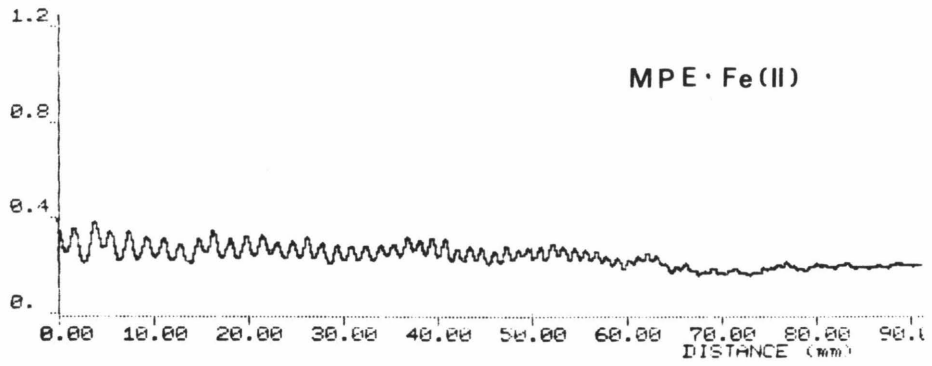
**MPE•Fe(II) Cleaves DNA with Lower Sequence Specificity than DNase**

**I:** MPE•Fe(II) cleavage of a 380 base pair DNA restriction fragment labeled at either the 3' or 5' end with <sup>32</sup>P affords a relatively uniform DNA cleavage pattern on a Maxam-Gilbert sequencing gel. (Figures 30 and 31, lane 2) Densitometry reveals that the variation in average peak height is modest throughout the entire scan. Although MPE•Fe(II) cleavage of DNA is relatively non-specific, the reagent is not sequence neutral. DNase I exhibits a higher sequence specificity than MPE•Fe(II) as seen in both autoradiograms (Figures 30 and 31, lane 3). DNase I cleavage specificity over the span of a few base pairs can range one order of magnitude in absorbance intensity whereas MPE cleavages usually remains within  $\pm 0.1$  absorbance unit (Figure 32).

**Footprinting at Low Drug Binding Densities:** Actinomycin D, chromomycin A<sub>3</sub>, and distamycin A were equilibrated at low concentrations with the  $\sim 380$  base pair DNA restriction fragment (0.06 drug/DNA base pairs) followed by partial cleavage with MPE•Fe(II) or DNase I. The autoradiograms of the DNA cleavage inhibition patterns are shown in Figures 30 and 31. From densitometric analyses, the footprints on 70 base pairs of the 378-382 bp DNA fragment are shown in Figure 33. For actinomycin D, DNase I affords a footprint 6 to 12 base pairs in size while MPE•Fe(II) does not detect a strongly bound drug site. For chromomycin, DNase I reports three footprints while MPE•Fe(II) reports

**Figure 32**

Densitometer scans comparing MPE and DNase generated patterns. Left to right corresponds to the bottom to middle of the gel autoradiogram shown in Figure 30. Lanes are (from top to bottom): (2) MPE·Fe(II) control, (12) 12.5  $\mu$ M distamycin cleaved by MPE, (3) DNase I control, (13) 12.5  $\mu$ M distamycin cleaved by DNase. Notice the uniformity in cleavage intensity for MPE, while DNase varies considerably. Both 12.5  $\mu$ M distamycin lanes exhibit a single footprint.



five which are smaller in size. For distamycin A, the single binding site detected by DNase I is 9 base pairs in size whereas the MPE•Fe(II) footprint is 5 base pairs in size (Figure 34).

**Footprinting at High Drug Binding Densities:** The three drugs were allowed to equilibrate with the same DNA restriction fragment at higher concentrations (0.25 drug/DNA base pairs) followed by partial cleavage with either MPE•Fe(II) or DNase I. The autoradiograms of the corresponding footprints are shown in Figures 30 and 31. From densitometric analyses, the footprints on 70 base pairs of the 378-382 bp DNA fragment are shown in Figure 33. For actinomycin D, MPE•Fe(II) partial cleavage reveals six footprints 2-5 base pairs in size. DNase I partial cleavage exhibits three footprints, two 5-6 base pairs and one 36 base pairs in size which encompasses three of the discrete MPE•Fe(II) footprints. For chromomycin A<sub>3</sub>, MPE•Fe(II) partial cleavage reveals seven footprints. DNase I reports four footprints, one of which is 36 base pairs in size. For distamycin, MPE•Fe(II) partial cleavage reveals four discrete footprints 5-6 base pairs in size. DNase I partial cleavage exhibits three footprints, one 7 base pairs and two 16 and 25 base pairs in size, respectively (Figure 34).

**Comparisons of MPE and DNase I Small Molecule Footprints:** There are two significant differences between small molecule binding sites reported by MPE and DNase I footprinting methods. While both methods report footprints centered around the same sequences, DNase I consistently affords larger footprints. This is especially evident at elevated small molecule/base pairs DNA ratios ( $\sim$  1:4) where multiple discrete MPE footprints may be contained in a single large DNase

### Figure 33

MPE·Fe(II) and DNase I footprints on both strands of 70 nucleotides of the 380 bp DNA fragment corresponding to bottom to middle of autoradiograms in Figures 30 and 31. The DNase I footprints are shown as light and dark bars due to partial and complete cleavage inhibition, respectively. The MPE·Fe(II) footprints are shown as histograms. Bottom strand footprints are from Figure 30. Top strand footprints are from Figure 31. Two binding densities are shown for each inhibiting small molecule; top is 0.06 antibiotic/base pair, bottom is 0.25 antibiotic/base pair.

Actinomycin D

5'CGCGTAGTCGATAGTGGCTCCAAGTAGCGAAGCGAGCAGGACTGGGCGGGCCAAAGCGGTTCGGACAGT  
 340 320 300 280  
 3'GCGCATCAGCTATCACCGAGGTTTCATCGCTTCGCTCGTCCTGACCCGCCGCCGGTTTCGCCAGCCTGTCA

Actinomycin D

5'CGCGTAGTCGATAGTGGCTCCAAGTAGCGAAGCGAGCAGGACTGGGCGGGCCAAAGCGGTTCGGACAGT  
 340 320 300 280  
 3'GCGCATCAGCTATCACCGAGGTTTCATCGCTTCGCTCGTCCTGACCCGCCGCCGGTTTCGCCAGCCTGTCA

Chromomycin A<sub>3</sub>

5'CGCGTAGTCGATAGTGGCTCCAAGTAGCGAAGCGAGCAGGACTGGGCGGGCCAAAGCGGTTCGGACAGT  
 340 320 300 280  
 3'GCGCATCAGCTATCACCGAGGTTTCATCGCTTCGCTCGTCCTGACCCGCCGCCGGTTTCGCCAGCCTGTCA

Chromomycin A<sub>3</sub>

5'CGCGTAGTCGATAGTGGCTCCAAGTAGCGAAGCGAGCAGGACTGGGCGGGCCAAAGCGGTTCGGACAGT  
 340 320 300 280  
 3'GCGCATCAGCTATCACCGAGGTTTCATCGCTTCGCTCGTCCTGACCCGCCGCCGGTTTCGCCAGCCTGTCA

Distamycin A

5'CGCGTAGTCGATAGTGGCTCCAAGTAGCGAAGCGAGCAGGACTGGGCGGGCCAAAGCGGTTCGGACAGT  
 340 320 300 280  
 3'GCGCATCAGCTATCACCGAGGTTTCATCGCTTCGCTCGTCCTGACCCGCCGCCGGTTTCGCCAGCCTGTCA

Distamycin A

5'CGCGTAGTCGATAGTGGCTCCAAGTAGCGAAGCGAGCAGGACTGGGCGGGCCAAAGCGGTTCGGACAGT  
 340 320 300 280  
 3'GCGCATCAGCTATCACCGAGGTTTCATCGCTTCGCTCGTCCTGACCCGCCGCCGGTTTCGCCAGCCTGTCA

Actinomycin



Chromomycin



Distamycin

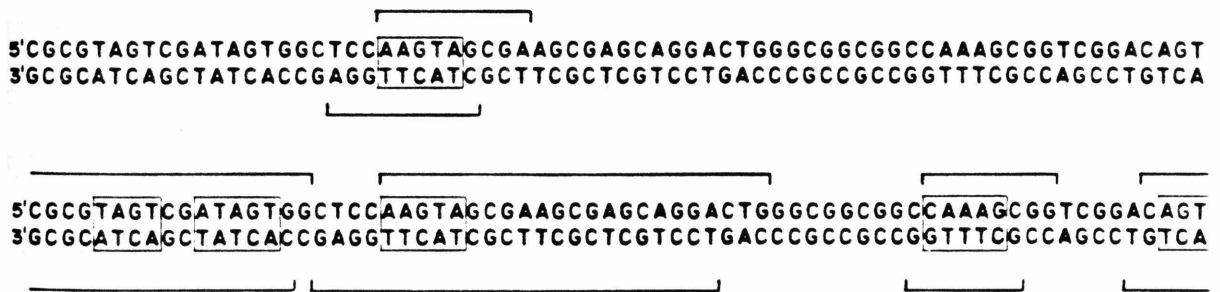


Figure 34

Illustration of MPE·Fe(II) footprints (boxes) and DNase I footprints (brackets) from Figure 33.

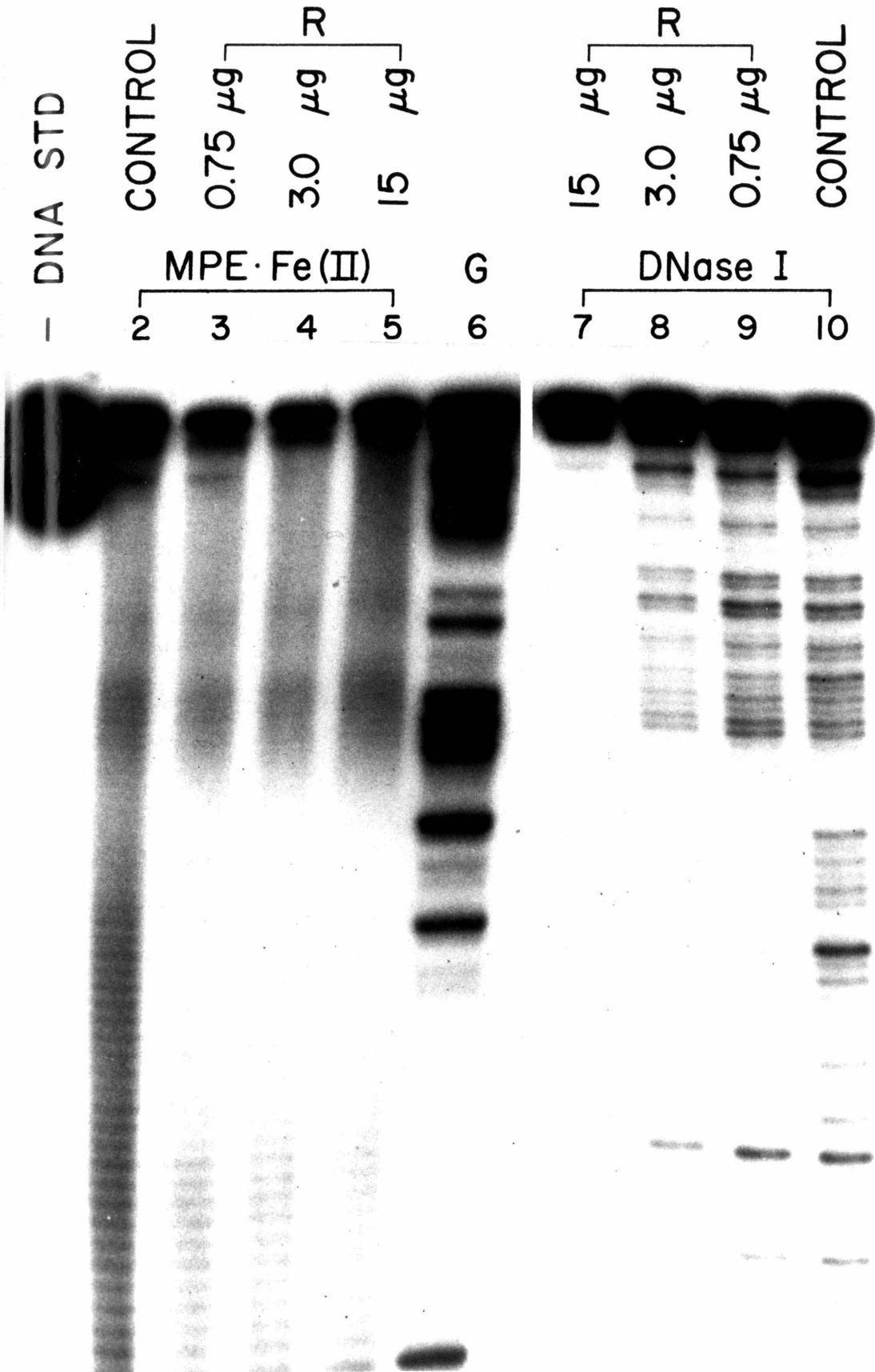
footprint. Smaller footprinting sizes allows for greater precision in determining the extents and locations of small molecule binding sites. DNase footprinting appears more sensitive, demonstrating footprints at lower small molecule concentrations where MPE·Fe(II) footprinting shows none (see 0.06 act/bp, Figure 30). Upon increasing concentration, MPE footprinting eventually demonstrates footprints at these previously invisible sites.

#### **MPE·Fe(II) Footprint of the lac Repressor<sup>172</sup>**

For comparison the characterized lac repressor-operator system was examined by both footprinting methods (Figure 35). A 3' <sup>32</sup>P end labeled 117 base pair DNA restriction fragment containing one copy of the UV-5 lac operon mutation, preequilibrated with several concentrations of the lac repressor protein (0.75 to 15 μg), were subjected to either MPE·Fe(II) or DNase I partial cleavage. Identical footprinting patterns are observed by both methods at the low lac repressor binding levels (0.75 and 3 μg) as seen in Figure 36. At 15 μg lac repressor DNase I cleavage is sufficiently inhibited such that a discrete footprint is no longer visible (Figure 35, lane 7). MPE·Fe(II) footprints lac repressor throughout the concentration range tested.

**Figure 35**  
**Comparison of lac repressor binding site by MPE**  
**and DNase footprinting methods**

Autoradiogram of 3' end labeled 117 bp DNA fragment containing a copy of the lac operon promoter-operator. Lane 1 contained the intact buffered DNA. Lane 6 was the Maxam-Gilbert G lane. Lanes 2-5 contained 10 mM Tris·Cl [pH 7.4], 50 mM NaCl, 100  $\mu$ M base pairs DNA, 4 mM DTT, and 10  $\mu$ M MPE·Fe(II) as final concentrations in 10  $\mu$ l reaction volumes. Lanes 7-10 contained 10 mM Na cacodylate [pH 8], 10 mM MgCl<sub>2</sub>, 5 mM CaCl<sub>2</sub>, 10  $\mu$ M base pairs DNA, 0.1 mM DTT, and 0.1  $\mu$ g/ml DNase I as final concentrations in 100  $\mu$ l reaction volumes. The amount of lac repressor present in each reaction was none (lanes 2 and 10), 0.75  $\mu$ g (lanes 3 and 9), 3  $\mu$ g (lanes 4 and 8), and 15  $\mu$ g (lanes 5 and 7).



0.75  $\mu$ g *lac* repressor

5' ATAATGTGTGGAATTGTGAGCGGATAACAATTTACACAG 3'  
60' 80'  
3' TATTACACACCTTAACACTCGCCTATTGTTAAAGTGTGTC 5'

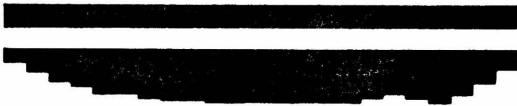


**Figure 36**

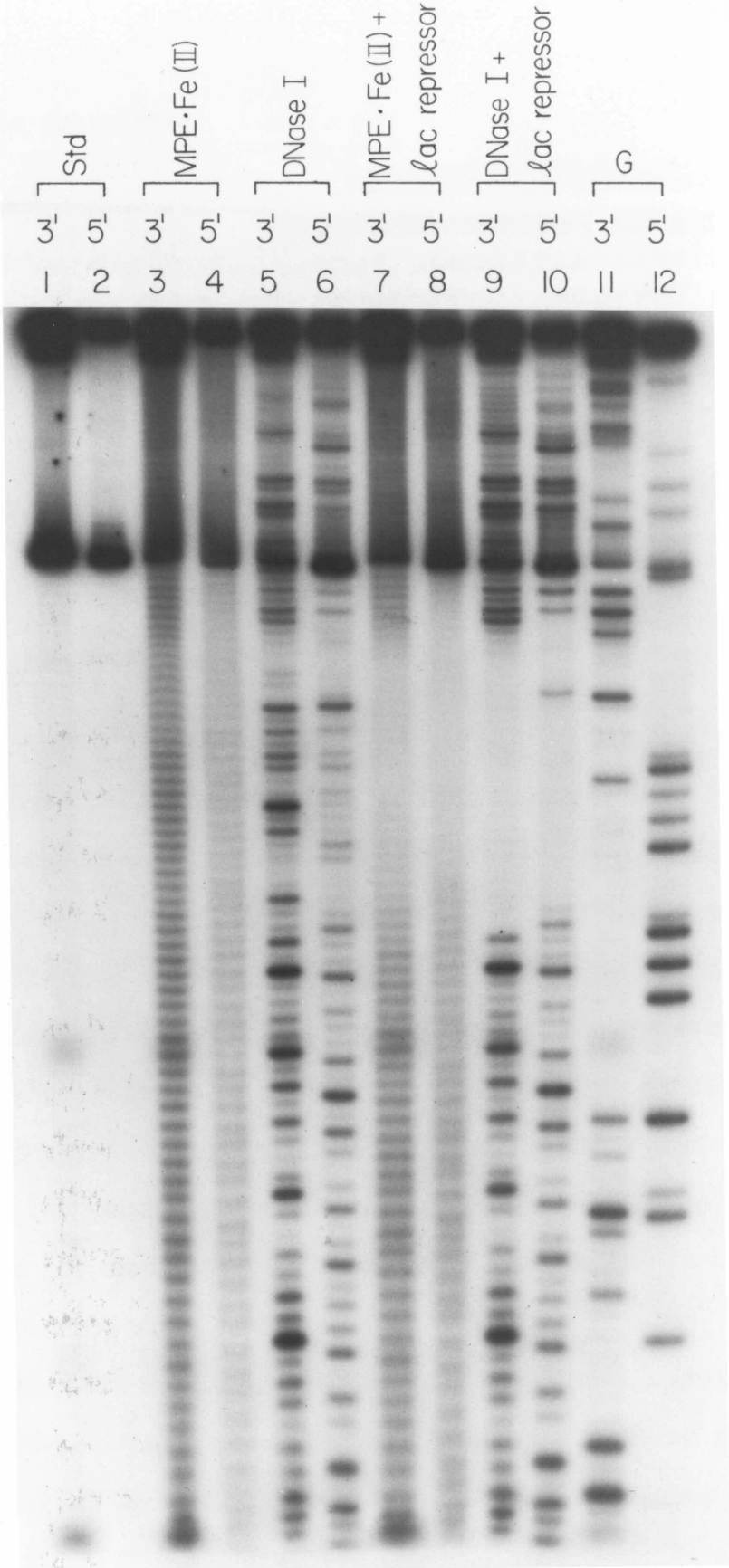
MPE·Fe(II) and DNase I footprint of *lac* repressor (7.5  $\mu$ g/ml) on 40 nucleotides of the 117 bp DNA fragment (Figure 36, lanes 3 and 9). The DNase I footprint is shown as a dark bar. The MPE·Fe(II) footprint is shown as a histogram.

For completeness an opposite strand analysis of *lac* repressor binding to its operator region was performed by both MPE and DNase I footprinting methods under optimum conditions. Either a 3' or 5' 32p end labeled 117 bp DNA restriction fragment containing a copy of the UV-5 *lac* operon mutation was preequilibrated with *lac* repressor at a final concentration of 58  $\mu$ g/ml and then subject to partial MPE·Fe(II) or DNase I digestion (see Figure 37). Under these reaction conditions both DNase I and MPE report similar footprints (Figure 38). Both methods exhibit 3 bp overhang on each 3' end of the asymmetric footprints. DNase shows footprints 24 bp long, while MPE has footprints 22 bp long in this experiment. One striking difference between these two methods is the absence of the accentuated DNase cleavage site within the footprint on the 5' labeled strand when footprinting is performed with MPE.

**Figure 37**

**Opposite strand analysis of lac repressor binding to the lac operon by MPE and DNase footprinting protocols.**

Autoradiogram of 3' and 5' end labeled 117 bp DNA fragments: Odd-numbered lanes (1,3,5,7,9,11) were 3' end labeled; even-numbered lanes (2,4,6,8,10,12) were 5' end labeled. Lanes 1 and 2 were the intact buffered DNAs. Lanes 11 and 12 were the Maxam-Gilbert G reactions. Lanes 3,4,7, and 8 contained 10 mM Tris·Cl [pH 7.4], 50 mM NaCl, 400  $\mu$ M base pairs DNA, 4 mM DTT, and 10  $\mu$ M MPE·Fe(II). Lanes 5,6,9, and 10 contained 10 mM Tris·Cl [pH 7.9], 10 mM KCl, 10 mM MgCl<sub>2</sub>, 5 mM CaCl<sub>2</sub>, 400  $\mu$ M base pairs DNA, 0.1 mM DTT and 0.2  $\mu$ g/ml DNase I. Lanes 7,8,9,10 also contained 58  $\mu$ g/ml lac repressor. Lanes 3 and 4 were the MPE cleavage controls; lanes 5 and 6 were the DNase cleavage controls.



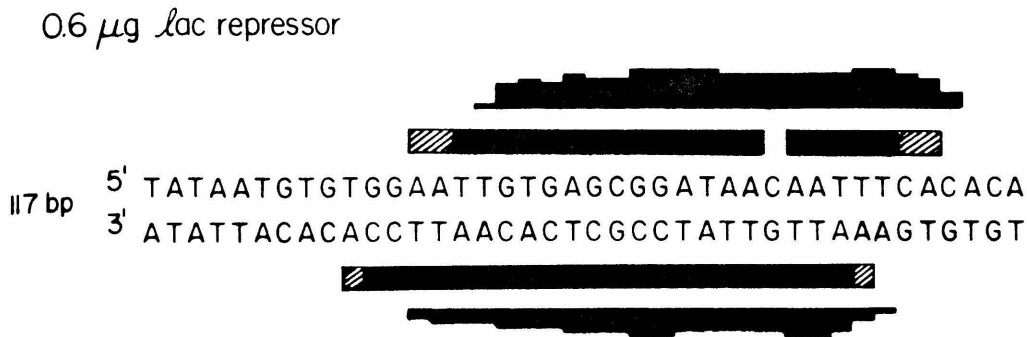


**Figure 38**

MPE·Fe(II) and DNase I footprints of *lac* repressor (7.5  $\mu$ g/ml) on 40 base pairs of the 117 bp DNA fragment (Figure 37, lanes 7-10) DNase footprints are represented as horizontal bars. Solid bars indicate complete cleavage inhibition; hatched bars, approximately 1/2 cleavage inhibition. MPE footprints are represented as histograms, their height indicative of the amount of cleavage inhibition.

### **Echinomycin Binding to DNA<sup>173</sup>**

Echinomycin is a quinoxaline antibiotic composed of two chromophores connected to a cyclic octadepsipeptide.<sup>110</sup> The chromophores are capable of simultaneously being intercalated at locations separated by two base pairs, i.e. bisintercalation.<sup>113</sup> The peptide ring lies in the minor groove and is postulated in conferring the observed guanine specificity through hydrogen bonding interactions.<sup>114</sup> Equilibrium binding studies suggest that the optimum binding site involves all four bases in the recognition process. The employment of MPE footprinting should aid in the elucidation of those sequences present in the optimum echinomycin binding site.

For an investigation of echinomycin DNA cleavage inhibition a variety of DNA substrates were prepared. Two were isolated from pLJ3, the 117 bp and 168 bp restriction fragments, each containing a copy of the lactose operon promoter-operator region. These were 3' end-labeled, thus allowing complementary DNA strands to be investigated. A total of

4 restriction fragments were isolated from pBR322 and either 3' or 5' end labeled, thus allowing opposite strand analyses. These were the 167 and 517 bp fragments containing the putative P<sub>1</sub>, 2, and 3 promoter regions; and the 274 (278) and 378 (382) bp fragments containing parts of the tetracycline resistance gene. Cleavage reactions were performed with either MPE or DNase I following conventional procedures. Electrophoresis was performed on 8% polyacrylamide, 1:20 crosslinked, 50% urea containing gels. The autoradiograms obtained from these experiments are shown in Figures 39-42.

**Controls:** As described earlier in the Results, MPE·Fe(II) exhibits relatively little sequence specificity on many fragments. The only examples contrary to these are the 167 and 517 bp DNA fragments, both of which exhibit MPE cleavage specificities whose difference in cleavage intensities resemble typical footprints (Figure 42, lanes 5,6,13,14). Errors associated in determining footprints near regions of intrinsic MPE cleavage inhibition are minimized through use of the "subtractive" method of footprint determination, described in the Experimental.

**Echinomycin, Footprints as a Function of Concentration:** Three series of footprinting experiments were investigated as a function of echinomycin concentration (Figures 39-41). Footprinting patterns first appear at concentrations equivalent to 1 echinomycin:32 base pairs DNA, but are readable only upon a four-fold increase in concentration (1:8) (Figure 39, lanes 6-9 and 16-19). Those footprints which appear at higher concentrations (1:4 - 1:2) typically are present at lower binding densities. Very few new sites appear. This is very similar to the

**Figure 39**

**Echinomycin-derived footprints as obtained by both MPE  
and DNase protocols: an opposite strand analysis**

Autoradiogram of 3' end labeled 382 bp and 5' end labeled 378 bp DNA fragments: Lanes 1-10 were 3' and lanes 11-20 were 5' end labeled. Lanes 1 and 11 were the intact buffered DNAs. Lanes 10 and 20 were the Maxam-Gilbert G reactions. Even numbered lanes 2,4,6,8 and 12,14,16,18 contained 10 mM Tris·Cl [pH 7.4], 50 mM NaCl, 200  $\mu$ M base pairs DNA, 4 mM DTT, 10% THF, and 10  $\mu$ M MPE·Fe(II). Odd numbered lanes 3,5,7,9 and 13,15,17,19 contained 10 mM Tris·Cl [pH 7.9], 10 mM KCl, 10 mM MgCl<sub>2</sub>, 5 mM CaCl<sub>2</sub>, 200  $\mu$ M base pairs DNA, 0.1 mM DTT, 10% THF, and 0.5  $\mu$ g/ml DNase I. Lanes 4,5,14, and 15 contained 1.6  $\mu$ M **ech**. Lanes 6,7,16, and 17 contained 6.25  $\mu$ M **ech**. Lanes 8,9,18 and 19 contained 25  $\mu$ M **ech**. Lanes 2 and 12 were the MPE·Fe(II) cleavage controls. Lanes 3 and 13 were the DNase cleavage controls.

Std	MPE · Fe(II)	DNase I	Echinomycin						G	Std	MPE · Fe(II)	DNase I	Echinomycin						G
	m	d	1/128		1/32		1/8			m	d		1/128		1/32		1/8		
1	2	3	4	5	6	7	8	9	10	11	12	13	14	15	16	17	18	19	20

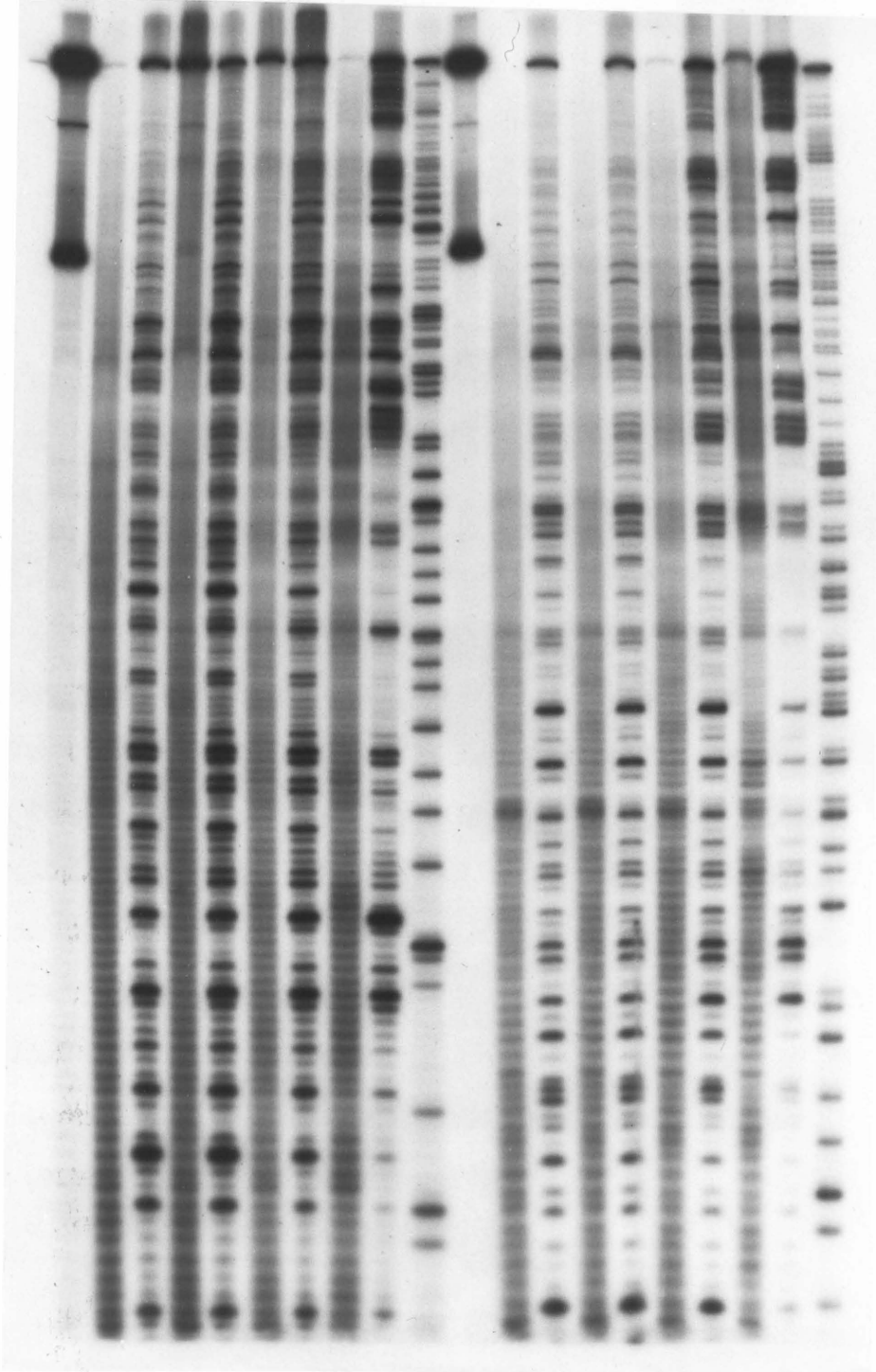


**Figure 40**

**Echinomycin footprints on opposite DNA strands as  
obtained by both MPE and DNase protocols**

Autoradiogram of 3' end labeled 278 bp and 5' end labeled 274 bp DNA fragments: Odd numbered lanes (1,3,5,7,9,11,13, and 15) were 3' end labeled; even numbered lanes (2,4,6,8,10,12,14, and 16) were 5' end labeled. Lanes 1 and 2 are the intact buffered DNAs. Lanes 15 and 16 were the Maxam-Gilbert G reactions. Lanes 3,4,7,8,11, and 12 contained 10 mM Tris·Cl [pH 7.4], 50 mM NaCl, 400  $\mu$ M base pairs DNA, 4 mM DTT, 10% THF, and 10 M MPE·Fe(II). Lanes 5,6,9,10,13, and 14 contained 10 mM Tris·Cl [pH 7.9], 10 mM KCl, 10 mM MgCl<sub>2</sub>, 5 mM CaCl<sub>2</sub>, 400  $\mu$ M base pairs DNA, 0.1 mM DTT, 10% THF, and 0.4  $\mu$ g/ml DNase I. Lanes 7,8,9, and 10 contained 115  $\mu$ M ech. Lanes 11,12,13, and 14 contained 46  $\mu$ M ech. Lanes 3 and 4 were the MPE cleavage controls. Lanes 5 and 6 were the DNase cleavage controls.

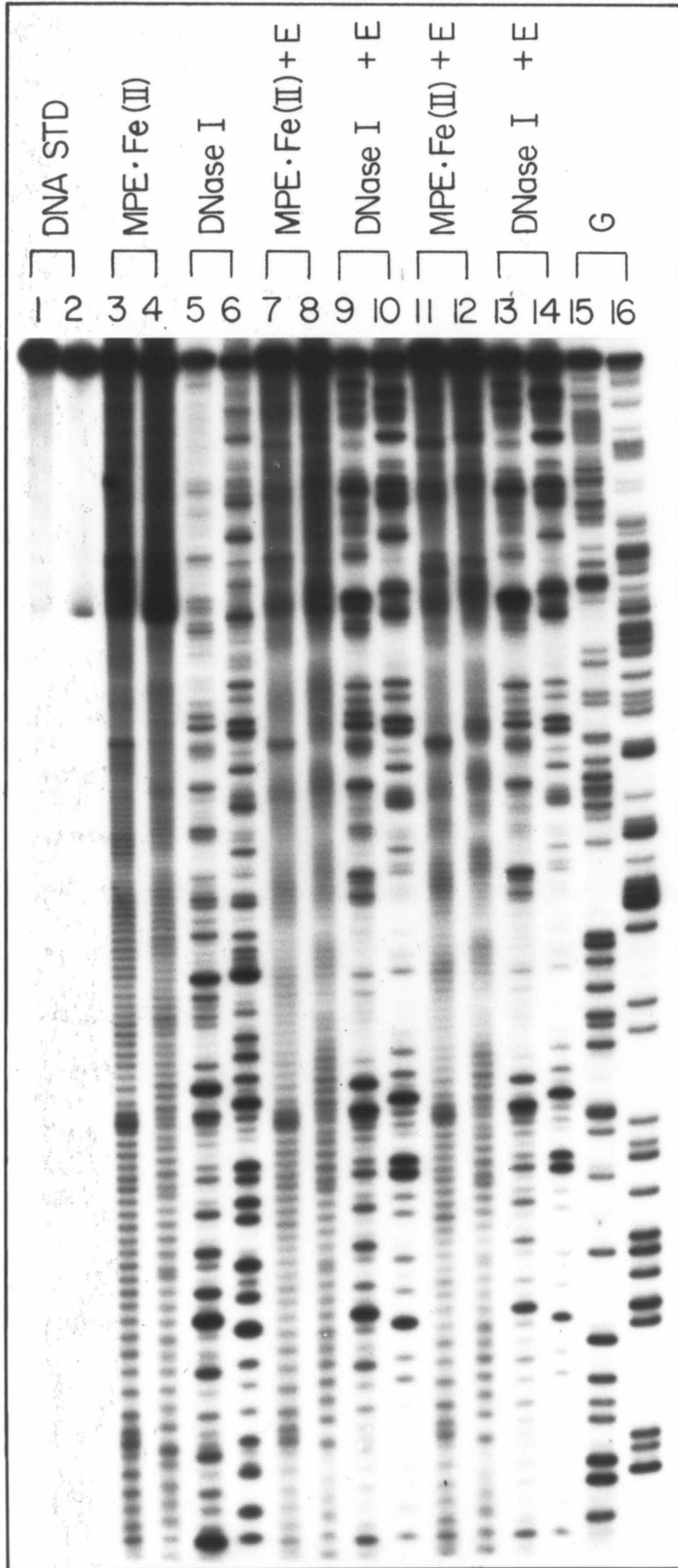


**Figure 41**

**Complementary strand analysis of echinomycin-binding sites.**

Autoradiogram of 3' end labeled 117 bp and 168 bp DNA fragments: Lanes 1-5 were 117 bp and lanes 6-10 were 168 bp DNA. Primed number lanes (example 4') correspond to their unprimed counterparts except that they had been electrophoresed twice as long (7 hr vs 3.5). This allows for greater resolution of the longer DNA cleavage fragments. Lanes 1 and 6 were the intact buffered DNA. Lanes 5 and 10 were the Maxam-Gilbert G reactions. Lanes 2-4 and 7-9 contained 10 mM Tris·Cl [pH 7.4], 50 mM NaCl, 400  $\mu$ M base pairs DNA, 4 mM DTT, 10% THF, and 10  $\mu$ M MPE·Fe(II). Pairs of lanes 2 and 7, 3 and 8, 4 and 9 contained 0, 50, and 200  $\mu$ M ech., respectively.

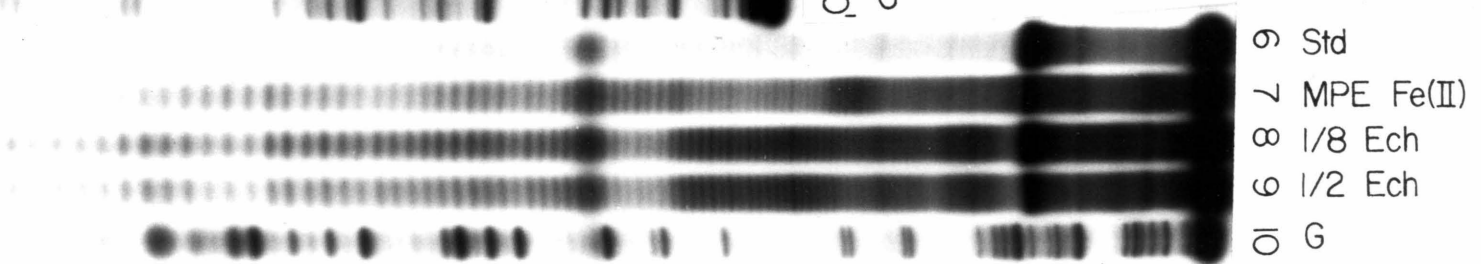
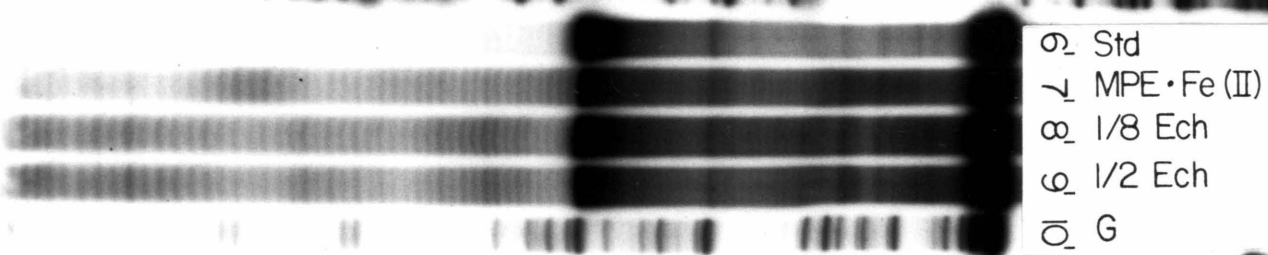
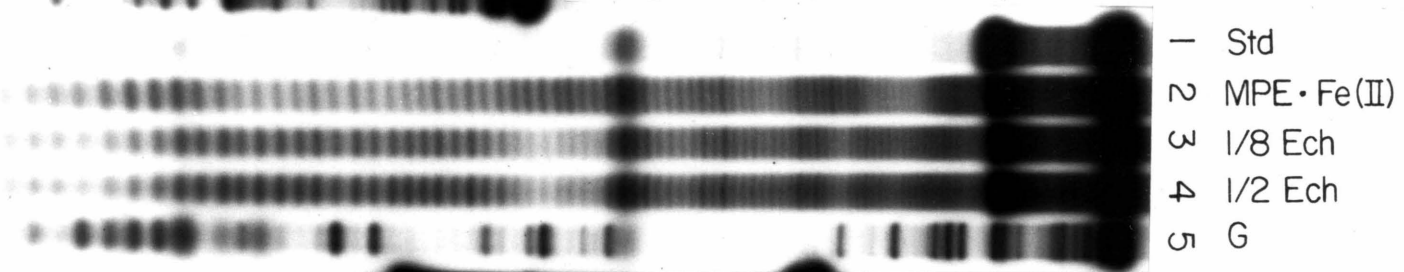
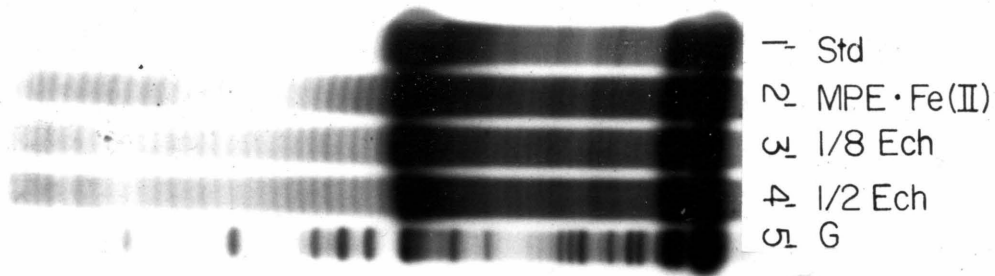
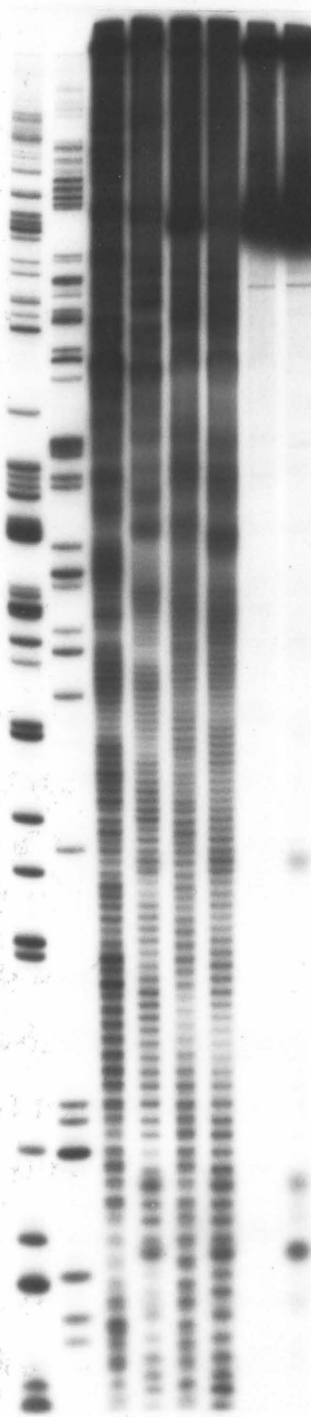


**Figure 42**

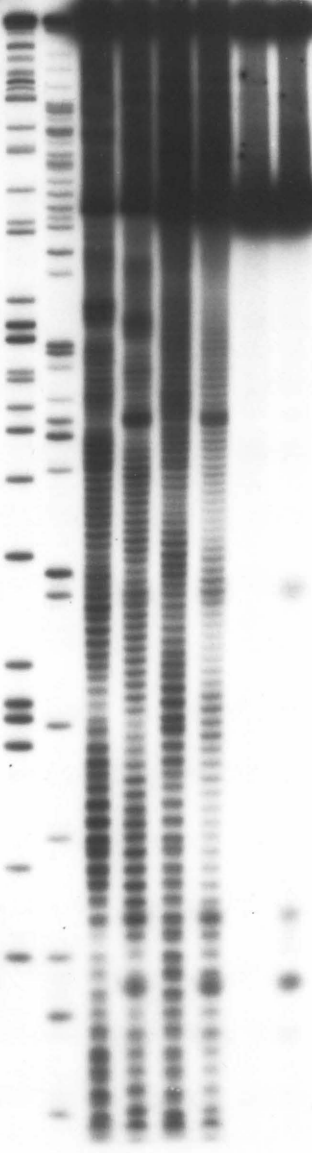
**Opposite strand analysis of echinomycin-binding sites.**

Autoradiogram of 3' and 5' end labeled 167 bp and 517 bp DNA restriction fragments: Odd numbered lanes were 5' end labeled; even-numbered lanes were 3'. Lanes 1-8 were the 517 bp DNA; lanes 9-16 were the 167 bp DNA. Lanes 1,2,9, and 10 were the Maxam-Gilbert G reactions. Lanes 7,8,15, and 16 were the intact buffered DNAs. Lanes 3-6 and 11-14 contained 10 mM Tris·Cl [pH 7.4], 50 mM NaCl, 400 μM base pairs DNA, 4 mM DTT, 10% THF, and 10 μM MPE·Fe(II). Lanes 3,4,11, and 12 also contained 200 μM **ech**. Lanes 5,6,14, and 15 were the MPE·Fe(II) cleavage controls. Note in these lanes the slight specificity inherent in MPE- directed DNA cleavage.

1 2 3 4 5 6 7 8  
] G  
] MPE · Fe(II) + E  
] MPE · Fe(II)  
] DNA STD



9 10 11 12 13 14 15 16  
] G  
] MPE · Fe(III) + E  
] MPE · Fe(II)  
] DNA STD



footprinting of actinomycin. Upon increasing echinomycin concentration some enlargement of the footprinting sites occurs, yet this is far less than the coalescence phenomenon observed with distamycin and netropsin. Densitometric analyses were performed on these footprinting lanes. The histograms and interpreted binding sites are shown in Figures 43-48

**MPE versus DNase Footprinting of Echinomycin:** These two methods of footprinting were compared on two DNA restriction fragments (274/278 bp and 378/382 bp) with echinomycin. At low echinomycin concentrations (1:32 bp), both methods indicated similar regions of cleavage inhibition (Figure 39, lanes 6,7,16,17 and Figure 40, lanes 5-8). Thus DNase exhibits little if any increased sensitivity over MPE, unlike the case with actinomycin. No increased DNase cleavages (hypersensitivity) were observed adjacent to the footprints. No changes in the sequence specificity of DNase cleavages was noted. Typically echinomycin exhibited larger footprints with DNase (up to 23 bp) than with MPE (9 bp max). Often a single region of DNase cleavage inhibition was resolvable into multiple MPE footprints. Thus MPE footprinting should be the method of choice for determining the preferred echinomycin binding sites.

**Echinomycin Binding Sites:** 360 base pairs of heterogeneous DNAs were investigated by MPE footprinting with echinomycin present at a range of 1:8 to 1:2 base pairs. 23 footprints were observed. All MPE footprints demonstrated 3' overprotection on the order of 1-3 bp. Typical protected regions were between 3-9 bp in length, with the average minimum binding site size being 4 bp. Using the 4 bp binding site size as a model, the histogram footprints were interpreted thusly.

### Figures 43-48

Footprinting histograms and interpreted preferred binding sites for echinomycin. MPE footprints are shown as histograms. DNase I footprints are shown as hatched and solid bars reflecting partial and complete cleavage inhibition, respectively. Individual figures are:

**43** (top) MPE and DNase I footprints on 54 base pairs of the 378/382 bp DNA fragment; echinomycin 1:8 bp. (bottom) Interpreted preferred binding sites. Autoradiogram is found in Figure 44.

**44** MPE and DNase I footprints on 70 base pair of the 274/278 bp DNA fragment; a) echinomycin 1:32 bp, b) echinomycin 1:8 bp. Autoradiogram is found in Figure 45.

**45** Interpreted binding sites from footprints in Figure 49. a) echinomycin 1:32 bp; b) echinomycin 1:8 bp.

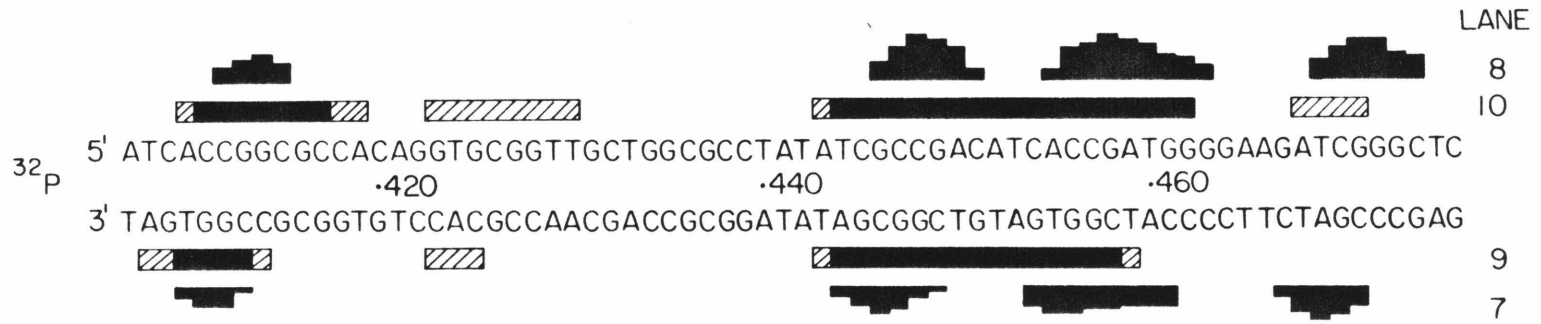
**46** (top) MPE footprints on 80 base pairs of the lac operon (117 & 168 bp fragments). Echinomycin 1:8 bp. (center) Echinomycin 1:2 bp. (bottom) Interpreted binding sites. Applicable to both echinomycin concentrations. Autoradiogram is found in Figure 46.

**47** (top) MPE footprints on 85 base pairs of the 517 bp DNA fragment; echinomycin 1:2 bp. (bottom) Interpreted binding sites. Autoradiogram is found in Figure 47.

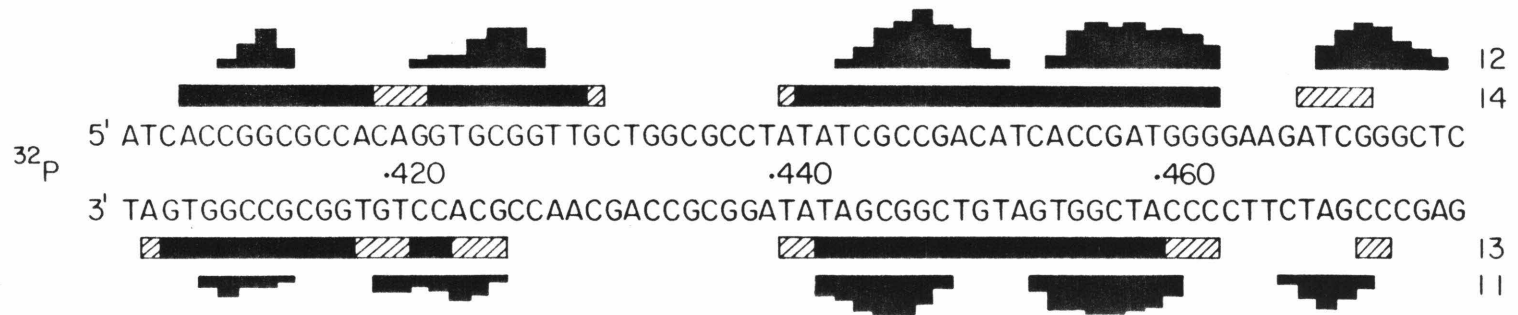
**48** (top) MPE footprints on 70 base pairs of the 167 bp DNA fragment; echinomycin 1:2 bp. (bottom) Interpreted binding sites. Autoradiogram is found in Figure 47.



a



b



a



b



ech 1:8 lac operon 80 bp

5' CATTAGGCACCCAGGCTTTACACTTTATGCTTCCGGCTC  
17 3' GTAATCCGTGGGGTCCGAAATGTGAAATACGAAGGCCGAG

GTATAATGTGTGGAATTGTGAGCGGATAACAATTTACACA 3' 168  
CATATTACACACCTTAACACTCGCCTATTGTTAAAGTGTGT 5'

ech 1:2 lac operon 80 bp

5' CATTAGGCACCCAGGCTTTACACTTTATGCTTCCGGCTC  
117 3' GTAATCCGTGGGGTCCGAAATGTGAAATACGAAGGCCGAG

GTATAATGTGTGGAATTGTGAGCGGATAACAATTTACACA 3' 168  
CATATTACACACCTTAACACTCGCCTATTGTTAAAGTGTGT 5'

5' CATTAGGCACCCAGGCTTTACACTTTATGCTTCCGGCTC  
117 3' GTAATCCGTGGGGTCCGAAATGTGAAATACGAAGGCCGAG

GTATAATGTGTGGAATTGTGAGCGGATAACAATTTACACA 3' 168  
CATATTACACACCTTAACACTCGCCTATTGTTAAAGTGTGT 5'

517 bp Rsa I → Eco RI 1:2 ech 85 bp



517

Eco RI... 5' GGCC TCGT GAT ACGC CTATTTTTAT AGGTTAATGTCATGATAATA  
 •4340 •4320  
 3' CCGGAGCACTATGCGGATAAAAATATCCAATTACAGTACTATTAT

ATGGTTTCTTAGACGTCAGGTGGCACTTTTCGGGGAAATG 3'  
 •4300 •4280  
 TACCAAAGAATCTGCAGTCCACCGTGAAAAGCCCCTTTAC 5' ... Rsa I

167 bp Eco RI → Rsa I 1:2 ech 70 bp



-80-

167



Echinomycin afforded protection to 117 base pairs on these DNAs, 83 base pairs (71%) were G+C in nature.

#### **Small Molecules Which Apparently Do Not Footprint**

There are many small molecules which do not demonstrate footprinting patterns by our protocol at this time. Typically they indicate some manner of DNA interaction by the diminution of MPE cleavage equally throughout the entire pattern upon increasing small molecule concentration. These small molecules, their binding characteristics and structures have been previously listed in the introduction of this thesis. Two typical series, the quinoxaline and anthracycline antibiotics, also contain members which have demonstrated sequence-specific MPE footprinting patterns. Short descriptions of their investigations follow.

**Anthracyclines:** Those anthracycline antibiotics studied during the course of this work include adriamycin, daunomycin, nogalamycin, and 7-con-O-methylnogarol (*ngr*). Daunomycin was shown not to footprint in the initial studies of MPE cleavage inhibition used to determine small molecule preferred binding sites (Figure 15). Further investigations included a complementary-strand MPE footprinting analysis, the autoradiogram of which is shown in Figure 49.

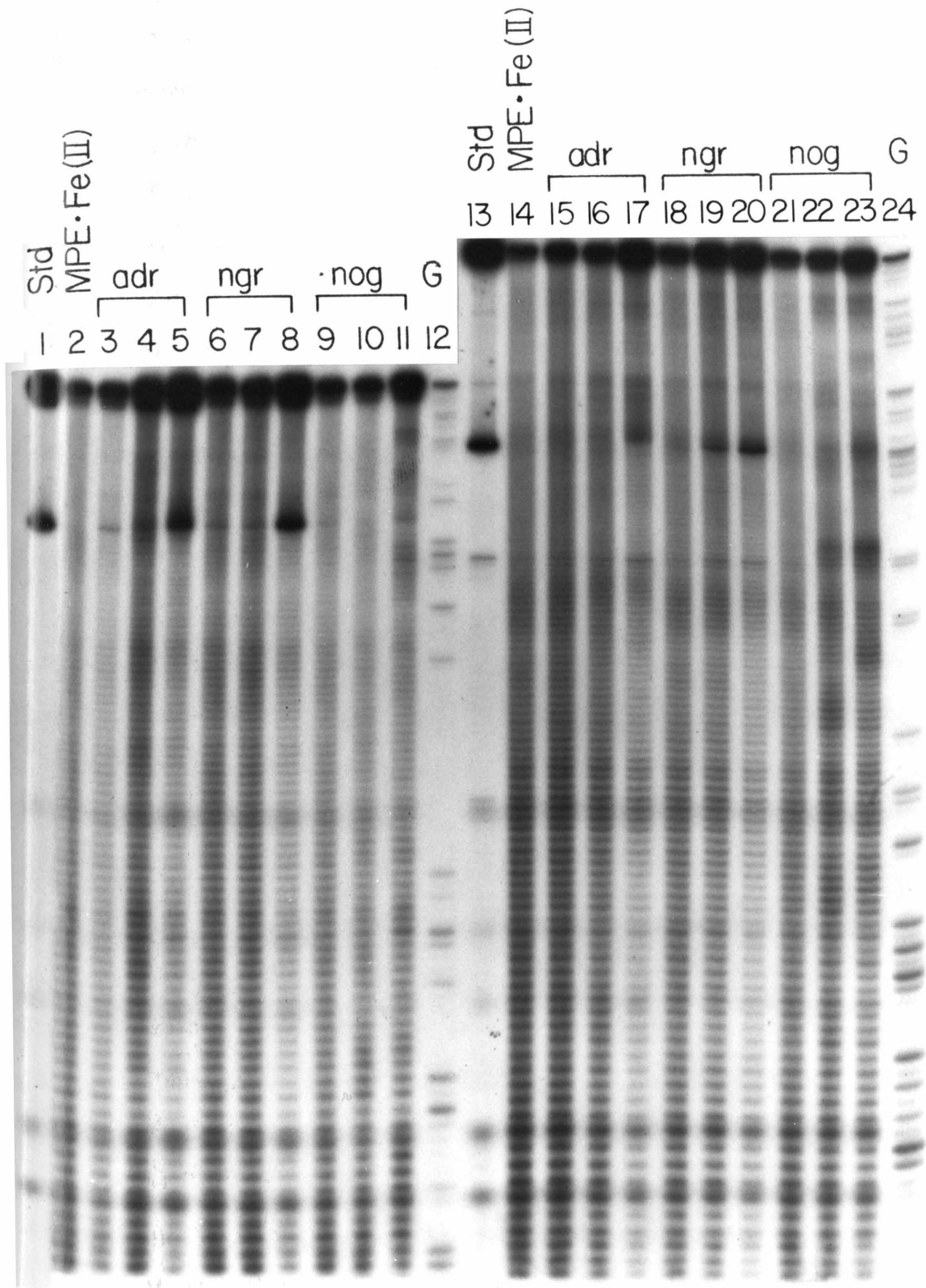
Two DNA restriction fragments, each containing the lactose operon promoter-operator region, were 3' end labeled on complementary strands. MPE·Fe(II) partial digests were performed with various concentrations of anthracyclines; the exact values listed in the figure legend. Cleavage was terminated by freezing and lyophilization. Electrophoresis was performed under denaturing conditions resolving

**Figure 49**

**Complementary-strand footprinting of the anthracyclines:**

**Adriamycin, 7-con-O-methylnogarol, and Nogalamycin.**

Autoradiogram of 3' end labeled 117 bp and 168 bp DNA fragments: Lanes 1-12 contained 117 bp, and lanes 13-24 contained 168 bp DNA. Lanes 12 and 24 were the Maxam-Gilbert G reactions. Lanes 1 and 13 were the intact buffered DNAs. Lanes 2-11 and 14-23 contained 10 mM Tris·Cl [pH 7.4], 50 mM NaCl, 100  $\mu$ M base pairs DNA, 4 mM DTT, and 10  $\mu$ M MPE·Fe(II). Lanes 3-5 and 15-17 contained 6.3, 2.5, and 100  $\mu$ M **adr**, respectively. Lanes 6-8 and 18-20 contained 6.3, 2.5, and 100  $\mu$ M **ngr**, respectively. Lanes 2 and 14 were the MPE·Fe(II) cleavage controls.



fragments from 22 to approximately 90 nucleotides in length.

The MPE cleavage controls (lanes 2 and 14) exhibited relatively even cleavage patterns, indicative of a lack of MPE specificity on these DNA fragments. For adriamycin, nogalamycin, and ngr at 6.3  $\mu\text{M}$  concentrations (1 anthracycline: 16 bp), no change in the otherwise uniform cleavage pattern resulted. Increasing concentrations of adriamycin and ngr to 100  $\mu\text{M}$  show no footprints but do demonstrate an increased amount of nondenatured, intact DNA (nondenatured DNA corresponds to lower dark band as seen in DNA standards, also lanes 5,8,17 and 20), together with a general lightening throughout the uniform cleavage pattern. These two phenomena are thought to represent non-sequence-specific MPE cleavage inhibition, the result of non-sequence specific small molecules competitively binding to the DNA. Thus as determined by MPE footprinting, the anthracyclines adriamycin, daunomycin, and 7-con-O-methylnogarol bind heterogeneous double stranded DNA without any sequence preference.

The anthracycline antibiotic, nogalamycin, performs differently at higher concentrations (1:4 bp - 1:1 bp) when footprinted by MPE (lanes 10,11,12, and 23). Alternating regions of lighter and darker bands are observed, the lightened regions being footprints. While rigorous sequence analysis of these footprints are part of the continuing studies under K. Harshman (Caltech) it should be evident that nogalamycin demonstrates some sequence specificity in binding to DNA as determined by MPE footprinting.

**Quinoxalines:** Those quinoxaline antibiotics investigated by MPE and DNase footprinting methods included the natural products echinomycin

and triostin A together with the synthetic triostin analogs tandem, AY-285, and AY-206. Echinomycin was generously provided by the National Institutes of Health, triostin A and analogs were the gifts of R. K. Olsen (Utah State). Three separate samples of Tandem were provided due to concerns over possible degradation. All were used as solutions in tetrahydrofuran (THF); concentrations determined spectrophotometrically ( $\epsilon_{325\text{nm}} = 12,000$ ).<sup>114,115,130</sup>

A 278 bp 3' end-labeled DNA restriction fragment consisting of a part of the tetracycline resistance gene was used as the substrate for quinoxaline binding. MPE·Fe(II) or DNase I partial digests were performed with various concentrations of antibiotics; the exact values are listed in the figure legend (Figure 50). Reactions and work-ups followed the usual procedures described in the Experimental. DNA fragments 25 to 100 bp long are resolved in the autoradiogram shown.

For this experiment the controls appear satisfactory: DNA standard is without visible levels of spurious nicks; MPE and DNase cleavage controls have adequate levels of denatured, intact DNA indicative of "one-hit kinetics" (lane 1; lanes 2 and 3, respectively). MPE cleavage pattern is relatively uniform, indicative of a lack of MPE specificity for the DNA fragment. All three tandem samples show no change in either the MPE or DNase standard cleavage pattern (lanes 4-9). It is therefore concluded that these tandem samples exhibit no sequence specific DNA binding, as determined by either footprinting assay. Triostin, while demonstrating no change in the MPE cleavage pattern (lane 10), did cause a slight diminution in the band intensities around the middle of the DNase pattern. This region, 69-89 bp from the labeled

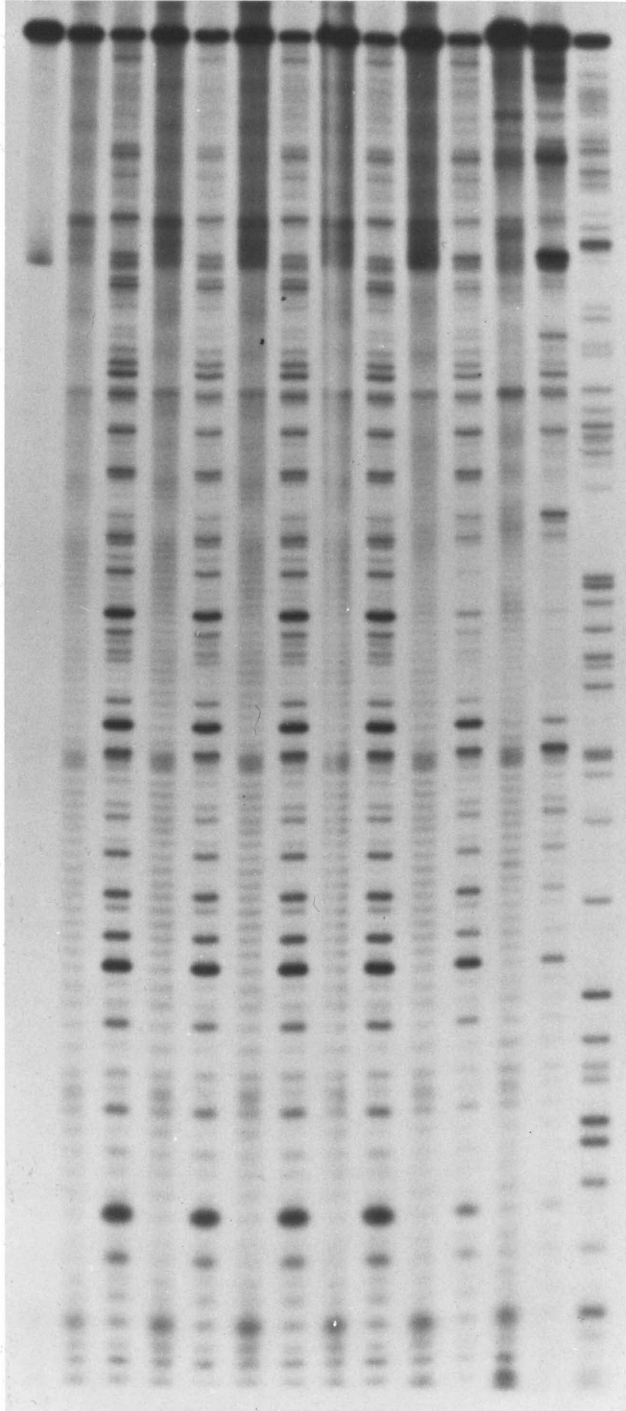
**Figure 50**

**Quinoxalines and their footprinting patterns by both MPE and DNase footprinting protocols.**

Autoradiograms of 3' end labeled 278 bp DNA fragment: Lane 1 was the intact buffered DNA. Lane 14 was the Maxam-Gilbert G reaction. Even numbered lanes (2,4,6,8,10,12) were MPE footprinting reactions containing 10 mM Tris·Cl [pH 7.4], 50 mM NaCl, 400  $\mu$ M base pairs DNA, 4 mM DTT, 10% THF, and 10  $\mu$ M MPE·Fe(II). Odd numbered lanes (3,5,7,9,11,13) were DNase footprinting reactions containing 10 mM Tris·Cl [pH 7.9], 10 mM KCl, 10 mM MgCl<sub>2</sub>, 5 mM CaCl<sub>2</sub>, 400  $\mu$ M base pairs DNA, 0.1 mM DTT, 10% THF, and 0.4  $\mu$ g/ml DNase I. Lanes 4 and 5 contained 100  $\mu$ M **tan** (sample #1). Lanes 6 and 7 contained 100  $\mu$ M **tan** (sample #2). Lanes 8 and 9 contained 100  $\mu$ M **tan** (sample #3). Lanes 10 and 11 contained 108  $\mu$ M **tri**. Lanes 12 and 13 contained 235  $\mu$ M **ech**. Lanes 2 and 3 were the MPE and DNase cleavage controls, respectively.

Std  
MPE·Fe (II)  
DNase I  
Tan<sub>1</sub>  
Tan<sub>2</sub>  
Tan<sub>3</sub>  
Tri  
Ech  
G

m d m d m d m d m d m d m  
1 2 3 4 5 6 7 8 9 10 11 12 13 14



end, is a G·C rich region (67%) which also demonstrates cleavage inhibition when echinomycin is present. Triostin A may therefore also be a sequence specific DNA binder, though not to the same degree as echinomycin. Echinomycin demonstrates footprints by both MPE and DNase techniques (lanes 12 and 13) as has previously been described.

These findings concur with the literature expectations for sequence specific DNA binding by quinoxalines except for the case of tandem. Tandem has demonstrated high AT specificity in equilibrium binding studies to various natural DNAs and homopolymers. Anticipated reduction of the disulfide crosslink and subsequent loss of rigid cyclic octadepsipeptide conformation necessary for DNA binding is a possibility in both MPE and DNase cases (4 mM and 0.1 mM DTT, respectively), though the slight footprinting observed for the similar triostin A molecule (lane 11) seems to contradict this. Most likely is the possibility that the tandem samples provided were degraded, as evident by their UV-vis absorption spectra when compared with those of triostin, AY-206, and AY-285 (see Figure 51).

#### **Attempted MPE·Fe(II) Footprinting of Z DNA**

Certain B form DNAs containing alternating purine-pyrimidine sequences undergo a reversible conformational transition to the left handed Z form upon increasing salt concentration.<sup>174</sup> Recent x-ray analysis of oligonucleotide crystals containing alternating d(pCpG) sequences have verified the left-handed helical structure of Z DNA.<sup>175</sup> In solution, a plasmid containing a d(pCpG)<sub>16</sub>·d(pCpG)<sub>16</sub> insert in B form

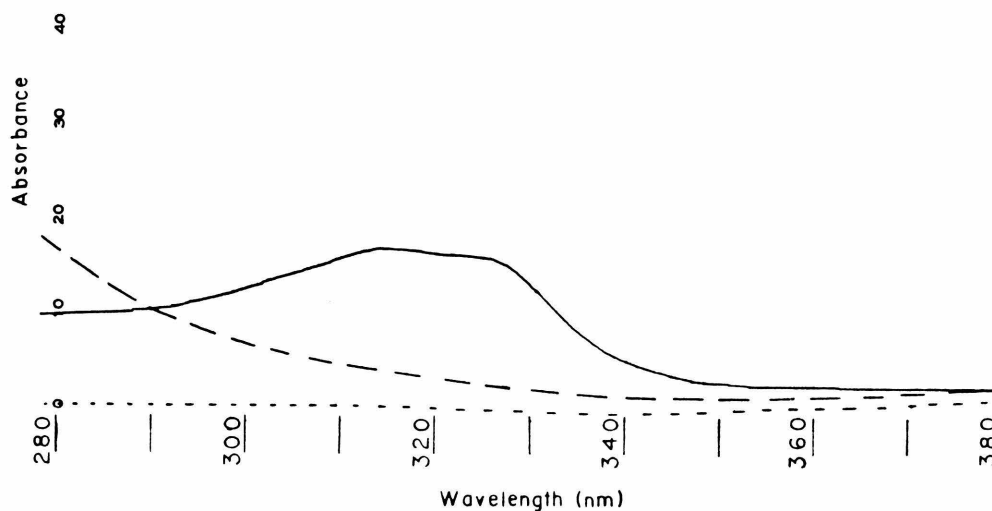


**Figure 51**

Partial UV-vis spectra of triostin A and tandem (**tan**) in isopropanol. The solid line (a) corresponds to triostin; the dashed line (b), **tan**; the dotted line (c), isopropanol standard. Notice absence of quinoxaline absorbances (313 and 327 nm) in **tan**, spectra.

was shown to go to Z under conditions of high salt, Co(III), or negative supercoiling of the plasmid.<sup>176</sup> This conformational change can be observed by an inversion of the circular dichroism (CD) spectrum,<sup>174</sup> a large reduction in electrophoretic mobility for plasmids containing Z DNA inserts,<sup>176</sup> and by S1 nuclease cleavage of B-Z DNA junctions.<sup>177</sup> Thus it was found that B DNA can exist in close proximity with Z DNA.<sup>178</sup> Given our MPE footprinting methods as a probe, we were interested in changes in either the intrinsic MPE cleavage pattern or the sequence specific binding of small molecules on Z or nearby B DNA.

For these investigations a 259 bp Nar I → Eco RV restriction fragment containing a 32 bp d(pCpG)<sub>16</sub>·d(pCpG)<sub>16</sub> insert at the Bam HI

site was isolated from the plasmid pLP 32, a gift of L. Peck (Harvard). For comparison the equivalent 227 bp Nar → Eco RV fragment, sans CG insert, was isolated from pBR-322. Both were 3' end labeled at their Nar I restriction site before Eco RV digestion. MPE partial cleavages, both with and without inhibiting small molecules present, were performed in the usual fashion on both singularly 3' end labeled DNA fragments under conditions favoring either B or Z conformations. Exact reaction conditions and the resulting autoradiograms are shown in Figures 52 and 53.

MPE•Fe(II) cleaves the 227b bp DNA fragment uniformly, demonstrating no intrinsic sequence specificity (Figure 52, lane 2), whereas there is a distinct darkening of bands in the CG insert region of the 259 bp fragment (Figure 52, lane 12 and Figure 53, lane 2). Bands in this CG region demonstrate anomalous electrophoretic mobilities, indicative of hairpinning under these electrophoresis conditions. The presence of 0.1 mM  $\text{Co}(\text{NH}_3)_6^{3+}$  or 2.65 M  $\text{Na}^+$  does not affect the MPE cleavage patterns for either fragment (227 bp, Co(III): Figure 52, lane 3; 259 bp, Co(III): Figure 52, lane 13; 259 bp,  $\text{Na}^+$ : Figure 53, lane 3). MPE cleavage also does not appear diminished in either case.

For the MPE footprinting of small molecules, the presence of the CG insert does not appreciably affect their adjacent sequence specific binding sites. (Figure 52) Actinomycin > chromomycin >> distamycin prefer to bind to this  $(\text{CG})_{16}$  region as determined by inhibition (or promotion) of MPE cleavage. The addition of 0.1 mM  $\text{Co}(\text{NH}_3)_6^{3+}$ , supposedly inducing Z conformation in the CG insert, does not alter the

**Figure 52**

**The effect of an alternating (CG)<sub>16</sub> insert on the sequence specific binding of small molecules.**

Autoradiograms of 3' end labeled DNA fragments: Lanes 1-10 contained the 227 bp Nar I → Eco RV fragment from pBR-322. Lanes 11-20 contained the similar 259 bp Nar I → Eco RV fragment from pLP32 with a 32 base pair 5' {CG}<sub>16</sub> 3' insert at the Bam HI site. Lanes 10 and 20 were the Maxam-Gilbert G reactions. Lanes 1 and 11 were the intact buffered DNAs. Lanes 2-9 and 12-19 contained 10 mM Tris·Cl [pH 7.4], 50 mM NaCl, 200 μM base pair DNA, 4 mM DTT, and 10 μM MPE·Fe(II). Plus (+) lanes contained 100 μM Co(NH<sub>3</sub>)<sub>6</sub><sup>3+</sup> and should have had their CG inserts in a Z conformation. Lanes 4,5,14, and 15 contained 130 μM **act**. Lanes 6,7,16, and 17 contained 210 μM **chr**. and 420 μM Mg<sup>2+</sup>. Lanes 8,9,18, and 19 contained 53 μM **dis**. Lanes 2,3,12, and 13 were the MPE·Fe(II) cleavage controls.

Std	MPE·Fe (II)		Act		Chr		Dis		G	Std	MPE·Fe (II)		Act		Chr		Dis		G
	-	+	-	+	-	+	-	+			-	+	-	+	-	+	-	+	
1	2	3	4	5	6	7	8	9	10	11	12	13	14	15	16	17	18	19	20

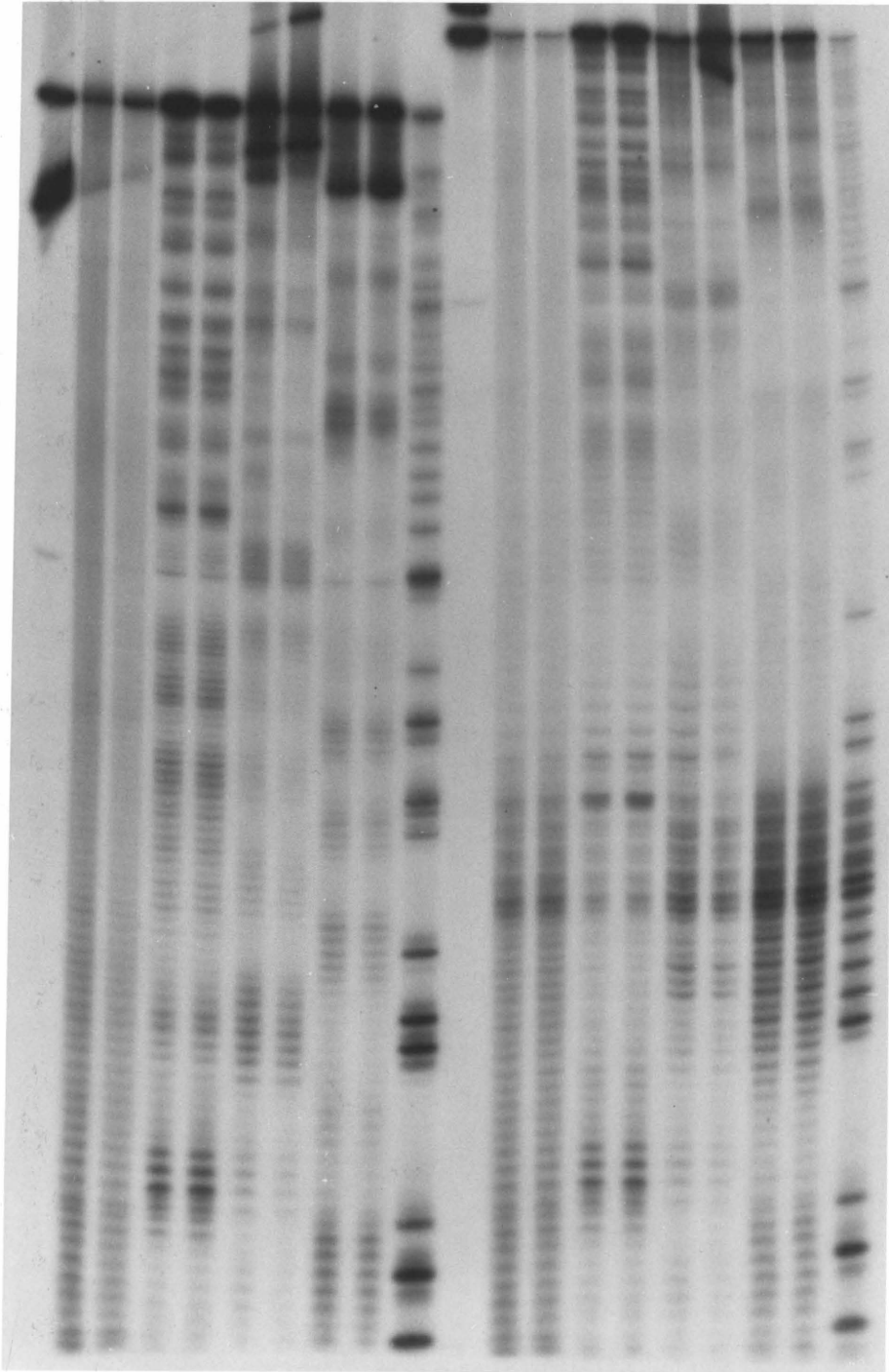
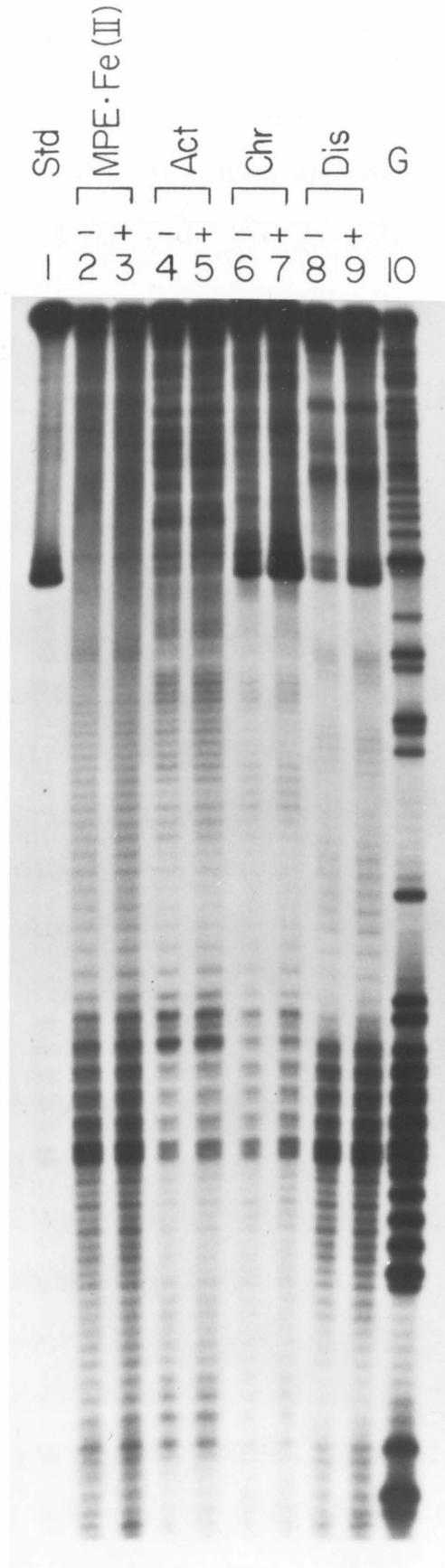


**Figure 53**

**The effect of alternating (CG)<sub>16</sub> insert on the sequence  
specific binding of small molecules.**

Autoradiogram of 3' end labeled 259 bp DNA fragments: Lane 1 contained the intact DNA. Lane 10 was the Maxam-Gilbert G lane. Lanes 2-9 contained 10 mM Tris·Cl [pH 7.4], 50 mM NaCl, 200 μM base pairs DNA, 4 mM DTT and 10 μM MPE·Fe(II). Plus (+) lanes had an additional 2.6 μM NaCl, for a total of 2.65 M NaCl final concentration. Lanes 4 and 5 contained 50 μM **act.** Lanes 6 and 7 contained 50 μM **chr.** and 100 μM Mg<sup>2+</sup>. Lanes 8 and 9 contained 50 μM **dis.** Lanes 2 and 3 were the MPE·Fe(II) cleavage controls. High salt reactions were ethanol precipitated prior to electrophoresis.



footprinting patterns of either actinomycin, chromomycin, or distamycin (Figure 52, compare even versus odd-numbered lanes 4-9 and 14-19) on both DNA fragments. Similarly, high salt does not affect the footprinting patterns under conditions capable of inducing Z form DNA (Figure 53, lanes 4-9).

It has previously been shown that small molecules like ethidium, actinomycin, distamycin, and mithramycin interact preferentially with B form DNA over a modified Z\* form (10 mM Mg<sup>+</sup> and 10% EtOH) DNA.<sup>179</sup> This binding preference ranges from  $k_{Z^* \text{ DNA}}/k_{B \text{ DNA}} = 0.2$  for ethidium to 0.6 mithramycin, with no observable binding for distamycin to poly[d(G-C)] under either B or Z conditions. Ethidium and mithramycin appeared to convert a substantial amount of the Z\* DNA to B form. This has been independently confirmed in the observation that low binding levels of ethidium (1:20 bp), BMSp (~1:45 bp), or actinomycin (1:450 bp) inhibited the B → Z transition.<sup>186</sup> Thus it may not be possible to have Z form DNA, let alone being able to MPE cleave in its presence, under the conditions of MPE footprinting. Optimized EDTA·Fe(II)-induced DNA cleavages may be one of the only means of probing Z-form DNA. Ideally one anticipated observation which might occur is the reversal of the MPE cleavage asymmetry to 5' overhanging regions on left-handed Z-form DNAs. Small molecule footprinting should still remain unlikely.

#### **Investigation of Small Molecule Induced Allosteric Transitions in DNA Structure by Footprinting**

A molecule bound to DNA at one site may influence the subsequent binding of other molecules to nearby sites. This co-operative effect may proceed through two means: either a direct physical interaction as

In the inhibition of RNA polymerase binding to the lac operon in the presence of bound repressor,<sup>181</sup> or by means of a structural alteration of the DNA between the bound molecule and the virtual site. Examples of the latter case include the neighbor exclusion effect of intercalative binding<sup>182</sup> and the transmission of a long range allosteric effect in the Z → B conformational transition upon ethidium binding to Z form poly d(GC).<sup>183</sup> The co-operative binding of many small molecules to natural DNAs, including actinomycin, distamycin, and daunomycin, ethidium and others have been investigated by spectroscopic means.<sup>184-187</sup> This effect tends to occur at low binding densities, typically from 1:50 bp (dis) to 1:17 bp (act) and appear independent of base pair composition. With regulatory proteins, the cAMP-binding gene-activating protein (crp) is also believed to exert a long range conformation change in the lac operon, thus affecting polymerase binding.<sup>188-190</sup> We chose to investigate the effect of both regulatory proteins alteration of nearby small molecule binding sites as determined by MPE or DNase footprinting, and the influence of site-specifically bound small molecules on the sequence specific cleavage by distamycin-EDTA·Fe(II), [DE·Fe(II)].

For these investigations the complementary 3' end labeled 117 and 168 bp DNA fragments from plasmid pLJ3, each containing a copy of the E. coli lactose promoter-operator, were prepared. From Maxam-Gilbert sequencing analysis, their published nucleotide sequences were verified. Unfortunately it was discovered that neither contained an intact crp binding site, thus precluding any work involving that regulatory protein. Protocols used followed standard experimental procedures; the exact concentration values being listed in the figure legends.

In the first experiment small molecules like **act**, **chr**, and **dis** were preequilibrated with the DNA prior to cleavage by MPE or DE. The resulting autoradiogram of the electrophoretically separated cleavage fragments is shown in Figure 54. Under conditions which demonstrate MPE footprinting patterns for each of the small molecules (**act**: lanes 4 and 14, **chr**: lanes 6 and 16, **dis**: lanes 8 and 18), DE cleavage was also performed. Actinomycin appeared to diminish the weakly cleaved DE sites, without affecting the pair of sites exhibiting strong DE cleavage (lanes 5 and 15). Chromomycin/Mg<sup>2+</sup> appeared to have very little effect on the intensities of DE cleavage throughout its pattern (lanes 7 and 17). Distamycin abolished all DE cleavage on these fragments. None of these small molecules seemed to affect the locations, sizes, and relative orientation preferences of DE cleavage, only changing the intensities of cleavage at certain sites. Usually these sites corresponded directly with the observed footprinting sites of the inhibitory small molecules, though in the case of actinomycin inhibiting cleavages at the weak DE sites this effect seems to occur at distances up to 7 bp from a presumed **act** binding site. This may be an example of small-molecule-induced allosteric transitions in the DNA structure, though more studies are needed on other DNA substrates to verify this.

Similar experiments were performed with preequilibrated **lac** repressor bound to its site on the **lac** operon, and its influence on the subsequent binding of small molecules as probed by MPE and DNase. Again the 117 bp 3' end labeled DNA fragment was used as substrate, and **act**, **chr**, and **dis** served as inhibiting small molecules. MPE and DNase I partial digestions were performed in the usual manner. The resulting

**Figure 54**

**Comparison of MPE and Distamycin-EDTA (DE)-mediated  
footprinting patterns for the antibiotics actinomycin,  
chromomycin, and distamycin.**

Autoradiogram of 3' end labeled 117 bp and 168 bp DNA fragments:  
Lanes 1-10 were 117 bp, and lanes 11-20 were 168 bp DNA. Lanes 1 and 11  
were the intact buffered DNAs. Lanes 10 and 20 were the Maxam-Gilbert G  
reactions. Lanes 2-9 and 12-19 contained 10 mM Tris·HCl [pH 7.4], 50 mM  
NaCl, 400  $\mu$ M base pairs DNA, and 4 mM DTT. Lanes with a small m  
contained 10  $\mu$ M MPE·Fe(II); lanes with a capital D contained 40  $\mu$ M  
DE·Fe(II). Lanes 4,5,14, and 15 contained 50  $\mu$ M act. Lanes 6,7,16, and  
17 contained 50  $\mu$ M chr. and 100  $\mu$ M Mg<sup>2+</sup>. Lanes 8,9,18, and 19 contained  
50  $\mu$ M dis. Lanes 2 and 12 were the MPE·Fe(II) cleavage controls. Lanes  
3 and 13 were the DE·Fe(II) cleavage controls.

Std MPE·Fe(II) DE·Fe(II) Act Chr Dis G  
m D m D m D m D m D  
1 2 3 4 5 6 7 8 9 10

Std MPE·Fe(II) DE·Fe(II) Act Chr Dis G  
m D m D m D m D m D  
11 12 13 14 15 16 17 18 19 20

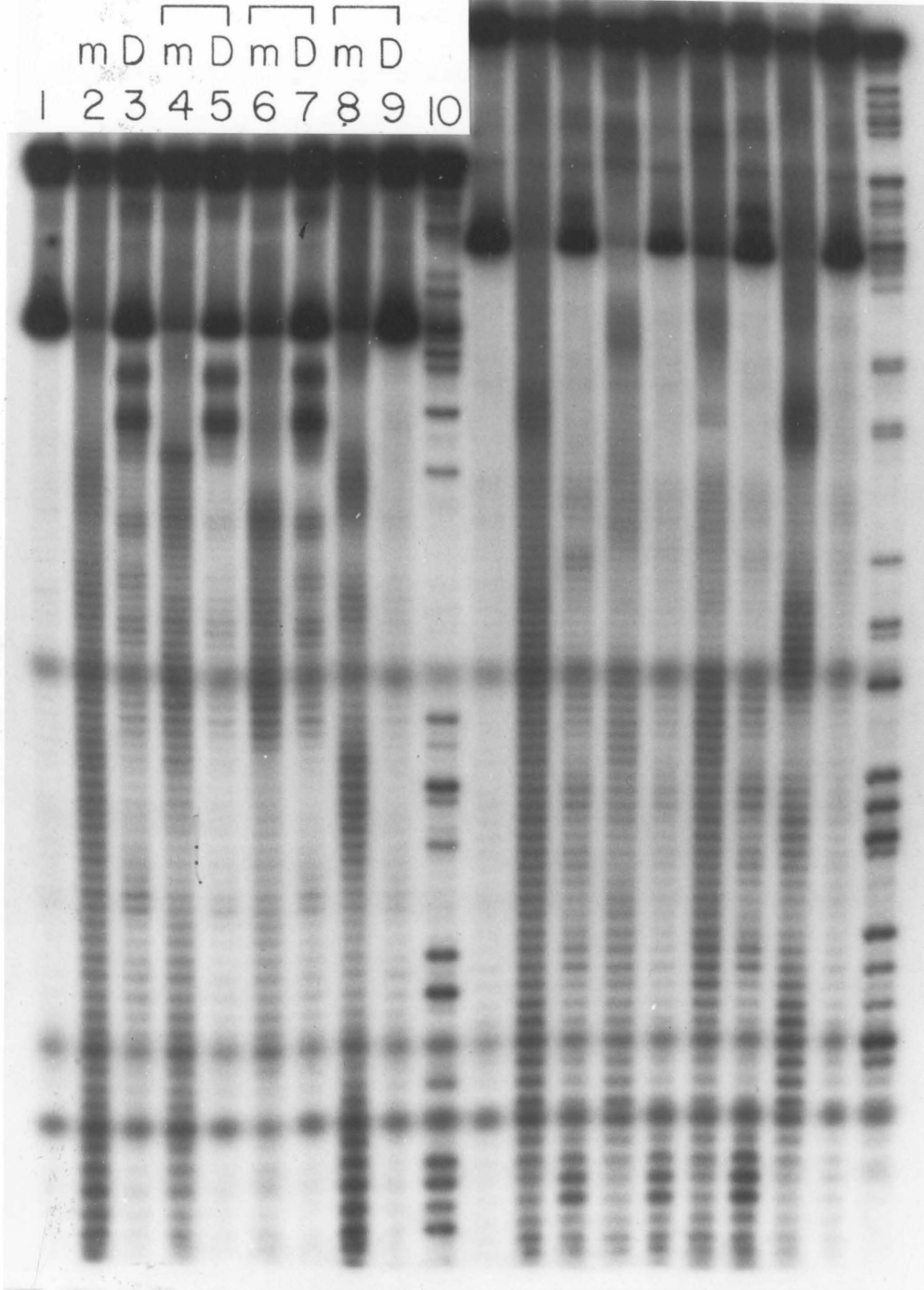
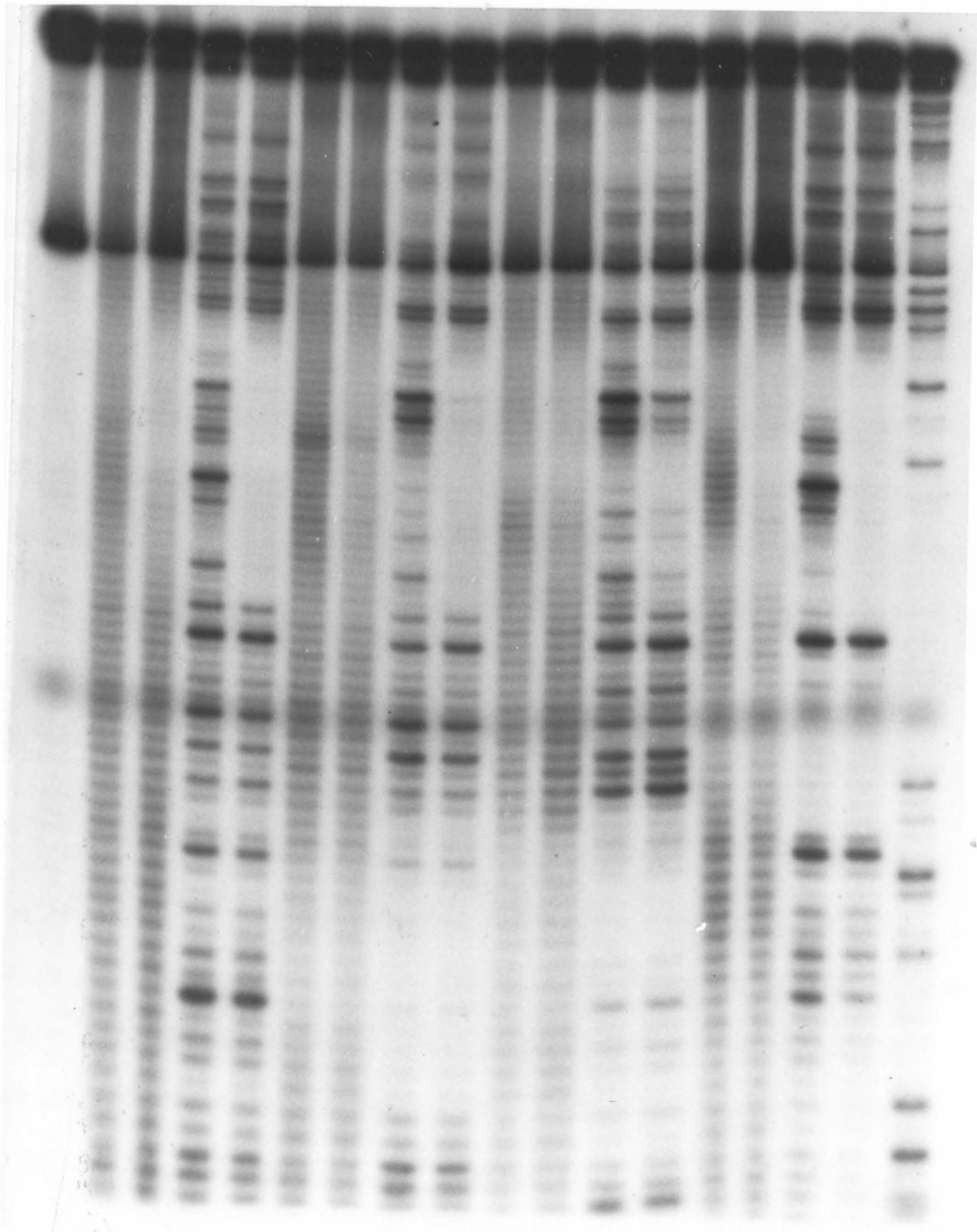


**Figure 55**

**Allosterics of *lac* repressor binding on the subsequent  
binding of antibodies as determined by MPE- and  
DNase-footprinting protocols.**

Autoradiogram of 3' end labeled 117 bp DNA fragments: Lane 1 was the intact buffered DNA. Lane 18 was the Maxam-Gilbert G reaction. Lanes with a small **m** contained 10 mM Tris·Cl [pH 7.4], 50 mM NaCl, 400  $\mu$ M base pairs DNA, 4 mM DTT, and 10  $\mu$ M MPE·Fe(II). Lanes with a small **d** contained 10 mM Tris·Cl [pH 7.9], 10 mM KCl, 10 mM MgCl<sub>2</sub>, 5 mM CaCl<sub>2</sub>, 400  $\mu$ M base pairs DNA, 0.1 mM DTT, and 0.2  $\mu$ g/ml DNase I. Lanes with a plus (+) sign also contained 58  $\mu$ g/ml *lac* repressor, this being added after prior equilibration with an inhibitory small molecule (**act**, **chr**, or **dis**) if present. Lanes 6,7,8, and 9 contained 50  $\mu$ M **act**. Lanes 10,11,12, and 13 contained 50  $\mu$ M **chr** and 100  $\mu$ M Mg<sup>2+</sup>. Lanes 14,15,16, and 17 contained 50  $\mu$ M **dis**. Lanes 2 and 3 were the MPE·Fe(II) cleavage controls. Lanes 4 and 5 were the DNase cleavage controls.

Std	MPE·Fe(II)		DNase I		Act				Chr				Dis				G
	m	m	d	d	m	m	d	d	m	m	d	d	m	m	d	d	
	-	+	-	+	-	+	-	+	-	+	-	+	-	+	-	+	
1	2	3	4	5	6	7	8	9	10	11	12	13	14	15	16	17	18



autoradiogram is shown in Figure 55. lac repressor itself was weakly footprinted by MPE (lane 3) and clearly footprinted by DNase (lane 5). Typically the MPE and DNase I footprinting patterns for any of the small molecules alone corresponded fairly well in terms of the number of binding sites and their locations. The addition of lac repressor was only marginally observed by MPE footprinting (lane 7), though was quite visible by DNase footprinting (lane 9) in the case of a prior act, equilibrated template. Chr binding appears to largely attenuate subsequent lac repressor binding as ascertained by both footprinting methods (lanes 7 and 9), while dis does not seem to effect lac repressor binding (lanes 15 and 17). DNase I also showed no conformational changes in the form of cleavage enhancements due to the presence of bound small molecules. In all cases the small molecule footprints outside the lac repressor binding site observed by either footprinting method are unchanged upon addition of lac repressor, indicated of no protein induced allosteric transitions in this experiment. This could be anticipated, lac repressor is not believed to induce any nearby DNA conformational changes upon binding to its operator.<sup>191</sup> Further work employing the crp protein should prove more promising.

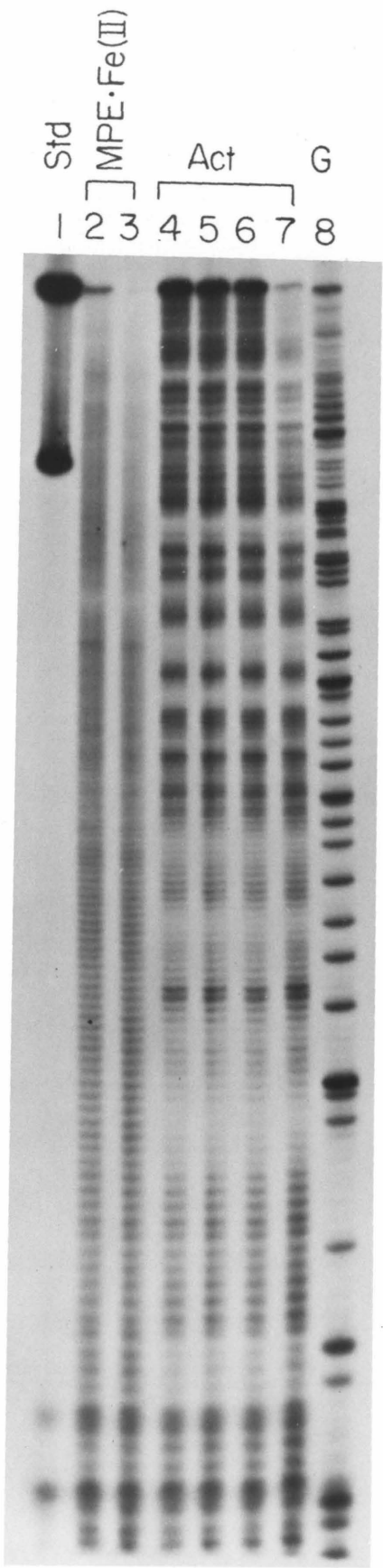
#### **Equilibrium Conditions on MPE•Fe(II) Footprinting**

Footprinting with MPE•Fe(II) is assumed to proceed under equilibrium conditions. Those small molecules which bind stronger to a particular site will remain there for a large fraction of DNA fragments during the time which cleavage takes place. Under kinetic control those sites which exhibit slower rates of small molecule dissociation would appear protected if  $t_{1/2\text{dissoc}} >$  the time in which MPE•Fe(II) is

**Figure 56**

**Equilibration conditions on MPE cleavage and actinomycin  
footprinting.**

Autoradiogram of 3' end labeled 382 bp DNA fragment:  
Lane 1 was the buffered intact DNA. Lane 8 was the  
Maxam-Gilbert G lane. Lanes 2-7 contained 10 mM Tris·Cl [pH  
7.4], 50 mM NaCl, 200  $\mu$ M base pairs DNA, 4 mM DTT, and 10  $\mu$ M  
MPE·Fe(II). Lanes 4-7 also contained 50  $\mu$ M **act**. Lane 2,  
sample was equilibrated at room temperature 30 min prior to  
MPE·Fe(II)/DTT addition and cleavage initiation. Lane 3,  
sample was equilibrated for 15 min at room temperature, then  
15 min at 37°C prior to MPE·Fe(II)/DTT addition. Lane 4 was  
equilibrated with **act** for < 5 min at room temperature prior  
to cleavage initiation. Lane 5 was equilibrated with **act**  
for 30 min at room temperature prior to cleavage initiation.  
Lane 6 was equilibrated with **act** for 15 min at room  
temperature, then 15 min at 37°C prior to cleavage  
initiation. Lane 7, sample containing **act** was equilibrated  
at room temperature for 15 min, then equilibrated with  
MPE·Fe(II) for 15 min at 37°C. Cleavage was initiated by  
the subsequent addition of DTT. For all reactions, cleavage  
proceeded at 37°C for 15 min.



present. To ascertain the circumstance in a typical footprinting reaction, a series of footprinting reactions were performed with actinomycin D ( $\tau = 25$  min) under different conditions of equilibration. The autoradiogram is shown in Figure 56. No change in footprinting pattern is observed. Thus there appears to be an independence or equilibration condition for MPE·Fe(II) footprinting, given the typical reaction conditions (15 min at 37°C).

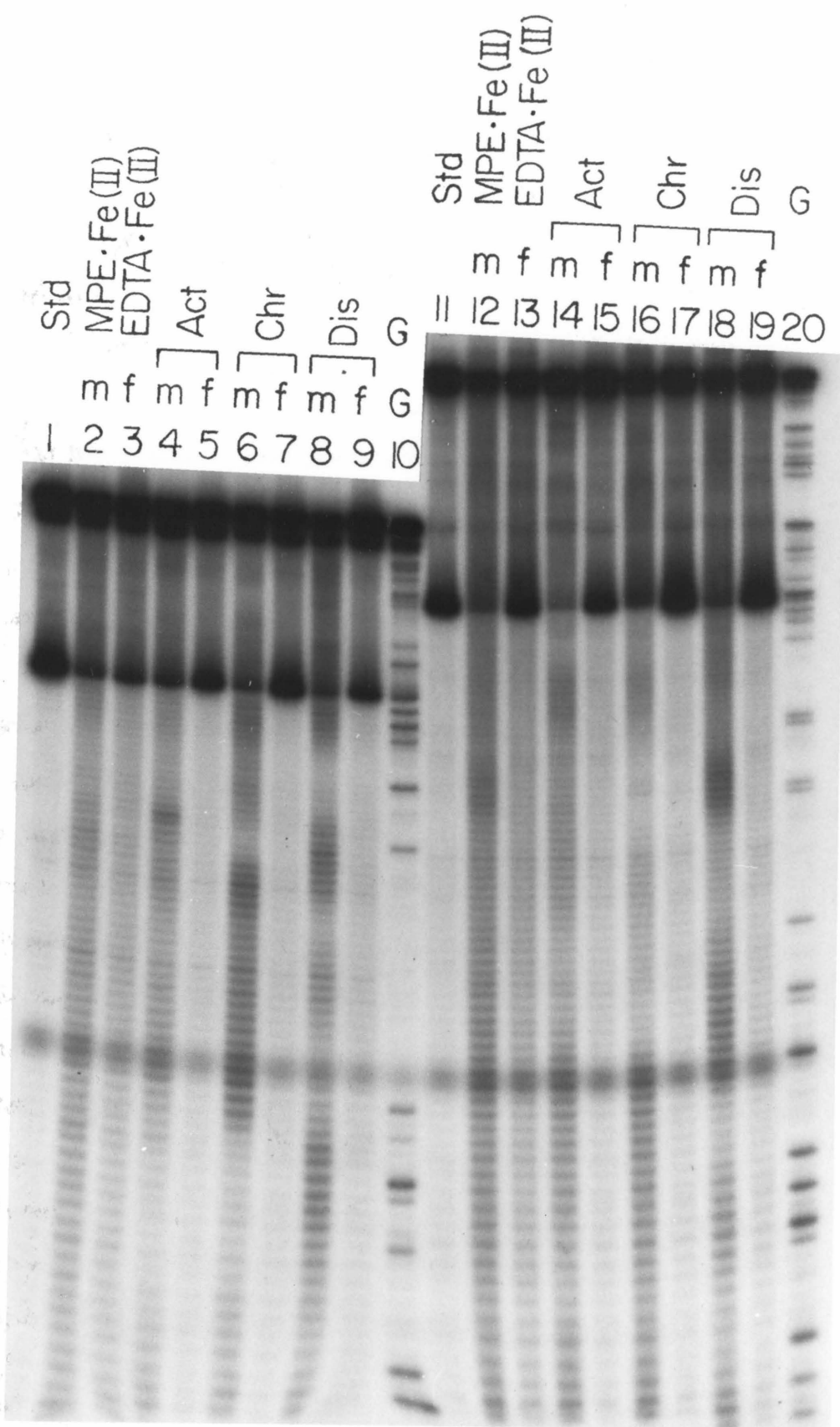
#### **Comparison of MPE·Fe(II)- and EDTA·Fe(II)-mediated Footprinting**

With regards to the cleaving reaction present in MPE·Fe(II) footprinting, it is believed that an EDTA chelated Fe is involved in the creation of a diffusible reactive oxygen species.<sup>51</sup> Evidence points towards the intermediacy of ·OH.<sup>52</sup> This reactive species then may cleave the DNA through a non-sequence specific oxidative degradation of the deoxyriboses. Cleavage inhibition may be affected by ·OH capture on the part of the protecting small molecule. If this were the sole case, it should be possible to footprint with EDTA·Fe(II) alone. Attempts were made to footprint actinomycin, chromomycin, as distamycin with either MPE·Fe(II) or EDTA·Fe(II) under conditions where each would provide sufficient DNA cleavage on unprotected DNA. The autoradiogram is shown in Figure 57. EDTA·Fe(II)-mediated DNA cleavage is greatly diminished throughout the DNA sequence when protecting small molecules are present under condition where MPE·Fe(II) shows distinct footprints. This concurs with other researchers who have found EDTA·Fe(II) unsuitable for use as a footprinting reagent.<sup>137</sup>

**Figure 57**

**Comparison of MPE- and EDTA·Fe(II)-mediated footprinting patterns for the antibiotics actinomycin, chromomycin and distamycin.**

Autoradiogram of 3' end labeled 117 bp and 168 bp DNA fragments: Lanes 1-10 were 117 bp, and lanes 11-20 were 168 bp DNA. Lanes 1 and 11 were the intact buffered DNAs. Lanes 10 and 20 were the Maxam-Gilbert G reactions. Lanes 2-9 and 12-19 contained 10 mM Tris·Cl [pH 7.4], 50 mM NaCl, 400  $\mu$ M base pairs DNA, and 4 mM DTT. Lanes with a small **m** contained 10  $\mu$ M MPE·Fe(II); lanes with a small **f** contained 2 mM EDTA·Fe(II). Lanes 4,5,14, and 15 contained 50  $\mu$ M **act**. Lanes 6,7,16, and 17 contained 50  $\mu$ M **chr** and 100  $\mu$ M **Mg<sup>2+</sup>**. Lanes 8,9,18, and 19 contained 50  $\mu$ M **dis**. Lanes 2 and 12 were the MPE·Fe(II) cleavage controls. Lanes 3 and 13 were the EDTA·Fe(II) cleavage controls.



### **Reproducibility of MPE·Fe(II) and DNase I Footprinting of Small Molecules**

Given the large number of variables which are present in each footprinting experiment (quantities, reaction volumes, reaction times, etc.) it would be interesting to see how reproducible these footprinting patterns would be. A series of six experiments were performed attempting to reproduce the MPE·Fe(II) and DNase I footprinting of the small molecules actinomycin, chromomycin, and distamycin on the 3' end labelled 382 bp DNA fragment (see autoradiograms in Figure 58a-f). What is observed is the variability in size and intensity for various footprinting patterns. Large differences may occur on occasion (Figure 58 a vs b, lane 15). However, the location of these footprints do not change. It is therefore necessary to do a gradual increase in small molecule concentration (factors of 2) or else multiple footprinting trials to properly fix the footprint sizes.

### **DNA Affinity Cleavage and MPE Footprinting**

Recently Schultz, Taylor and Dervan have synthesized the DNA cleaving molecule, distamycin-EDTA [DE], which consists of the DNA minor groove binder distamycin and the metal chelator EDTA linked together by a propyl hydrocarbon tether.<sup>192</sup> Both MPE·Fe(II) footprinting of distamycin and DNA affinity cleaving by DE show common binding locations and site sizes.<sup>193</sup> Each binds 5 bp sites with a preference for poly(dA)·poly(dT) regions. The equivalence in binding sites can be envisioned as a form of self-footprinting in the case of affinity cleavage. This is shown graphically in Figure 59.

**Figure 58**

**Reproducibility for MPE and DNase  
footprinting of small molecules**

A series of six autoradiograms (a-f) which were repetitions of the identical reaction conditions. Each contained the 3' end labeled 382 bp DNA fragment. Lane 1 contained the intact DNA. Lane 16 was the Maxam-Gilbert G lane. All other even-numbered lanes (2,4,6,8,10,12,14) contained 10 mM Tris·Cl [pH 7.4], 50 mM NaCl, 400  $\mu$ M base pairs DNA, 4 mM DTT, and 10  $\mu$ M MPE·Fe(II). All other odd-numbered lanes (3,5,7,9,11,13,15) contained 10 mM Tris·Cl [pH 7.9], 10 mM KCl, 10 mM MgCl<sub>2</sub>, 5 mM CaCl<sub>2</sub>, 400  $\mu$ M base pairs DNA, 0.1 mM DTT, and 0.2  $\mu$ g/ml DNase I. Inhibiting drugs in these reactions were: lanes 4 and 5, 25  $\mu$ M **act**; lanes 6 and 7, 100  $\mu$ M **act**; lanes 8 and 9, 25  $\mu$ M **chr**, and 50  $\mu$ M Mg<sup>2+</sup>; lanes 10 and 11, 100  $\mu$ M **chr** at 200  $\mu$ M Mg<sup>2+</sup>; lanes 12 and 13, 25  $\mu$ M **dis**; lanes 14 and 15, 100  $\mu$ M **dis**.

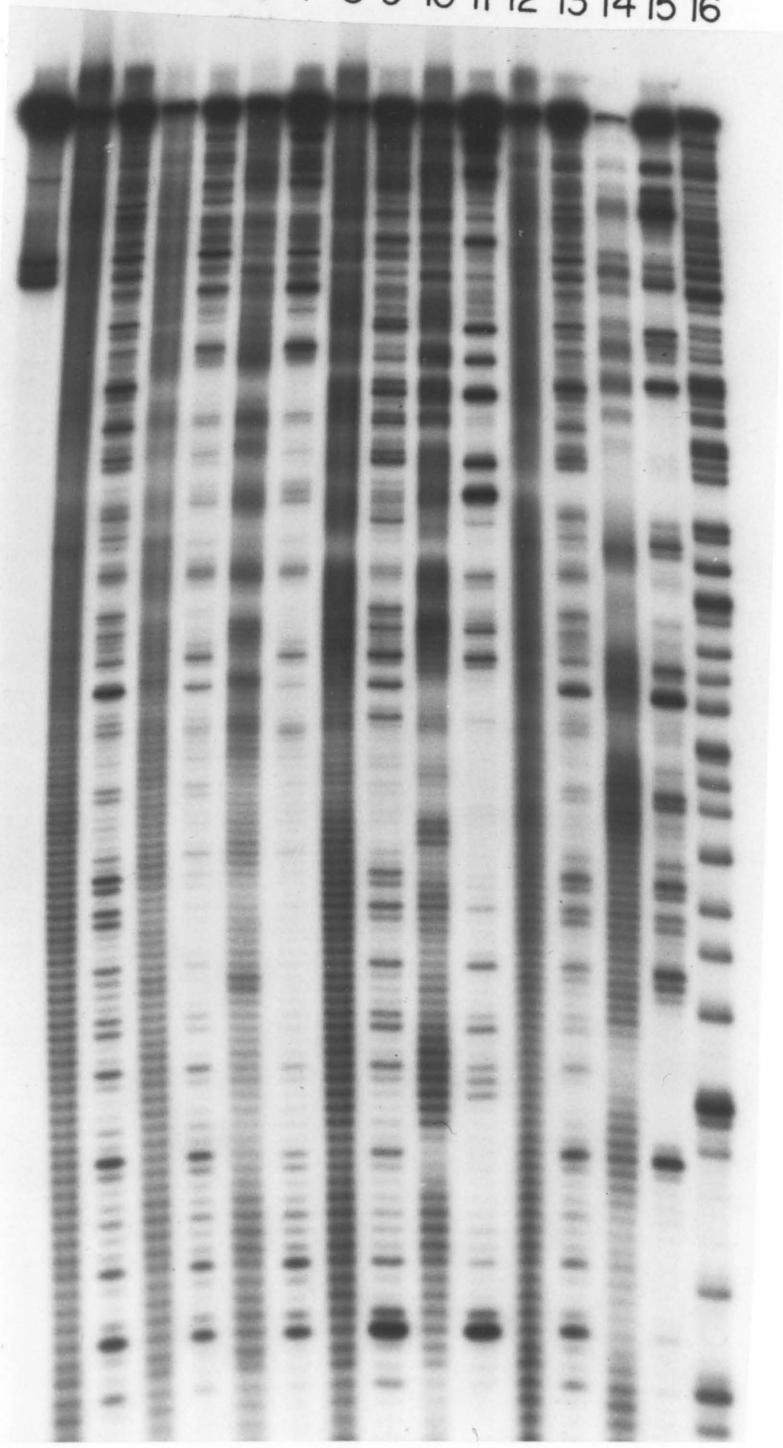
Exceptions: In figure (d), 0.4  $\mu$ g/ml DNase I was employed in the odd-numbered lanes (3,5,7,9,11,13,15) . Notice also the inversion of lanes 13 and 12.





DNA STD  
MPE · Fe (II)  
DNase I

ACT      CHR      DIST      G  
1 2 3 4 5 6 7 8 9 10 11 12 13 14 15 16



DNA STD  
MPE · Fe(II)  
DNase I

ACT            CHR            DIST    G

1 2 3 4 5 6 7 8 9 10 11 13 12 14 15 16



DNA STD  
MPE · Fe(II)  
DNase I

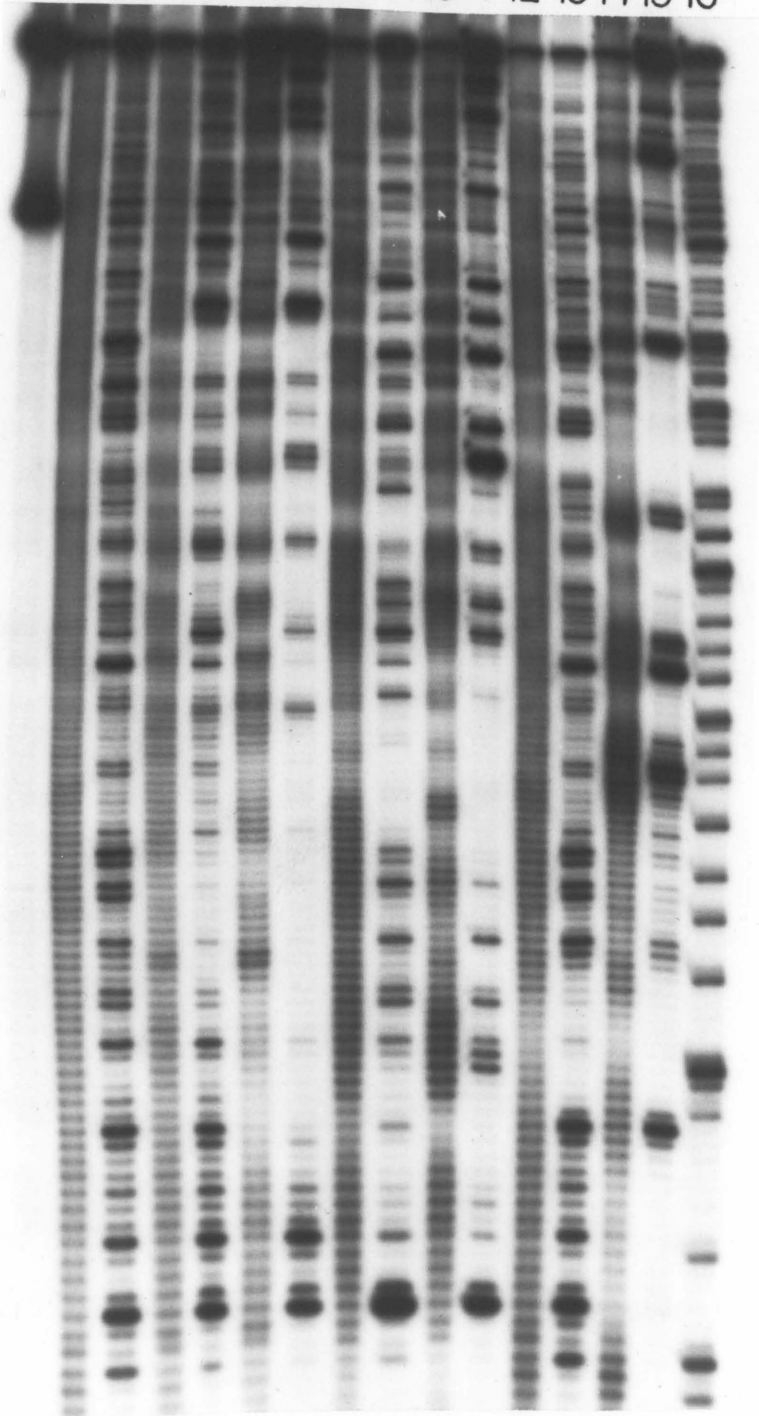
ACT      CHR      DIST      G

1 2 3 4 5 6 7 8 9 10 11 12 13 14 15 16



DNA STD  
MPE · Fe (II)  
DNase I

ACT      CHR      DIST      G  
1 2 3 4 5 6 7 8 9 10 11 12 13 14 15 16



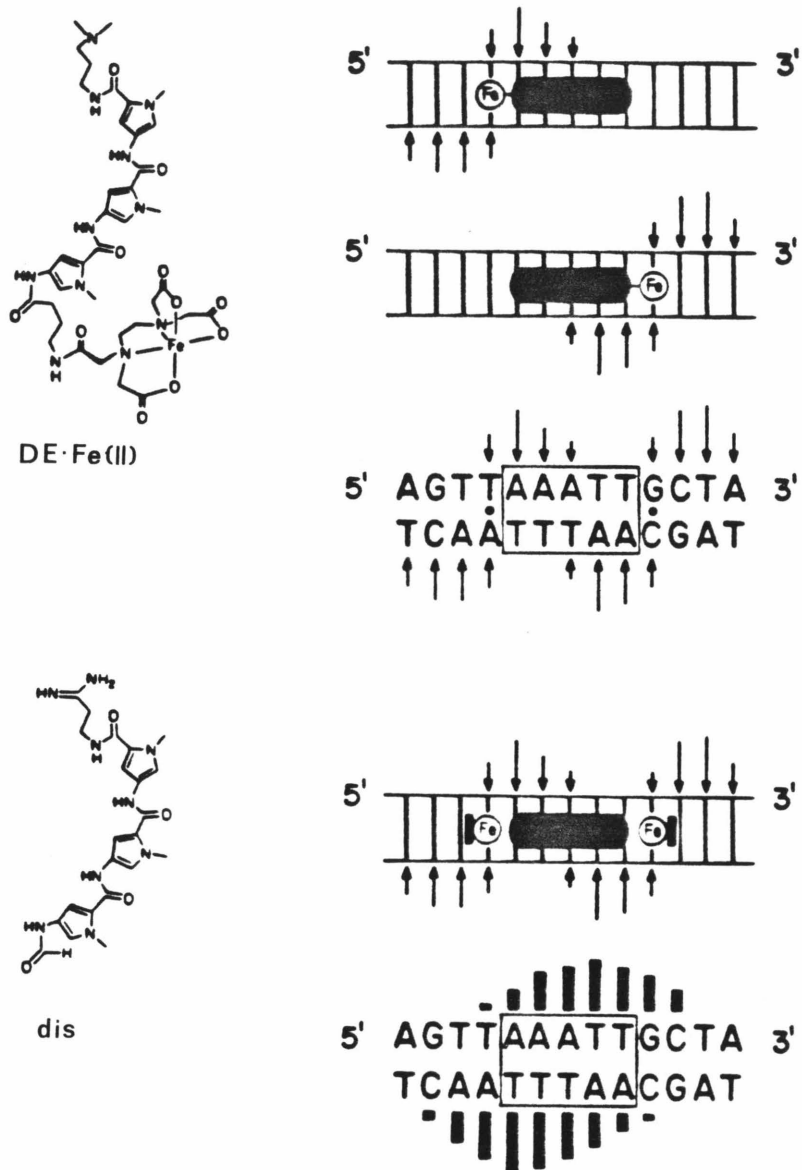


Figure 59

(Top) Structure of DE·Fe(II) and model for DNA affinity cleaving relating binding site to DNA cleavage patterns.

(Bottom) structure of distamycin and model for MPE·Fe(II) footprinting relating binding site to cleavage inhibition patterns.

### **Actinomycin D Binding Model**

Actinomycin D binds to double helical DNA by intercalation,<sup>65</sup> with the cyclic pentapeptide rings located in the minor groove.<sup>81</sup> The binding geometry of the actinomycin:DNA complex has been investigated by x-ray crystallography,<sup>80,82</sup> NMR,<sup>83-85</sup> and optical spectroscopy on known sequence homopolymers.<sup>29,78</sup> Binding on heterogeneous DNAs has also been investigated by MPE and DNase footprinting methods.<sup>164,169-171</sup> With this collection of information, it is possible to postulate a model describing the sequence specificity of actinomycin binding to DNA.

From a 2:1 deoxyguanosine:actinomycin crystal study,<sup>80</sup> the positioning of the phenoxazone chromophore parallel to the bases comprising the intercalation site was verified. The cyclic pentapeptides, located in the minor groove, were either above the plane of the chromophore (quinoid half of chromophore), or below the plane of the chromophore (benzoid half of chromophore). Both cyclic peptides occupied the whole of the minor groove, extending just beyond the nucleotides involved in the intercalation site. Strong hydrogen bonding interactions connected the 2-amino functionalities of the guanines on the 5' ends of the intercalation site with the carbonyl oxygens of the L-threonines in the two cyclic pentapeptides. Weaker hydrogen bonds could be formed between the amide N-H of L-threonine and the N(3) ring nitrogen of purines (G or A). Crystal studies on a 2:1 d(GpC): actinomycin pseudo-intercalated complex showed that the relative orientation of the peptide rings was independent of which portion of the chromophore was present.<sup>82</sup> Proton and <sup>31</sup>P NMR investigations of actinomycin interactions with mono-, di-, and larger oligonucleotides

demonstrated the importance of stacking interactions (hydrophobic) in the stabilization of the bound complex.<sup>83,84</sup> Different sequences infer different complex conformations, leading to very different rates of dissociation.<sup>78</sup> Together these spectroscopic studies leads towards a model which must concur with the observed preferred binding sites obtained from equilibrium binding studies on homopolymers and footprinting studies on heterogenous DNAs.

A simple model explaining the sequence specificity binding is shown in Figure 60. Note that only the two base pairs of the intercalation site need be involved. Further base pairs probably do have an influence on actinomycin binding, but their effect is most likely conformational in nature. In this model the chromophore is intercalated between the two base pairs, with the orientation of the benzoid and quinoid portions not defined. The chromophore-cyclic peptide amide bond points toward the 5' side. This allows for the strong hydrogen bonds from the L-threonine to be involved in the complex formations. Also this orientation avoids possible unfavorable steric interactions between the prolines of the cyclic pentapeptides and the 2-amines of guanine. In this model only purine bases contribute towards stabilizing stacking interactions. There is at maximum only two possible stacking interactions per bound actinomycin molecule, this occurring only when both portions of the chromophore are involved.

Comparisons between the ranked dinucleotides and homopolymers binding studies exhibits a high degree of correlation. The observed<sup>29</sup> the order of binding 5' GC > GG > GT, GGT > GA, GAA, GTA >> GAT, AT, AA has dinucleotides sites present which fit quite well with the proposed

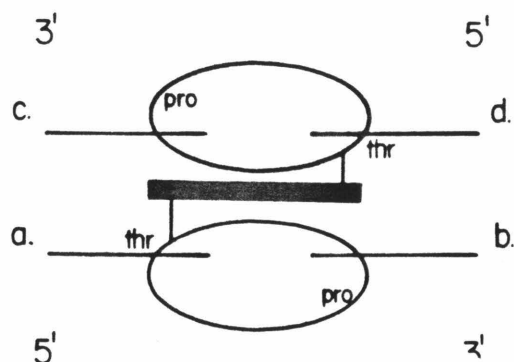


**Figure 60**

Proposed model for actinomycin binding to DNA. Actinomycin is represented here as the dark rectangle intercalated between the two base pairs a-b and c-d. Intercalation site is viewed from the minor groove. Cyclic pentapeptide substituents are represented as ovals, with the amino acid residues L-threonine (**thr**) and L-proline (**pro**) shown. Potential actinomycin:DNA interactions include: 1) two hydrogen bonds, one strong connecting the the guanine 2-NH<sub>2</sub> group with the carbonyl oxygen of **thr**, and one weak connecting the N-H group of **thr** to the N(3) ring nitrogen of either guanine or adenine. Both interactions involve bases a and d. 2) Steric interference between the 2-NH<sub>2</sub> group of guanines and the **pro** residues for bases b and c. 3) Stacking interactions between purines and the phenoxaxone chromophore for any of the four bases abcd. Given these interactions a hierarchy of preferred binding sites may be derived:

Preferred Actinomycin Binding Sites

	Bases 5'- <u>a</u> <u>c</u> -3'	# Hydrogen Bonds		# Stacking Interactions	# Steric Repulsions
		Strong	Weak		
binding	G C	2	2	2	0
	G T (AC)	1	2	2	0
	G A (TC)	1	1	2	0
	G G (CC)	1	1	2	1
	A T	0	1	2	0
	A A (TT)	0	1	2	0
	A G (CT)	0	1	2	1
	T A	0	0	2	2
	T G (CA)	0	0	2	1
	CG	0	0	2	2

model. The major exception is GG, which is a poor binding site in the model yet has an apparent strong binding constant for actinomycin.<sup>29</sup> Noteworthy is the number of nucleotides per binding site (91) as obtained by equilibrium binding studies. Actinomycin is anticipated to occupy a physically much smaller site. This enormous apparent site size may reflect the need for some unusual and infrequent conformational change in the DNA structure prior to binding.

Footprinting analyses of actinomycin binding to 223 nucleotides of heterogeneous DNAs have been investigated by a combination of MPE and DNase protocols. On the 120 base pairs total for which complementary strand analyses have been performed, 38 (32%) were afforded protection by actinomycin. Of these protected base pairs, 28 (74%) were G+C in composition. Average minimum protected site size was 3 base pairs. This may be indicative of a "sidedness" in actinomycin-mediated DNA protection from MPE cleavage. A list of the protected sites is provided, with postulated intercalation sites shown (Table III). Almost half the preferred binding sites employ intercalation between 5'-GC-3' base pairs; the remainders being evenly distributed among the other possible binding sites. No actinomycin binding to a postulated nonbonding site needs to be invoked to explain any observed footprints. Both potential intercalation sites in the base pairs triplets is involved with equal frequency. The two most preferred actinomycin binding sites are 5'-GC-3' flanked by A·T base pairs. While insufficient data exist to draw conclusions as to the ideal actinomycin binding site, especially with regards to the conformational input of flanking sequences, information derived from footprinting analyses do

Table III - List of Actinomycin D Binding Sites

117 bp & 168 bp:50 bp studied

5'-CAC  
|

GCT TCC GGC      best binding site, repeated MPE footprinting  
|

TGT GG  
|

TGA GC  
|

378 bp & 382 bp:70 bp

C  
|

TCC  
|

GCA      best binding site, DNase footprinting  
|

GCG  
|

AGC  
|

CGG  
|

| indicates potential intercalation site

concur with the postulated model.

### **Distamycin A Binding Model**

Distamycin A and netropsin bind to double helical DNA through multiple hydrogen bonding and electrostatic interactions.<sup>97</sup> Location of these molecules is in the minor groove of B-form DNA.<sup>87,98</sup> The solid-state geometry of netropsin, as determined by x-ray crystallography, requires a large curvature in the oligopeptide backbone with the amide -NHs located on the concave side.<sup>91</sup> NMR spectroscopy and proton NOE measurements require that each pyrrole H-3 proton of netropsin be juxtaposed against each inside adenosine H-2 protons and that the guanidine CH<sub>2</sub> protons be juxtaposed against the outside adenosine H-2 proton for the tetranucleotide 5'-AATT-3'.<sup>30</sup> These physical studies, combined with footprinting and cleavage affinity analyses, allow for the postulation for the sequence specific DNA binding of oligopeptide N-methylpyrrole antibiotics like distamycin and netropsin.

A model describing the specificity requirements for distamycin A binding is shown in Figure 61. The molecule is centered in the minor groove to minimize steric interference. Hydrogen bonding may proceed between each carboxamide NH in the distamycin molecule and the N(3) of adenine or O(2) of thymine on adjacent base pairs. The hydrogen bonds to thymine may be favored due to its closer proximity (0.5 Å) and better lone pair orientation.<sup>99</sup> Thus the molecule may orientate itself preferentially over one DNA strand over part of its binding site, then switching to the other strand for the remainder. The positively charged propionamidino group interacts electrostatically and by hydrogen bonding

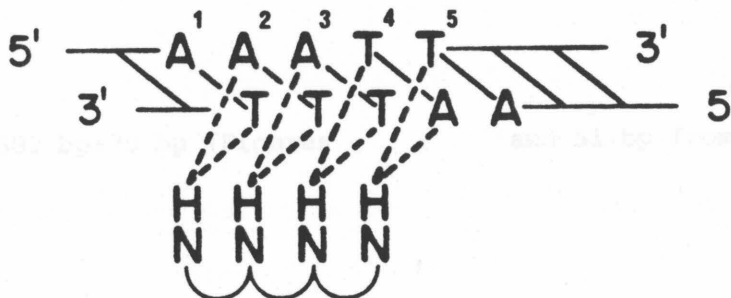


**Figure 61**

Proposed binding model for distamycin. Distamycin is represented as a series of four N-H amide functionalities tethered together. Located in the minor groove, distamycin is capable of four bifurcated hydrogen bonds to either the thymine O(2) or adenine N(3) acceptors. Optimally nucleotides 1-5 should all be either A or T. Base alternation leads to loss of hydrogen bonding. Thus the expected binding site preferences:

$A_5 > A_4T, A_3T_2 > A_3TA, A_2TA_2 > A_2TAT, ATA_2 > ATATA$

which is the series of 0,1,2,3, and 4 base alternations, respectively. In so far as hydrogen bonding is concerned, cytosine is equivalent to thymines. Guanines with their 2-NH<sub>2</sub> functionality, causes steric repulsion between distamycin and its binding site.

Table IV -- List of Distamycin A Binding Sites

117 bp & 168 bp:50 bp studied

5'-TTTAC ACTTT ATGCT

ATAAT

No strong DE cleavage sites

AATT

378 bp & 382 bp:70 bp (Figures

and 51 bp from P. Schultz

TAGT

ATAGT

AAGTA

CAAAG

AAATT

Strong DE cleavage site

ATATAG

167 bp:76 bp P. Schultz

TTTAA

AGTTT

AAATT

\*

Strong DE cleavage sites

GAAAT CTAAC AA

\*

516 bp:85 bp studied P. Schultz

TTTTT

Strong DE cleavage site

TTAAT

TAATA A

TCTTA

TTTTC

AAATG

to phosphate oxygens on the 3' side of the binding site. Five base pairs are involved in the binding site. Binding strength is proportional to the number of hydrogen bonds formed.<sup>97</sup> Alternating the base composition on each strand interferes with the formation of carboxamide - thymine O(2) or - adenine N(3) hydrogen bonds. Thus reducing binding. Cytosines are equivalent to thymines. The N(2) of guanine sterically interferes with the close distamycin:DNA interaction. The relative importance of guanine's steric interference and the loss of hydrogen bonding upon A+T alternation is not known.

Substantial MPE footprinting analyses have been performed on distamycin, together with cleavage affinity studies on the distamycin analog, DE. Both studies demonstrate preferred distamycin binding sites on polydA·polydT stretches with minimum base alternation present. Table VI lists a variety of these sites. On 332 total base pairs heterogeneous DNA investigated, 113 (34%) appear as distamycin binding sites. Of these 96 (85%) are A+T in composition. The typical minimum binding site size averages 5 base pairs. Strong DE cleavage sites are believed to occur at the most preferred distamycin binding sites. This follows from the reduced binding constant of DE, perhaps due to the steric interference of the EDTA moiety, as determined by DE/distamycin competition experiments (Figure 54). These cleavage sites have typically one or less alternation of nucleotides per strand and any guanines located outside the hydrogen binding sites (see Table IV). Such findings generally agree with the aforementioned model.

#### **Chromomycin A<sub>3</sub> Binding Model**

The aureolic acid family of antibiotics, chromomycin A<sub>3</sub>,

mithramycin, and olivomycin, all bind double helical DNA through a poorly understood mechanism. Absolute requirements for the 2-amino functionality of purines (guanine) and stoichiometric amounts of  $Mg^{2+}$  have been shown.<sup>107</sup> Binding is therefore felt to proceed through the minor groove. Sequence specificity studies have been limited to optical spectroscopy on homopolymer DNAs and our footprinting work. No crystallographic or NMR studies are available on these antibiotics at this time.

In the cases of the antibiotics actinomycin D, distamycin A, and netropsin, since a great deal of physical information is known about their DNA binding interactions, footprinting was a means of verifying their postulated binding models. However, with the aureolic acid family of antibiotics, the additional data provided by footprinting were necessary before a binding model could be formed. The preferred binding sites of the antibiotics chromomycin A<sub>3</sub>, mithramycin, and olivomycin have been compared at various concentrations on 70 base pairs of the *lac* operon by MPE footprinting techniques (Figure 24). Additionally, chromomycin A<sub>3</sub> has been investigated by both MPE and DNase footprinting on 70 base pairs of the *tet*<sup>R</sup> gene (Figures 30 and 31). In general, the protected sites average 2-3 base pairs long (by MPE footprinting) and are very G+C rich (88% at levels 1:4 antibiotic:base pairs). Almost universally there exists a 5'-GC-3' sequence present in the most preferred binding sites. There may be some conformational or steric influence on the quality of the binding site as a function of its flanking sequences. This is observed when identical binding sites exhibit different affinities for the antibiotics. All of the

antibiotics share similar, though not identical, binding sites. This may be dependent on the nature of the attached sugar substituents which vary among the three molecules. Since chromomycin A<sub>3</sub> has been most thoroughly investigated by ourselves and in the literature, it will herein serve as a model for the Mg<sup>2+</sup> chelative binding mode. A list of its preferred binding sites, in order of appearance as a function of chromomycin:bp DNA ratio, is shown (Table V).

Given what is known about the binding of chromomycin to DNA and its solution chemistry it was possible, with the aid of CPK space filling models, to devise some manner of model explaining the hydrogen bonding and electrostatic interactions present which is conducive to the observed 5'-GC-3' preference. One of the chromophore phenolic oxygens should be deprotonated at physiological pHs, this follows from the observed pK<sub>a</sub> (=5) of the similar compound, 1,8-dihydroxy-2-naphthaldehyde.<sup>194</sup> Most likely the outermost phenolic oxygen would ionize, allowing the innermost phenolic hydroxy to form an intramolecular hydrogen band which stabilizes the conjugate base. This anionic site could then chelate a Mg<sup>2+</sup> ion together with a phosphate on the DNA backbone, thus effecting charge neutralization. Location of the chromophore within the DNA minor groove in such a way as to minimize steric interactions between the substituent polysaccharides and the DNA necessitates an orientation of the chromophore as 5'-disaccharide-chromophore-trisaccharide-3', this following the curvature of a right-handed double helix. Now in order to maintain a chromophore-Mg-phosphate linkage while allowing some form of hydrogen bonding interactions with the preferred 5'-GC-3' site, a binding model

Table V - List of Chromomycin A<sub>3</sub> Binding Sites

Preferred Chromomycin A<sub>3</sub> Binding Sites

117 bp & 168 bp: 70 bp studied

<u>1:16</u>	<u>1:4</u>	<u>1:1</u> <u>chr:bp DNA</u>
(A)CCC(C)	(C)GGC(T)	(A)CAC(T)
(G)GCT(T)	(G)CGG(A)	(T)GCT(T)
		(T)GGA(A)

378 bp & 382 bp:70 bp

(C)GC(G)	(A)GC(G)
(G)GC(T)	(G)GGA(C)
(G)GCG(G)	
(C)GGC(C)	
(A)AGC(G)	

( ) nucleotides in parentheses are adjacent to the determined binding sites.

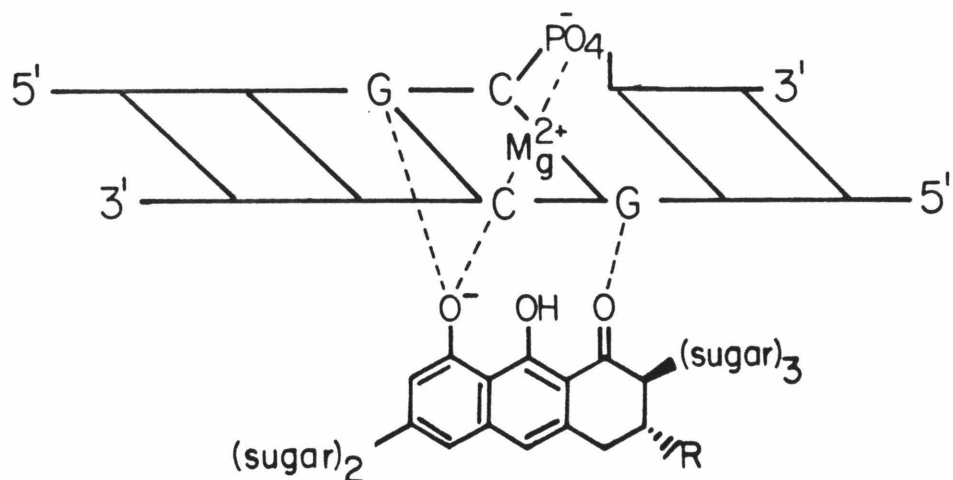


**Figure 62**

Proposed binding model for chromomycin. Chromomycin, represented by its chromophore, lies in the DNA minor groove. An anionic phenoxy substituent jointly chelates a  $Mg^{2+}$  ion with a phosphate 3' from the 2 base pair binding sites. Further hydrogen binding is postulated between that phenoxy and the 2-amino functionality of guanine, and the chromophore carbonyl and the 2-amino of guanine on the opposite strand. Binding site preferences would therefore be: 5'-GC > GG,GT,GA > CG,CT,CA with at least one guanine required in the binding site.

on the order of that shown (Figure 62) looks promising. The phosphate 3' oxygen of the GC base pairs is closest to the ionically-bound  $Mg^{2+}$  ion. This allows a hydrogen bond to form between a 5'G (2) amino function and the phenolic oxygen involved in the  $Mg^{2+}$  chelation. Another hydrogen bond is also possible between N-(2) of guanine located on the opposite DNA strand and the ketone carbonyl on the tricyclic portion of the chromophore. Adjacent base pairs may determine the relative orientation of the bound molecule by steric preference for or against a particular substituted polysaccharide present. Further physical investigations will be necessary to verify this particular binding model.

#### **Echinomycin Binding Model**

Echinomycin is a member of the quinoxaline family of antibiotics which exhibits a strong G·C preference.<sup>114</sup> Homopolymer DNA binding preferences are: poly(dG)·poly(dC) > poly(dG-dC) > poly(dA-dT) >> poly(dA)·poly(dT).<sup>114</sup> This was the first example of a bisintercalative DNA binding molecule studied.<sup>113</sup> Binding site size (5 bp) indicates nearest-neighbor exclusion for the bisintercalation event.<sup>114</sup> Minor groove location of the antibiotic follows from binding studies with phage T2. The cyclic octapeptide ring would provide several possible candidates for hydrogen bonding interaction with the functionalities present in guanine and cytosine in the minor groove. The highest binding affinity was obtained with *M. lysodeikticus* DNA (72% G+C) and not with poly(dG)·poly(dC) or poly(dG-dC) DNAs, suggesting that all four bases in the binding site may be important in the recognition process. Conformational recognition may also be involved, given the tendency of

poly(dG)·poly(dC) to assume an A-like structure<sup>195</sup> while poly(dA)·poly(dT) will not.<sup>196</sup> NMR<sup>117</sup> studies and empirical potential energy calculations<sup>118</sup> point towards a rigid symmetrical peptide ring with parallel quinoxaline chromophores extending roughly perpendicular to the plane of the ring in one direction (up) while the 5-methyl functionality of the thioacetyl cross-bridge points in the other (down). Up is defined as towards the DNA when binding occurs. In this model the Ala carbonyls are up and may be involved in hydrogen bonds with the N-(2) of guanines. Cys carbonyls are down and should not interact with the DNA. No NMR investigations have been performed in the presence of DNA. No crystal structures exist of either echinomycin or its complex with DNA.

Substantial MPE (and DNase) footprinting analyses have been performed on echinomycin. Investigations on 360 base pairs of heterogeneous DNAs indicates numerous footprints. Liberal interpretation of these binding sites indicates a typical size of 4 base pairs which are moderately (71%) G+C rich. Amazingly, most of the stronger sites (67%) contain a central 5'-CG-3' sequence, with the sequences 5'-GG-3' and 5'-CC-3' a distant second (21%). No similar correlation can be made with the outside two base pairs. A list of all the putative echinomycin binding sites is provided (Table VI). From these data the importance of the central two base pairs is demonstrated, with the sequence 5'-CG-3' being preferred. On the basis of such binding specificity, together with earlier spectroscopic studies, it should be possible to formulate a reasonable DNA binding model for echinomycin.

The model we postulate for the preferred binding of echinomycin

Table VI. List of Echinomycin Binding Sites

117 bp & 168 bp lac operon: 80 bp studied (figure 51)

5' CCCA CCGGCT\* GCGG 3'

378 (382) bp & 274 (278) bp tet<sup>R</sup> gene: 125 bp studied (figures 48, 50)

5' GCGT TCGA GCGAAGCG TGGGCGGC 3'

5' CCGG AGGTGCGG<sub>(w)</sub> TCGCCGA\* CCGATGG\* TCGG 3'

167 bp & 517 bp promoter-rich regions (P1,2,3): 155 bp studied (figures 52, 53)

5' TCGA GCGG ACGC<sub>(w)</sub> ACCG<sub>(w)</sub> 3'

5' TCGT ACGC AGGT<sub>(w)</sub> TGTC<sub>(w)</sub> 3'

5' ACGT AGGT TCGG 3'

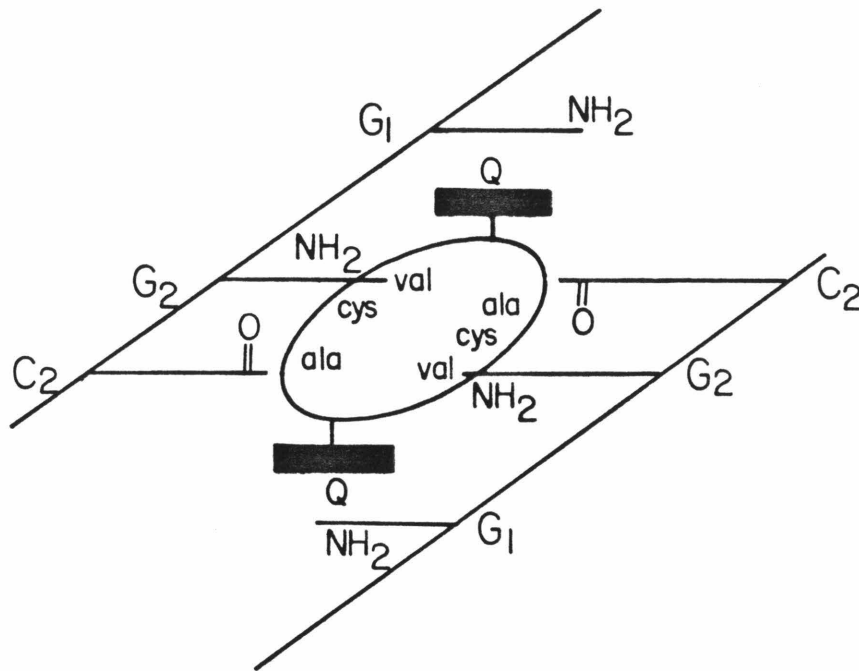


**Figure 63**

Proposed model for echinomycin binding to DNA.

Echinomycin is represented as two rectangular quinoxalines intercalated between four base pairs with one exclude site between these (bisintercalation). DNA is viewed from the minor groove. A cyclic octapeptide links the two chromophores; the amino acid residues L-alanine (**ala**), N-methyl-L-cysteine (**cys**), and L-N-methylvaline (**val**) being shown. Hydrogen bonds are postulated to connect 1) **ala** N-H and cytosine(2)O-(2), 2) NH<sub>2</sub>-(2) of guanine(2) and amide carbonyl of either **cys** or **val**, 3) NH<sub>2</sub>-(2) of guanine(1) and the amide carbonyl of quinoxaline. Binding strength should be proportional to the number of hydrogen bonds formed, with the central 5'-CG-3' base pairs being essential. Thus the series of binding preferences:



might be expected.

to DNA is shown in Figure 63. Optimally six hydrogen bonds are involved: two connecting the cytosine O(2) carbonyls with the amide •NH's of L-alanine, two connecting the guanine N(2) hydrogens with either the amide carbonyls of Me<sub>2</sub>-L-cysteine or the lactone carbonyls of L-N-Me-valine, and two connecting the quinoxaline amide carbonyls with the N(2) hydrogens of the outer guanines. All this hydrogen bonding is made possible by the two-fold symmetry of both echinomycin and the 5'-CCGG-3' sequence. The conformation of the echinomycin molecule is such that the quinoxaline chromophores lie in parallel planes perpendicular to the cyclic peptide yet offset slightly to afford maximum capability for bisintercalation. The cyclic octapeptide then assumes a slightly skewed orientation, keeping in line with the right-handed helical twist of both A and B form DNAs. The orientations of the amide bonds capable of hydrogen bonding within The cyclic octapeptide are: D-Ser carbonyl, down; L-ala-NH, up; L-Ala carbonyl, down; N-Me-L-Cys carbonyl, up; L-N-MeVal carbonyl, up. The quinoxaline amide carbonyls are also oriented towards the DNA. This conformation is allied with that postulated in nonpolar solution by NMR, only that the starting point for amide bond orientation alternation has been changed. This simple model predicts the following order for echinomycin affinity to G-containing homopolymers 5'-C<sub>2</sub>G<sub>2</sub> > C<sub>3</sub>G > CG > CC-3' without regard to conformational preferences intrinsic to each. Future x-ray crystallographic studies will ascertain the validity of this model.

#### Footprinting of Proteins

Lac repressor binding to its specific site on the E.coli lactose operator is a classical example of protein:DNA interaction which proved

the potential of DNase I footprinting. Results by Galas and Schmitz<sup>41,42</sup> showed lac repressor protecting 25 nucleotides on the upper, and 24 nucleotides on the lower strand of DNA from DNase I-mediated phosphodiester bond hydrolysis. This protection was asymmetric, overhanging 3-4 nucleotides on each strand towards the 3' end (see Figure 64). Their findings concur quite well with the expected lac repressor binding site as determined by repressor/5-bromodeoxyuridine crosslinking,<sup>197</sup> constitutive operator mutations,<sup>198,199</sup> and methylation protection experiments.<sup>200</sup> Overprotection to DNase I digestion is from 2-3 nucleotides on each strand. Such accuracy is considered a high degree of precision.

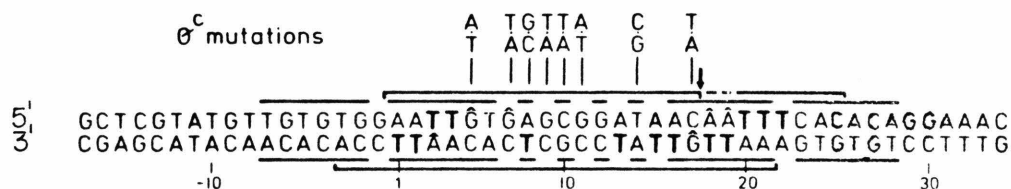


**Figure 64**

Characterization of the lac operator by four different methods. 1) DNase I footprints of lac repressor are shown as brackets along side the DNA sequence. The arrow above the upper strand points to the repressor-induced site of enhanced DNase I cleavage. 2) Constitutive operator mutations are shown above the sequence. These weaken the repressor-operator interaction. 3) Bold fact **Ts** represent sites of repressor/5'-bromodeoxyuridine crosslinking after UV radiation. 4) Nucleotides capped with a circumflex represent repressor-induced sites of protection against methylatsion. Those horizontal lines nearest the nucleotide sequence indicate the two-fold symmetry present.

Comparing MPE- and DNase I footprinting of proteins on DNA, the lac repressor:operator complex was chosen as an example. DNase I footprinting, both an earlier 3' labeled and a later opposite strand analysis, showed protection for 24 nucleotides on each strand, with equivalent 3' overhangs of 3 nucleotides apiece on each end. An

accentuated DNase I cleavage site within the footprint was also observed. These results are almost identical with those already mentioned. MPE footprinting of the same complex gave slightly smaller footprints (22 nucleotides) with the same apparent asymmetry. This cleavage asymmetry, 3 nucleotides toward the 3' end, is identical for both MPE and DNase I footprinting. While this asymmetry might reflect a certain protein:DNA geometry of interaction, allowing differential accessibility for the cleaving agent to either strand, both MPE and DNase are known to generate staggered cuts on naked DNA. Most remarkable is the loss of the internal accentuated cleavage site on the upper strand with MPE footprinting. The simplest explanation would require that the protein influenced modified DNA structure at that site is easily recognized by DNase I but does not afford a suitable binding site for MPE. With a greater understanding of the conformation recognition of DNA by DNase I and its influence on the rate of strand cleavage, it should be possible to compare MPE- and DNase I footprinting patterns of protein:DNA complexes and directly determine the modes of action for various regulatory proteins, for example the destabilization of double-helical DNA by cAMP-CRP binding.<sup>188</sup>

## **SUMMARY**

Many small molecules, including several antibiotics employed in cancer chemotherapy, bind to double helical DNA noncovalently and evince their therapeutic action through impediments to the progress of DNA-directed, RNA and DNA polymerases. Understanding the sequence specificities should aid in the understanding of the molecular basis of antibiotic action.

With the synthesis of MPE there became available a small synthetic scissors which efficiently induce single-strand cleavages into double helical DNA with low sequence specificity. Applying MPE in a fashion similar to the DNase I footprinting of proteins it was possible to directly determine the preferred binding sites of several small molecules on heterogeneous DNA among those small molecules investigated are the antibiotics actinomycin D, chromomycin A<sub>3</sub>, distamycin A, echinomycin, mithramycin, netropsin, and olivomycin. From their footprinting data models were devised to explain their interactions with DNA. These models could then be employed for the postulation of anticipated preferred binding sites on previously untested DNA segments.

Further investigations compared the relative usefulness of MPE versus DNase I-based footprinting for determining the preferred binding of both small molecules and proteins. DNase proved more sensitive in several cases, but afforded significantly poorer resolution than MPE. MPE was capable of being used under a wider variety of conditions {ionic strength, pH, absence of divalent cations}. Thus MPE•Fe(II) footprinting is the method of choice for determining the binding location and site sizes of antibiotics to DNA and a useful complement to

the DNase footprinting of proteins.

In conclusion, MPE·Fe(II) footprinting provides a simple, rapid, and direct means for assaying hundreds of potential equilibrium binding sites for both small molecules and proteins in vitro.

MPE·Fe(II) footprinting exhibits a wide operating range, demonstrates a high degree of reproducibility, and possesses a relatively well understood mechanism of operation. These factors combine to give an extensive applicability to the MPE footprinting method and increased confidence in its results. This may eventually lead to the development of improved antibiotics.

## **EXPERIMENTAL**

### **DNA**

#### Varieties and Sources

For investigations of small molecule footprinting on natural DNAs, three varieties of bacterial plasmids were used. Plasmid pBR-322<sup>201</sup> was a gift from J. Campbell and was grown in E.coli strain HB101. Plasmid pLJ 3,<sup>202</sup> containing a 285 base pair insert with two copies of the lactose operon promoter-operator sequence in the same orientation, was a gift from D. Galas and was grown in E.coli strain MM294. Plasmid pLP 32,<sup>176</sup> containing a 32 base pair repeating 5'(CG)<sub>16</sub>3' insert, was a gift from L. Peck and was grown in E.coli strain HB101. Bacterial plasmids were chosen as the source of heterogeneous DNA since they could be produced in large quantity and high purity. Plasmid integrity, as defined as the absence of single-stranded DNA cleavages, could in this system be easily ascertained by noting the ratio of open-circular to superhelical plasmids present after gel electrophoresis and ethidium staining. Nicked DNA would cause an undesirably high background cleavage ladder after high resolution gel electrophoresis, thus obscuring the weaker footprints.

Calf thymus DNA {type 1, Na<sup>+</sup> salt} was obtained from Sigma and deproteinized by phenol extraction. This material served as a carrier DNA in footprinting reactions, where its concentration in base pair relative to the radiolabeled restriction fragment was greater than two orders of magnitude.

### Growth and Purification of Plasmid DNAs

The growth and purification of plasmid DNAs generally followed the procedures of Tanaka and Weisblum.<sup>203</sup> A more elaborate description of the techniques involved is presented in "Molecular Cloning, A Laboratory Manual".<sup>204</sup> Below is stated a short summary of the individual procedures as presently employed in the course of this research (see also Figure 65).

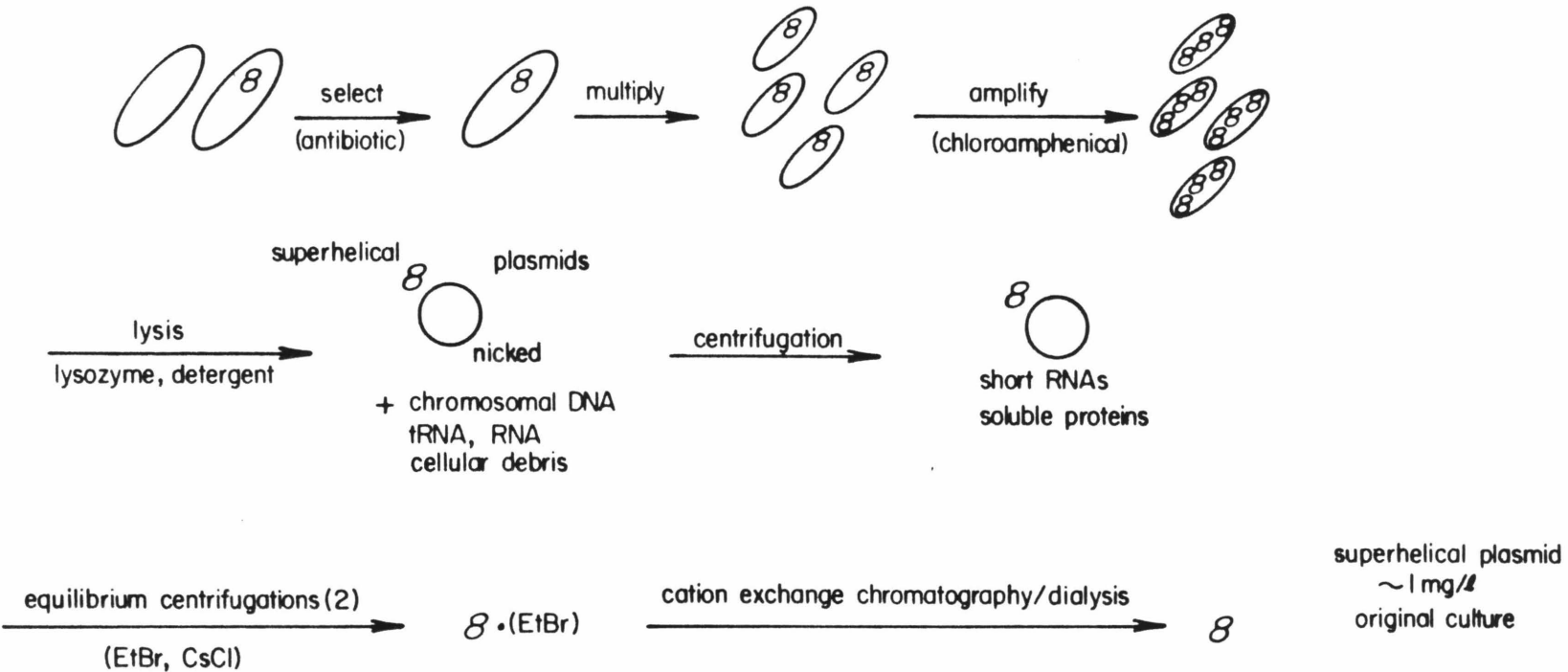
Isolation of individual colonies: Plasmid containing bacterial hosts provided in soft agar stabs were streaked onto antibiotic containing agar petri dishes in such a fashion as to obtain isolated single colonies. pBR-322 was selected on 35  $\mu\text{g/ml}$  ampicillin and 15  $\mu\text{g/ml}$  tetracycline containing plates. pLJ3 was selected on 15  $\mu\text{g/ml}$  tetracycline plates. pLP32 was selected on 50  $\mu\text{g/ml}$  ampicillin plates. Streaked plates were incubated at 37°C overnight. An individual colony was transferred to a flask containing one quarter its volume in sterile rich media without antibiotics and incubated overnight at 37°C in a shaker. This constituted the starter broth.

Amplification of plasmids: Bacterial hosts containing selected plasmids were grown at 37°C in minimal media until reaching an optical density (at 590 nm) of 0.7-0.9. Thereupon chloroamphenicol (Chloromycetin Sodium Succinate, Parke-Davis) was added to a concentration of 200  $\mu\text{g/ml}$  and flasks were allowed to continue shaking at 37°C for an additional 12 h. Bacteria were then harvested by centrifugation at 8000 rpm for 15' at 4°C in a Sorvall rotor.

Extraction and purification of plasmids: Bacteria was lyzed by the Triton X-100 method (see Practical Protocols). Plasmid containing

Figure 65

### E. coli Plasmid Preparations



supernatant was made to a density of  $\rho = 1.55$  with solid CsCl and 400  $\mu\text{g/ml}$  ethidium bromide. Equilibrium centrifugation was achieved after spinning in a Ti70 rotor at 40,000 rpm for 48 h at 14°C. Bands were visualized by long-wave UV irradiation and isolated by peristaltic pumping. The lower, denser band constituted the desired superhelical material and saved. The equilibrium centrifugation procedure was repeated once more to minimize random RNA contamination. Ethidium bromide was removed by passage through a Dowex 50W-X4 cation exchange resin equilibrated to pH 8.

Plasmids were dialyzed exhaustively against TNE buffer (10 mM Tris [pH 7.4], 50 mM NaCl, 1 mM EDTA). Concentration was determined by absorbance at 260 nm ( $\epsilon = 11800$  per mole base pairs).

#### Preparation of Restriction Fragments

Site specific cleavage of DNA by restriction endonucleases was employed in two circumstances. First, to prepare a selected site or sites on a plasmid for radioactive end labeling. Second, to unevenly divide a DNA restriction fragment labeled on both its 3' (or 5') ends so as to obtain singularly end-labeled DNA fragments suitable for Maxam-Gilbert sequencing and footprinting. Restriction endonucleases used in the first case included Bam HI, Eco RI, and Nar I; for the second case, Eco RI, Eco RV, Hae III, Rsa I, and Sal I.

All endonucleases were obtained from New England Biolabs. Digestions were performed following the manufacturer's instructions.

A table of the DNA restriction fragments which were utilized in the course of this thesis work is presented (Table VII). Included is such data as their lengths, strand which is labeled, plasmid of origin, restriction sites of both ends, and each fragment's relative importance. Figure 66 shows the locations of these fragments on their respective plasmids. Throughout this thesis a particular DNA restriction fragment will be referred to by its length. For all restriction fragments herein described, their nucleotide sequences have been previously determined (pBR-322,205 pLJ-3,206 pLP-32.176. Sequences for those regions investigated by footprinting are listed with both their respective histograms and corresponding site determinations.

#### End-labeling of DNA Restriction Fragments

Singularly end-labeled DNA fragments, usually radiolabeled with  $^{32}\text{P}$ , are the basic substrate for Maxam-Gilbert sequencing and allied footprinting protocols. Through the judicious use of restriction endonucleases and labeling procedures, regions of particular interest on a plasmid may be rendered suitable with a minimum of manipulation.

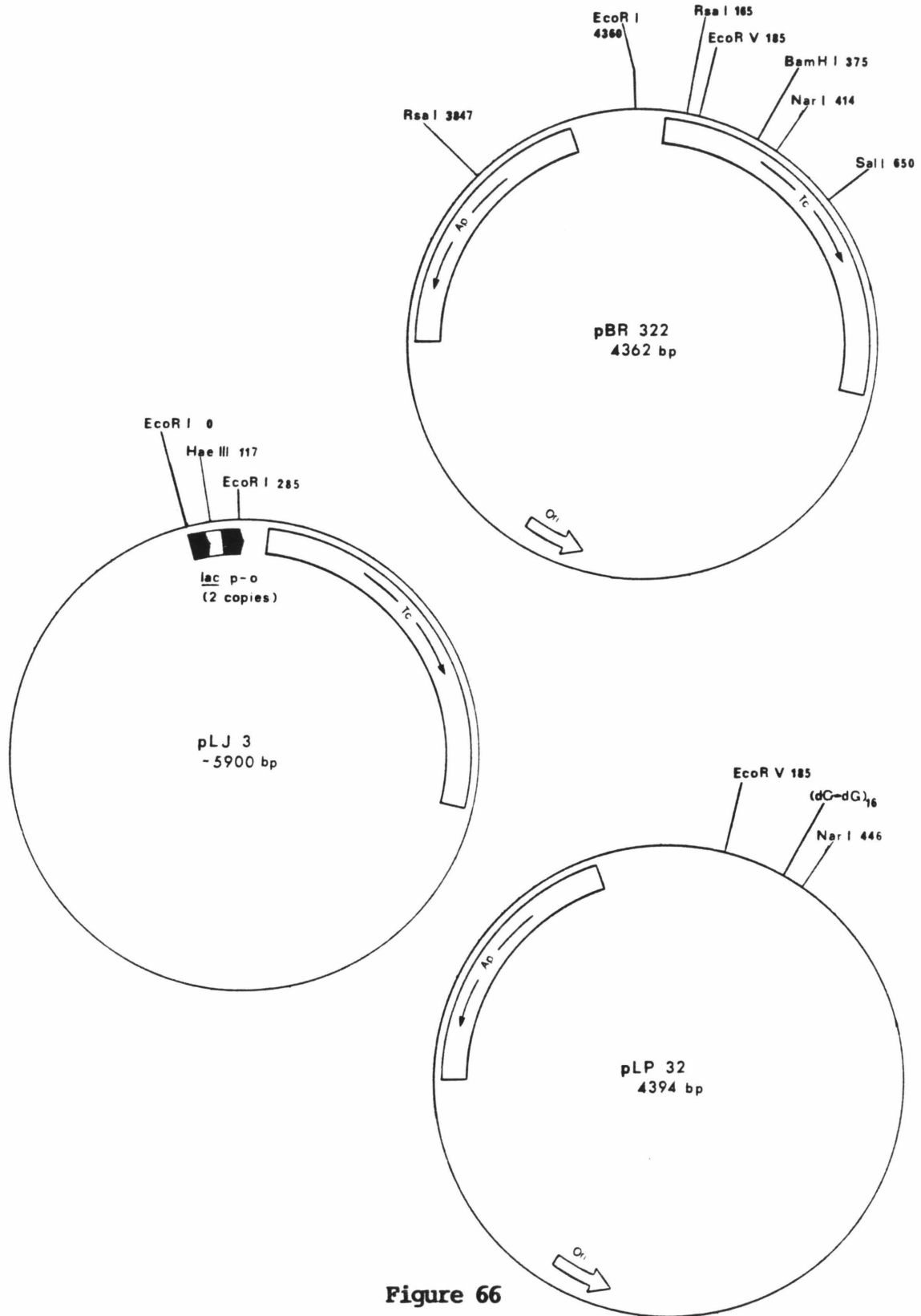
Initially to avoid any predisposed bias, fragments which were conveniently accessible were investigated. Usually this entailed an initial cleavage at a specific single site on a plasmid. After radiolabeling the proper ends of the linearized plasmid, a second restriction digest would render the whole plasmid into three or more dissimilar fragments, two of which being singularly end labeled. Ideally the two radiolabeled fragments should differ in length by greater than 10% for optimum resolution by gel electrophoresis, and have

Table VII DNA Restriction Fragments Serving as Substrates for Footprinting Assays

Length (base pairs)	End Labeled	1st digest*	2nd digest	Parent Plasmid	Other
378 382	5' 3'	Bam HI	Eco RI	pBR 322	contains portion of tetra- cycline resistance gene
274 <sup>+</sup> 278	5' 3'	Bam HI	Sal I	pBR 322	contains portion of tetra- cycline resistance gene
517	5' or 3'	Eco RI	Rsa I	pBR 322	contains long stretches of AT rich sequences with 200 bp of label
167	5' or 3'	Eco RI	Rsa I	pBR 322	contains both P1 and P2 (tet) transcription promoters
168 117	5' or 3' 5' or 3'	Eco RI	Hae III	pLJ 3	contains copy of <u>lac</u> operon used in complementary strand analyses
259	3'	Nar I	Eco RV	pLP 32	pBR 322 with a 32 bp 5'-(CG) <sub>16</sub> -3' insert at the Bam HI site. used in Z conformations studies
227	3'	Nar I	Eco RV	pBR 322	control for 259 bp experiments

\* Restriction Site Labeled

<sup>+</sup> 274/278 base pair restriction fragments are actually 276/280 bp.



**Figure 66**

Restriction enzyme map of the plasmids pBR 322, pLJ 3, and pLP 32. Map is limited to restriction fragments studied.

lengths between 100 and 500 base pairs for maximum recovery by standard elution methods.

3' end-labeling:  $\alpha$ - $^{32}\text{P}$  labeled nucleotide triphosphates and the large fragment of DNA polymerase I were used to fill in "sticky" restriction sites. Reaction conditions employed are those of Jacobsen et al.<sup>207</sup>

5' end-labeling: Enzymatically cleaved DNA with overhanging 5' ends had their terminal phosphates removed by the action of bacterial alkaline phosphatase. After protein removal and an ethanol precipitation, a radioactive label was placed on the 5' end by the action of polynucleotide kinase and high specific activity [ $\gamma$ - $^{32}\text{P}$ ]ATP. Procedure was from Chaconas and van de Sande.<sup>208</sup>

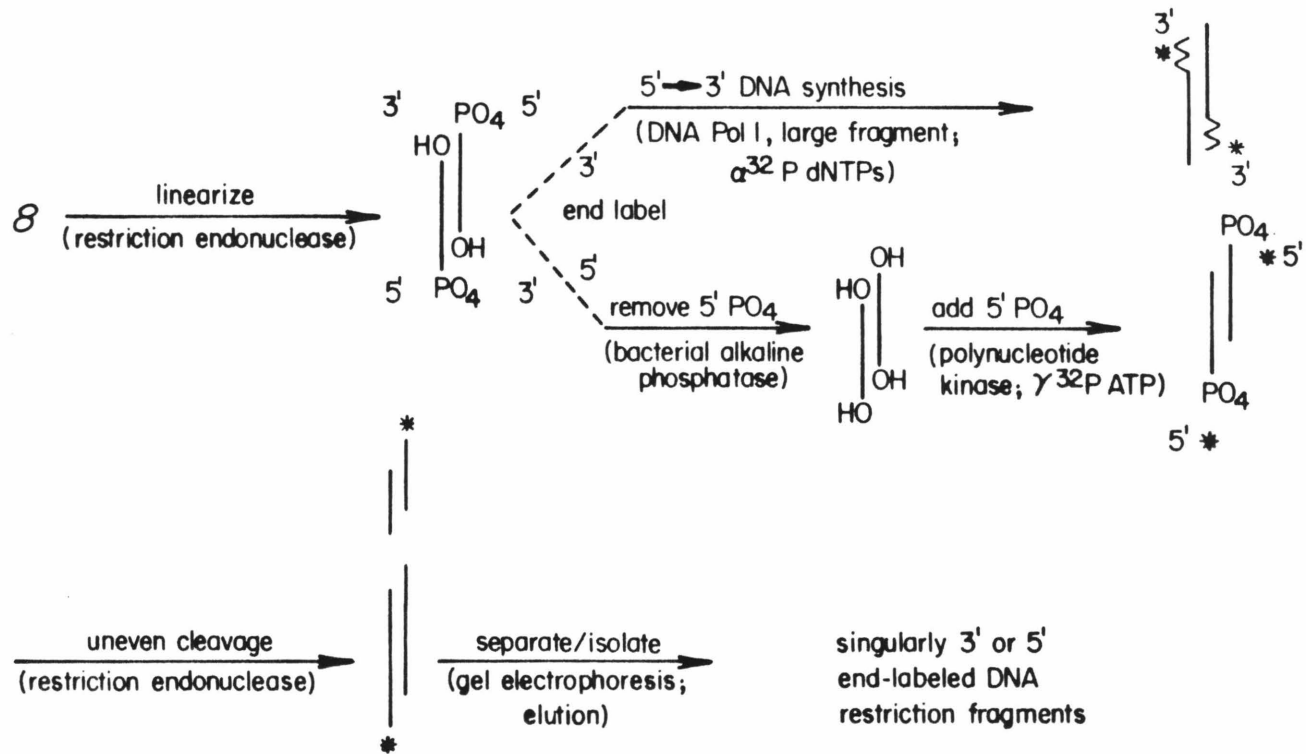
A flow chart describing the process from whole plasmid to radioactively end-labeled DNA restriction fragment is shown in Figure 67. Generally the steps are initial restriction digest, end labeling, second restriction digest, purification by gel electrophoresis and elution from gel matrix. Protocols for these individual steps may be found in Methods in Enzymology, Maxam and Gilbert,<sup>35</sup> or in the Molecular Cloning laboratory manual.

#### Maxam-Gilbert Sequencing

To determine the locations of alterations in an otherwise uniform cleavage pattern due to the sequence specific binding of small molecules, lanes containing base-specifically cleaved DNA fragments need to be run in parallel on high resolution gel electrophoresis. Since our

Figure 67

### END LABELING



substrate for footprinting was double-stranded, heterogeneous DNA, a chemical means of DNA sequencing was chosen. Initially four Maxam-Gilbert reactions (G, A>C, C, C+T) were employed to verify the literature sequences for the particular fragments investigated. On later experiments only a G-specific reaction was used in conjunction with the uniform MPE cleavage ladder as site markers.

Reaction conditions used in sequencing follow the methods of Maxam and Gilbert without change.

**Reagents:**

Methidiumpropyl-EDTA (MPE)

MPE is the DNA cleaving agent employed in MPE footprinting. 1 mg of the > 99% pure material was the generous gift of R. Hertzberg. Source of ferrous ion was  $\text{Fe}(\text{NH}_3)_2(\text{SO}_4)_2 \cdot 6\text{H}_2\text{O}$  [Fe(II)] {Baker reagent grade}, freshly dissolved in twice distilled  $\text{H}_2\text{O}$ . Prior to 7-82 (the complementary strand analyses of **chr**, **mit**, and **olv**) DNA cleavage was initiated by the simultaneous, separate additions of aqueous solutions containing MPE, Fe(II), followed by a reducing agent such as dithiothreitol (DTT) {Calbiochem}. After this time it was discovered that a pre-made MPE·Fe(II) complex was far more efficient in promoting DNA cleavage when DTT was present. A simplified procedure for making and storing the MPE·Fe(II) complex is presented in the Practical Protocols. Other than the autoradiograms presented in Figures 15-20, and 36 all other autoradiograms shown in this thesis used the improved method of MPE·Fe(II) preparation.

### Small Molecules Investigated by Footprinting

Small molecule is a generic term used in defining the assortment of substances investigated by MPE and DNase footprinting assays. Included in this series of DNA binding molecules are antitumor, viral, and bacterial antibiotics, drugs employed in combating trypanosomal, malarial, and other protozoal parasites, dyes, and miscellaneous other compounds. A list of those small molecules investigated as potential footprinting candidates is provided (Table VIII). Listed are their names, abbreviations used in this text, and the sources supplying these materials. Information concerning their interactions with DNA, together with their chemical structures, was presented in the introduction section of this thesis.

All small molecules were footprinted as obtained from the supplier, without further purification. The only exception was mithramycin (Sigma) which was supplied as a mixture of mannitol, sodium phosphate, and 2.5% antibiotic. This was purified by precipitation with 95% ethanol containing 2.5 mM each  $Mg(OAc)_2$  and  $CaCl_2$ , followed by additional salt-free ethanolic precipitations, until no white solids were observed.

Those small molecules which eventually exhibited footprints had their purities verified by thin-layer chromatography (TLC). This was performed to insure that no contaminants which might later be proven the actual cause of the footprinting were present. A list of these molecules, together with their solution compositions, molar absorptivities, and TLC conditions is provided (Table IX).

Table VIII: Small Molecules Investigate by Footprinting

<u>Name (abbreviation)</u>	<u>Source</u>	<u>Figure</u>	<u>Reference</u>
<b>Intercalators</b>			
<b>Anthracyclines:</b>			
adriamycin (adr)	Sigma	10	123
daunomycin (dau)	Calbiochem	7	58
7-con-O-methylnogarol (ngr)	Upjohn	10	129
nogalamycin (nog)	Upjohn	10	129
<b>Phenanthridines:</b>			
bismethidiumspermine (BMSp)	M. Becker, CIT	13	142
<b>Acridines:</b>			
proflavine (pro)	Sigma	13	152
<b>Phenoxazones:</b>			
actinomycin D (act)	Merck	7	78
<b>Tilerones:</b>			
2,7-bis(dimethylacteyl) fluorene•2NCl (002)	Sigma	12	132
3,6-bis[2-(dimethylamino)- ethoxy]-9H-xanthone-9- one•2HCl (874)	Sigma	12	132
2,6-bis[2-(dimethylamino)- ethoxy]-anthraquinone• 2HCl (043)	Sigma	12	132

Quinoxalines:

echinomycin (ech)	National Cancer Institute	9	114
Triostin A (tri)	R.K. Olsen, Utah State	11	130
Tandem (tan)	R.K. Olsen, Utah State	11	115
[Ala <sup>3</sup> , Ala <sup>7</sup> ]			
Tandem (285)	R.K. Olsen, Utah State	11	131
[L-Ser <sup>1</sup> , L-Ser <sup>5</sup> ]			
Tandem (206)	R.K. Olsen, Utah State	11	115

Bisthiazoles:

N-acetylbleomycin (ableo)	S. Hecht, U Virginia	13	137
---------------------------	----------------------	----	-----

**Nonintercalators**

Chromomycinone:

chromomycin A <sub>3</sub> (chr)	Calbiochem	8	101
mithramycin (mit)	Sigma	8	101
olivomycin (olv)	Calbiochem	8	101

Oligopeptide N-methylpyrroles:

netropsin (net)	D. Patel, Bell Labs.	7	86
-----------------	----------------------	---	----

distamycin A (dis)	Boehringer Mannheim	7	86
Other minor groove binders:			
berenil (ber)	Calbiochem	13	86
methyl green (MG)	Sigma	13	148
Miscellaneous:			
irehdiamine A (ire)	M. Becker, CIT	13	145
streptomycin (str)	Calbiochem	13	153

Table IX Solution Characteristics of Footprinted Molecules

Name	Solution Composition *	Molar Absorptivity	TLC Conditions
actinomycin D	50:50 H <sub>2</sub> O:EtOH	$\epsilon_{425} = 23500$	5% HOAc: on silic 5% MeOH:CH <sub>2</sub> Cl <sub>2</sub>
Netropsin distamycin A	H <sub>2</sub> O	(net) $\epsilon_{296} = 23400$ (dis) $\epsilon_{303} = 37000$	4% conc. NH <sub>4</sub> OH : MeOH on silica
chromomycin mithramycin olivomycin	[ 50:50 H <sub>2</sub> O = EtOH with twice molar excess MgCl <sub>2</sub> ]	$\epsilon_{410} = 11500$	10% iprOH:CH <sub>2</sub> Cl <sub>2</sub> on silica
echinomycin	THF	$\epsilon_{320} = 11500$	20% hexane:THF on silica

\* 1  $\mu$ l solution was added to aqueous solution

## Reactions:

### Methidiumpropyl-EDTA Footprinting

The partial cleavage of small molecule-protected, [<sup>32</sup>P] end-labeled DNA restriction fragments is the basis behind MPE footprinting. MPE, in the presence of ferrous ion, molecular oxygen, and a reducing agent induces single-stranded cleavages in double stranded DNA efficiently and with minimal sequence specificity. Discussed here are the conditions employed in these reactions during the course of this work.

Initially<sup>169,170</sup> footprinting reactions were performed at high drug:base pair ratios {1:4 to 4:1} for such antibiotics as **act** and **dis** 200  $\mu$ M bp DNA was buffered at twice its normal salt concentrations {20 mM Tris·Cl [pH 7.4] and 100 mM NaCl} and incubated at room temperature in the dark for typically 30 min with sufficient antibiotic for a total volume of 5  $\mu$ l. After this equilibration period MPE, Fe(II) and DTT were added to give final concentrations of 10  $\mu$ M, 10  $\mu$ M, and 4 mM, respectively in a final volume of 10  $\mu$ l. Reactions took place at 37°C over 15 min. Termination of reaction was done by freezing samples in dry ice and lyophilization. Banding results after gel electrophoresis and autoradiography are shown in Figures 15,19,20 and 36.

Later it was discovered that a pre-formed MPE·Fe(II) complex was more efficient at cleaving DNA.<sup>171</sup> Typical cleavage protocols of this time period entailed concentrated buffered DNA and antibiotic to be equilibrated at room temperature for 30 min, followed by addition of MPE·Fe(II) and DTT to final concentration of 10 mM Tris·Cl [pH 7.4], 50 mM NaCl, 100-200  $\mu$ M bp DNA, 4 mM DTT, 6-100  $\mu$ M antibiotic, and 10  $\mu$ M

MPE•Fe(II). Cleavage and work-up followed earlier procedures. Examples of this genre may be seen in Figures 24,25 and 49.

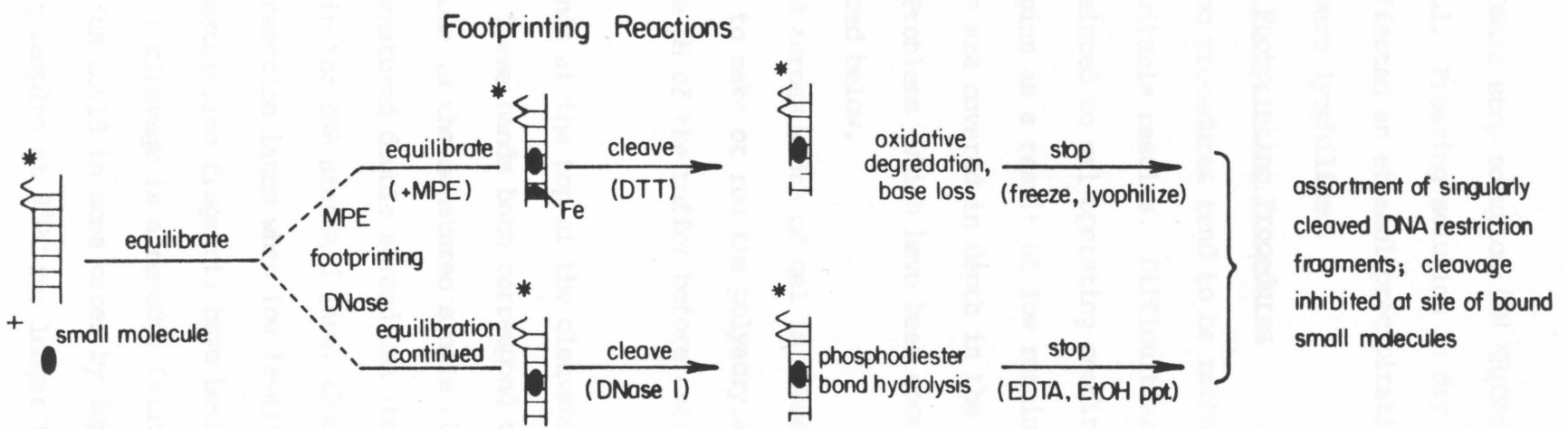
The optimal protocol was devised after attempts were made to improve the appearance of act footprints. Antibiotics were first equilibrated with buffered DNA in 8  $\mu$ l total volume for a period of 15 min at room temperature. Then 1  $\mu$ l of a 100  $\mu$ M MPE•Fe(II) solution was added, with competitive equilibration proceeding for 15 min at either room temperature or elevated temperature, depending on the binding kinetics of the particular antibiotic. Cleavage was initiated upon the addition of 1  $\mu$ l 40 mM DTT and continued at 37°C for 15 min until termination by freezing in dry ice and lyophilization. A generalized protocol is provided in the Practical Protocols. All other autoradiograms other than those previously listed followed this optimal procedure.<sup>172,173</sup>

#### DNase I Footprinting

DNase I footprinting is a complementary means of determining the binding sites of molecules (esp. proteins) on natural DNAs. Developed by Galas and Schmitz,<sup>41</sup> it was first applied to small molecules by Lane et al.<sup>164</sup> As a comparison against MPE•Fe(II) footprinting, I have employed a simplified modification of Galas's technique which insures singlet-hit kinetics. A step-by-step protocol is provided in the Practical Protocols.

A 9  $\mu$ l solution containing buffered DNA and antibiotic is allowed to equilibrate for 30 min at room temperature. Cleavage is initiated upon addition of 1  $\mu$ l of a 2  $\mu$ g/ml DNase I and 1 mM DTT solution. Reaction is quenched after 30 sec at room temperature with

Figure 68



the addition of 2.5  $\mu$ l DNase stop solution {3M  $\text{NH}_4\text{OAc}$  and 0.25M EDTA} followed by 40  $\mu$ l ethanol. Freezing solution in dry ice followed by a 10 min centrifugation effected an ethanol precipitation. 10  $\mu$ l  $\text{H}_2\text{O}$  was then added and samples were lyophilized.

#### Troubleshooting Footprinting Procedures

Both footprinting procedures tend to be rather straightforward and generally provide suitable results. Difficulties which are usually encountered are often related to gel operating conditions: band compression due to hairpins as a result of low running temperature, for example. These problems are covered in depth in the Methods in Enzymology article.<sup>37</sup> Problems which have been encountered in this thesis work, are described below.

1. A black band across width of gel is observed when the pH of tris-borate buffer used to make or run the polyacrylamide gel falls below pH 7.8. Check the pH of the buffer before use; it should be optimally pH 8.3.

2. Two dark bands at the top of the cleavage pattern (instead of one) are observed. These bands both correspond to the uncleaved complete DNA fragment, one is the denatured single stranded material (top) and the other undenatured double strand DNA (bottom). This is almost always observed in the DNA standard lane, though it also will appear in MPE or DNase reaction lanes when low levels of cleavage (less than one cleavage per restriction fragment) have been performed. While increasing MPE or DNase I cleavage is a remedy, failure to adhere to less-than-one-hit kinetics could in some cases be important. Incubating the formamide-containing samples at 90°C for longer than 90 sec, or

increasing the percentage of formamide from 50 to 80% sometimes helps reduce the amount of double stranded material present.

Often it is sufficient to merely reduce the separation between the denatured and undenatured bands to allow for information from a particular region on the DNA to be investigated. The variables which control this separation are unknown, therefore it may be necessary to repeat the gel electrophoresis until adequate results are obtained. See Figure 58a-f for examples.

3. No dark band at top of cleavage ladder indicates that excessive cleavage by MPE•Fe(II) or DNase has resulted. Should be most evident in MPE or DNase control lanes. The best remedy is to reduce the concentration of the cleavage agent present. In addition reductions in temperature or time have also been found effective.

Though excessive cleavage by MPE•Fe(II) or DNase, resulting in greater than one-hit kinetics {more than an average of one cleavage per labeled strand} has been advised against, empirically it has been found of little consequence in so far as defining the locations and sizes of molecule binding sites on DNA (see Figure 58d and e for comparisons).

4. Diffuse bands sometimes appear which grow darker with increasing age of the DNA sample: three bands usually appear at lengths corresponding to 25-26 bp, 29-31 bp, and 54-56 bp from the end-label on 8% polyacrylamide gels. They appear about two weeks after a DNA fragment has been 3' end labeled. The cause is unknown, but they are believed to be degradation products of the DNA after one radionuclide at a multiple labeled 3' gap filled end has decayed. Those bands which run faster (~ 25 and ~30 bp) may be eliminated if each sample is

individually ethanol precipitated prior to gel electrophoresis, as is done with DNase reactions. Otherwise the footprints need to be electrophoresed longer, i.e. until the offending bands have run off the bottom of the gel. It should be noted that the slower moving band ( $\sim 55$  bp) grows in far slower than the faster one (see Figure 24 for example).

5. Bands sometimes exhibit a chevron-like appearance, especially towards the bottom of the gel. This altered band shape, most evident in shorter (15-20 bp) DNA fragments, may also be observed in the bromophenol blue dye front while electrophoresing. This phenomenon is observed in situations where a large concentration ( $> 100$  mM) of salt was present in the reaction when electrophoresed. The altered band shape is believed to be caused by the presence of an ionic "bubble" before the bands, having the effect of perturbing the otherwise uniform potential gradient of the gel. The problem may be avoided by removing the excess salt by an ethanol precipitation prior to electrophoresis, as in the case of DNase reactions.

6. We believe that weak, indistinct footprints are indicative of some degree of sequence specific binding on the part of the small molecule, but such is insufficient to fully inhibit MPE or DNase cleavage at the same site on other DNA strands. Such may be the case if an insufficient concentration of small molecule is present, or if those small molecules which are present have experienced insufficient time to equilibriate at their optimal binding sites. The first case may be rectified by increasing the drug:bp ratio; the latter by either increasing the equilibrium period or its temperature. In some situations neither method will improve the appearance of a footprint.

These are then defined as weak binding sites.

7. Very large footprints not discernable as individual discrete drug binding sites occur when a sufficiently high concentration of drug was bound to the DNA at a number of adjacent sites such that a cleaving molecule like MPE or DNase would have no accessible cleavage sites present. This is more apt to occur in cases of DNase footprinting since this larger molecule appears to demonstrate larger footprints than MPE. In MPE footprinting, these large footprints are often observed at elevated binding ratios (1:4 bp or greater) of the minor groove binders **dis** and **net**. See Figures 15, 20 and 58d for examples. With MPE·Fe(II) footprinting this effect is usually minimized by reducing the amount of inhibiting drug present. With DNase footprinting this answer often has the effect of eliminating whole footprinted regions instead of the desired improvement in resolution.

8. Complete omission of cleavage might be the inactivation of the cleaving reagent either by the inhibiting small molecule or by its solvent carrier. This was observed in the case of quinoxalines dissolved in DMSO, a known radical scavenger. Changing to THF as cosolvent allowed the footprinting of **ech** by MPE.

9. The MPE·Fe(II) cleavage control lane in some cases shows a footprinting pattern. This is observed for DNA fragments whose sequences contain long stretches which are either uniformly G+C or A+T rich. The methidium chromophore is known to exhibit a modest G·C preference in its site of intercalation. While increasing amounts of radiolabeled DNA per band might obscure this observation, it is best to use this MPE cleavage pattern as a control against which small molecule

footprints are compared. This is known as the subtraction method of generating footprint histograms and is described later in the Experimental.

#### **Resolution of Data:**

##### Gel Electrophoresis and Autoradiography

Denatured samples in a formamide buffer were loaded onto high resolution polyacrylamide gels and electrophoresed, following the procedures of Maxam & Gilbert. Generally a 0.4 mm thick, 40 cm long, 8% polyacrylamide, 1:20 crosslinked sequencing gel containing 50% urea by weight was employed. This is capable of resolving approximately 100 nucleotide from the bottom of the gel, usually beginning 20 nucleotides from the labeled end when bromocresol purple is used as a marker. Electrophoresis was carried out between 1000 and 1250 V for 3 to 3.5 hr, voltage being kept constant throughout. Higher voltages tend to induce an undesirable curvature to the lanes, a phenomenon known as smiling.

Autoradiography was the means by which information such as fragment lengths and quantities was recorded. Initially sequencing gels, one glass plate removed and covered with a plastic wrap, were placed in intimate contact as a gel-film-intensification screen sandwich and left to expose at  $-60^{\circ}\text{C}$  overnight. The image obtained, was not of suitable quality for densitometric analysis or publication. Use of intensification screens, a calcium-tungstate containing phosphor, increases contrast and reduces resolution of bands. To generate a suitable autoradiogram it was necessary to carry out the autoradiography without intensification screen for a 10 times greater period of time, usually five days.

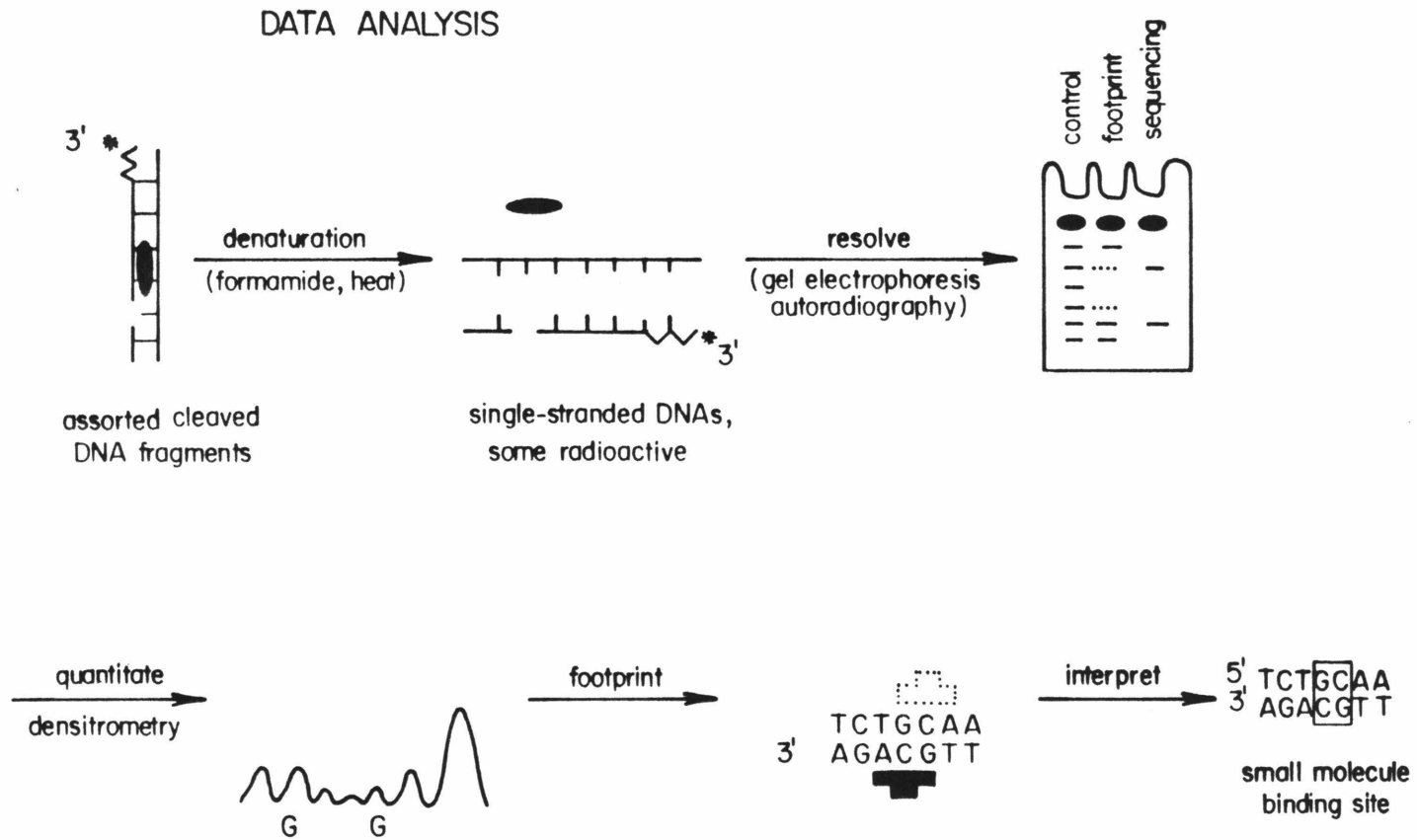
The film used was Kodak X-Omat AR, developed as per the manufacturer's instructions. The intensification screens used were Dupont Cronex Lightning-Plus, with writing-side placed against film.

#### Densitometry

Since the amount of DNA fragments of a particular length reflects the efficiency of cleavage at the site of its unlabeled end, and if one assumes that the efficiency of cleavage is directly proportional to the likelihood of MPE binding near the eventual cleavage sites, given that each DNA fragment has an equivalent amount of radiolabel, regardless of length, it should follow that under conditions of linear film response a measure of an autoradiogram band density in absorbance is a measure of how effectively MPE binding is inhibited near this site when compared with the same DNA fragment length band density in an MPE cleavage control experiment.

An 8 x 10" reduction was shot of the entire autoradiogram, and a contact positive was made of this negative on Kodak sheet film. A trimmed version of this copy positive was loaded into the Cary 219 spectrophotometer and scanned at 485 nm with an incident beam collimated to 0.2 mm utilizing the accompanying Master gel scanning program (Varian, 1981) and Apple microcomputer. Film base was arbitrarily set to  $A < 0.01$ . Usually a 150 mm length of each lane was scanned, this taking 12.8 min to complete. Data were visualized after scanning on the Apple CRT and absorbance limits were set at 0 and 0.9. Data were usually thermally printed in three separate 50 mm sections, these being pasted together later on. Examples of the final product, a complete densitometer scan of a given reaction lane, are seen in Figures

Figure 69



16,21,26, and 32.

### Footprints and Interpreting Binding Sites

Footprints appear as lightened regions in an otherwise uniformly dark cleavage pattern; quantification of their relative lightness is obtained by densitometry. The basis against which this quantification is made translates into the type of footprinting histograms derived, ultimately impacting on the interpretation of the preferred binding site. This section of the experimental defines the rationale behind the derivation of footprinting histograms and the interpretation of binding sites. The pros and cons of the various methods are discussed; references are made to those instances where personal bias has been incorporated. An example of the various steps employed in an ideal case of footprint determination and binding site interpretation is provided and follows the actual data presented in Figure 31, lane 14.

After densitometry, the data exist as a computer generated, dot-matrix plot of the film's absorbance as the y axis against the length of copy autoradiogram scanned as the x. If this is a scan of an MPE cleavage control lane performed at cleavage levels less than an average of one cleavage per strand on a DNA fragment containing no long stretches of either G+C or A+T rich base pairs, the resultant plot should show a series of up to 100 well-resolved peaks all with nearly uniform height. If a small amount of a DNA-binding ligand were also present in the original cleavage reaction, and this ligand exhibited a site-preferential inhibition of MPE-mediated DNA cleavage, then the product densitometer scan should be observed to contain peaks of non-uniform height, with regions of diminished intensity corresponding

to the lightened regions on the scanned copy autoradiogram. The quantification of these reductions in height for a series of neighboring peaks serves to delineate both the size and intensity of a footprint. Quantification is achieved by measuring the height differences between the peaks within a footprint and some basis of average anticipated MPE cleavage, whether defined by neighboring peak heights as in the "well" method or by an MPE cleavage control as in the "subtractive" method of footprint determination. Both methods are herein described.

The "well" method of footprint determination was the first employed and has been applied to all data present in this thesis except for the work involving echinomycin. This method is based on the premise that the average MPE cleavage pattern is perturbed by the simultaneous presence of inhibiting small molecules, even in regions where MPE cleavage continues to occur. For example, reduction in the number of available MPE cleavage sites should increase the average band intensity for those remaining regions still accessible to cleavage. Thus the most reasonable measure of anticipated MPE cleavage at a footprint would be a line defined by the average peak heights in the regions surrounding the footprint. An example is shown in Figure 70.

Measuring the differences in absorbance density between this imaginary line and the peaks within the footprint should provide the data necessary for generating the eventual histogram footprints as depicted throughout this work.

The other method of footprint determination, the "subtractive" method, is more recent. Here the scan from the MPE cleavage control lane which was run in parallel with the footprinting containing lane in

question serves as the basis for comparison. The assumption that cleavage intensities change on the average as number of MPE binding sites decreases is also assumed in this method. The only rejoinder is that relative cleavage intensities between different sites, as seen in the slight G·C vs A·T preference of MPE cleavage, is conserved regardless of the number of MPE binding sites present. Thus the MPE cleavage standard provides the best basis of comparison for increasing footprint-induced cleavage diminution. Such reasoning was employed in deriving the echinomycin footprints, Figures 48,51,52, and 53.

Of the two methods for footprinting determination, both have their merits and shortcomings. The "well" method allows the addressing of all lightened regions, even those flanked by regions of enhanced MPE cleavage, as footprints. Given a slanted basis line, allowances can be made in situations of overdigestion. The subtractive method is more accurate in the determination of size limits on a footprint, being less susceptible to labeling regions as footprints when they also appear in the MPE control lane. Perhaps the best procedure is to employ both methods, the "subtractive" one to define the footprint's limits and the "well" method for quantitation, when determining a footprint. An example of a comparison between the two methods is seen in Figure 70.

It may be noted that the typical footprinting histogram appears smaller in size than the densitometer scan would indicate. Earlier on in this work, each footprint present in a densitometer scan was visibly compared with its parent image in the original autoradiogram. There its size was made to conform to the number of bands present in the autoradiogram that were sufficiently lightened to be easily noticeable

upon inspection. This was equivalent to dropping the basis line halfway to the bottom of the "well". This first stage of interpretation, known as the half-maximal treatment, includes only those peaks defined as part of the footprint by the well method whose height diminution is greater than half that exhibited by the lowest peak. It may be rationalized that the slight cleavage inhibition observed adjacent to the actual small-molecule binding site is the result of a diminished hydroxyl radical flux at the cleavage point due to the absence of a contribution by an MPE molecule which could have been bound in place of the inhibiting small molecule. Subtracting out this effect should provide a more accurate representation of the true small-molecule binding site. The half-maximal interpretation was employed in the making of the footprint histogram shown in Figure 71 as an example.

Having determined the size and shape of a footprint by either method, it is necessary to locate this cleavage data on a particular DNA sequence. Working with DNA fragments of known nucleotide sequence, only a Maxam-Gilbert G lane electrophoresed in parallel is needed. By identifying each of the peaks in a scan, it is possible to translate the measurements for the "well" into blocks of varying height over a DNA sequence, generating the footprint histograms seen throughout this work. See also Figure 71. Earlier footprints were of an angular nature, they being contrived by "connecting-the-dots" where each value was the difference in peak height. Since each peak corresponds to a single nucleotide, their height differences with the basis are for discrete units and are probably most accurately described by a block histogram.

Given histograms on both strands of a DNA sequence, it is

possible to interpret the preferred binding sites for a small molecule. On first observation it should be noted that most of the footprint pairs are asymmetric displaced 2-4 nucleotides towards the 3' sides. From this finding and subsequent CRK model building we devised the "asymmetric model" for interpreting footprints, where the footprint is shifted at least one base pair to the 3' side of the inhibiting molecule binding site.<sup>170</sup> This is shown graphically in Figure 18. Assuming that MPE generates a hydroxyl radical a diffusible species the density of the ultimate cleaving species is inversely proportional to the distance separating the generating moiety EDTA·Fe(II) and the substrate DNA, this same model could be derived from the fact that two spatially closest deoxyriboses susceptible to ·OH attack are displaced by two nucleotides towards the 3' end in the right handed DNA. Work performed by P. Schultz and P. Dervan with the distamycin-derived affinity cleaving molecule DE·Fe(II) confirm this displacement, measuring it as showing footprints being 2 nucleotides overprotected on the 3' end and one nucleotide underprotected on the 5' strand for the actual five base pair binding site of distamycin.<sup>193</sup> This asymmetric model was applied on all small molecule binding site interpretations in this text, though the amount of overhang offset employed varied depending on the small molecule investigated.

When interpreting footprinting patterns containing multiple or overlapping binding sites, a certain amount of personal judgement is employed. Usually small definable individual binding sites serve as a guide to the nucleotide composition and binding site size. These are then applied to the larger footprints, aiding in their interpretation.

The determination of DNase I footprints and their interpretation as small molecule binding sites follow much the same procedures as those used for MPE·Fe(II) footprints. Here a subtractive method is used, the standard DNase I cleavage pattern itself exhibiting too great a variance in band cleavage intensity. Quantification of these subtractive differences is minimized, limited to defining those peaks exhibiting approximately 1/2, or greater than 3/4's cleavage inhibition. This simplification follows from the observation that DNase I footprints usually exhibit complete cleavage inhibition throughout the interior sequences of multiple closely spaced bound molecules. Subtraction of the nonspecific DNase cleavage standard would impose the differences in the DNase pattern on the footprint. From these footprints follow directly the assumed small molecule binding sites without further interpretation. This is fitting given the lack of knowledge as to how DNase I recognizes DNA perturbed by the sequence specific binding of a small molecule.

### **Practical Protocols**

#### **Lysis of E. coli, large scale preparation**

Lysis is the process of dissolving bacterial cell walls, thereby liberating the plasmids contained within. This method is quite gentle and results in very little shearing of plasmid DNA. Procedure is courtesy of J. Campbell (Caltech).

1. Resuspend the bacterial pellet from a 500 ml culture in 10 ml of a buffered sucrose solution {25% by weight sucrose, 50 mM Tris·Cl [pH 8.0]}. Transfer to a clean 50 ml beaker on ice.
2. Add 1.6 ml of a freshly prepared lysozyme solution {20 mg/ml

lysozyme, 0.25M Tris·HCl [pH 8.0]}. Stir gently by rotating the beaker. Let sit for 5 min at 0°C.

3. Add 3.2 ml of a 0.25M EDTA [pH 8.0] solution. Mix by rotation. Let sit for 10 min at 0°C.

4. Add 12.8 mls of a Triton X solution {10% Triton X-100, 60 mM EDTA [pH 8.0], 60 mM Tris·Cl [pH 8.0]} slowly with continual stirring by a glass rod. Solution will clear slightly, yet become increasingly viscous. Continue stirring for 15 min at 0°C to insure complete disruption of the bacteria.

5. Pour plasmid containing solution into polycarbonate centrifuge tubes (type #340382 Beckman) to a fill volume between 16 and 26.3 mls each. Tubes should weight within  $\pm 0.1g$  of each other to protect against rotor imbalance. **Caution:** the lysis solution acts like a non-Newtonian fluid which may exhibit self-siphoning phenomenon. Flow is best terminated by cutting the stream with a pair of scissors.

6. Place tubes opposite one another into a 70Ti rotor and centrifuge at 40,000 rpm for 60 min at 4°C. Rotor may be stopped with brake on.

7. Pour off and save supernatant. Plasmids contained in the supernatant will remain supercoiled for periods of several months when stored at 4°C.

#### **Preparation of methidiumpropyl-EDTA·Fe(II), [MPE·Fe(II)], solutions**

Methidiumpropyl-EDTA is the hybrid DNA binding/metal chelating molecule which, together with Fe(II) and dithiothreitol (DTT), cleaves DNA sufficiently for use in footprinting assays. Proper preparation and storage of MPE solutions insures high cleavage efficiency and

reproducibility over the longest solution lifetime.

Stock solutions:

1. Dissolve approximately 1 mg of  $\geq 99\%$  pure MPE in 250 doubly distilled  $H_2O_2$ . Molecular weight of R. Hertzberg's MPE preparations  $[MPE \cdot K^+ \cdot 4H_2O]$  is 785  $\mu g/mole$ . Concentration is best obtained by uv-vis spectroscopy. Molar absorptivities are  $\epsilon_{488} = 5994$  and  $\epsilon_{286} = 54,725$ , the former being preferred.

2. Dilute solution to 5 mM. This stock solution has an indefinite lifetime ( $> 4$  yr.) when stored frozen at  $-20^\circ C$  in the dark.

3. Purity may be ascertained by thin-layer chromatography on silica using a 4:1:2 solution of n-propanol, acetic acid, and  $H_2O$  as eluent.  $R_f$  is between 0.25 and 0.3. Spot appears fluorescent orange under long-wave ultraviolet irradiation. Typical impurities appear dirty brown under identical conditions and remain at the baseline.

Working solutions:

1. Prepare freshly a 10 mM  $Fe(NH_4)_2(SO_4)_2 \cdot 6H_2O$  [mol. wgt. 392.14, Baker reagent grade] by dissolving  $\sim 1$  mg in 255 twice-distilled  $H_2O$ . Store on ice.

2. To 2  $\mu l$  of MPE stock solution in a 450  $\mu l$  Eppendorf bullet vial, add 2  $\mu l$  of the above ferrous solution. Observe formation of a pink precipitate. Addition of 96  $\mu l$  twice distilled  $H_2O$  makes a 10  $\mu M$   $MPE \cdot 2Fe(II)$  working solution.

3. **Storage lifetimes of MPE working solutions are very temperature dependent!** It is always best to keep solution on ice when thawed, and to freeze in dry ice immediately after use. Solution lifetime, stored dark at  $-20^\circ C$ , is approximately 1-2 mo. Reduced

cutting efficiency is the first indication of MPE working solution degradation.

### **MPE Footprinting Reaction**

Listed here is a step-by-step protocol for performing a MPE footprinting reaction on a typical small molecule. This protocol consists of four steps: pre-equilibration, competitive equilibration, cleavage, and termination. The values stated here should only serve as a guideline. For example, each particular small molecule has its own optimum times and temperature for equilibration. Best results are often obtained through some trial and error.

1a. In a small bullet vial (450  $\mu\ell$ ) prepare the following buffered DNA solution (x times the number of reactions to be performed on a particular DNA fragment): 2  $\mu\ell$  2 mM (in base pairs) deproteinized calf thymus carrier DNA, 1  $\mu\ell$  10x TN buffer (100 mM Tris·Cl [pH 7.4], 500 mM NaCl), sufficient  $^{32}\text{P}$  end-labelled DNA to equal 1-3 mR/hr (= 3 x  $10^4$  cpm), twice distilled  $\text{H}_2\text{O}$  to make 7  $\mu\ell$  total. Aliquot 7  $\mu\ell$  to each reaction bullet vial.

b. To this is added 1  $\mu\ell$  of the particular small molecule to be investigated, dissolved in a suitable solvent {usually  $\text{H}_2\text{O}$ , ethanol, or THF, Never DMSO!} Typical concentrations range from 1 mM to 0.1 mM, producing final small molecule to base pair ratios on the order of 1:4 to 1:40. Remember to place 1  $\mu\ell$  of the solvent alone (without small molecule) in the MPE control reaction. All solutions are allowed to equilibrate at room temperature for 15 min.

2. 1  $\mu\ell$  of the 100  $\mu\text{M}$  MPE·2Fe(II) working solution is added to the above small molecule/DNA solution and allowed to competitively

equilibrate at room temperature for 15 min. For molecules with slow off rates, equilibrating at elevated temperatures often results in improved footprinting patterns.

3. To initiate cleavage, 1  $\mu\text{l}$  of a freshly prepared 40 mM dithiothreitol [DTT] solution is added to each reaction. Complete solution, 10  $\mu\text{l}$  final volume, is incubated at 37°C for 15 min.

4. Cleavage reactions are terminated by quickly freezing vial in dry ice and subsequent lyophilization. Samples are then ready for addition of a formamide buffer, heat denaturing, and loading on high resolution polyacrylamide gels, as described in the sequencing protocols of Maxam and Gilbert.

Rarely are any difficulties encountered in this procedure. If MPE cleavage levels are inadequate, a new working solution should be made. Cleavage levels are best optimized in the absence of inhibiting small molecules; optimal levels of cleavage being defined as one-hit kinetics. This is obtained when each band has roughly equivalent amounts of radioactive label present, and  $\sim 75\%$  of the label remains at the top.

#### **DNase I Footprinting Reaction**

This protocol is an adaptation of the procedure of Galas and Schmitz for footprinting proteins on DNA. Changes have been made with regard to volumes and work-up, attempting to keep the optimal reaction conditions of DNase I while simplifying the handling of multiple samples. Protocol consists of three stages: equilibration, cleavage, and work up. The values stated here for concentrations, times, and temperatures are less tolerant to variances than the MPE footprinting

conditions and should be considered optimal.

**1a.** In a small bullet vial (450  $\mu\text{l}$ ) prepare the following buffered DNA solution (x times number of reaction to be performed): 2  $\mu\text{l}$  2 mM base pairs deproteinized calf thymus DNA, 1  $\mu\text{l}$  10x TKMC (100 mM Tris·Cl [pH 7.9], 100 mM KCl, 100 mM MgCl<sub>2</sub>, 50 mM CaCl<sub>2</sub>); sufficient <sup>32</sup>P end-labelled DNA to equal 1-3 mR/hr (= 3 x 10<sup>4</sup> cpm); twice distilled H<sub>2</sub>O to make 8  $\mu\text{l}$  total. Aliquot 8  $\mu\text{l}$  above to each reaction bullet vial.

**b.** Same as **1b** in MPE footprinting protocol, except that equilibration is for 30 min at room temperature.

**2.** To initiate cleavage, 1  $\mu\text{l}$  of a 2  $\mu\text{g/ml}$  DNase I solution {equivalent to 1  $\mu\text{l}$  stock 1 mg/ml DNase I solution, Worthington DPFF, and 10  $\mu\text{l}$  50 mM DTT in 500  $\mu\text{l}$  twice distilled H<sub>2</sub>O, total final volume} is added. Sample is allowed to react for 30 sec at room temperature. Cleavage is halted upon addition of 2.5  $\mu\text{l}$  DNase stop solution {3M NH<sub>4</sub>OAc and 0.25M EDTA}, followed by 40  $\mu\text{l}$  ethanol.

**3.** Sample is placed on dry ice for 15 min, then centrifuged for 10 min in an Eppendorf microcentrifuge to effect precipitation of the DNA. Supernatant is pipetted off and discarded (check first to see if most radiation is in pellet and not in ethanol!). Pellet is resuspended in 10  $\mu\text{l}$  H<sub>2</sub>O, frozen, and lyophilized. Upon addition of formamide buffer and heat denaturing, sample is ready for gel electrophoresis.

#### **Densitometry Utilizing a Cary 219 Spectrophotometer**

Densitometry is the process by which band densities from an autoradiogram may be quantified, band densities being proportional to cleavage amounts. This process provides necessary information for the translation of a cleavage pattern into footprints. The protocol here

listed in compatible with the Cary 219 spectrophotometer and accompanying Master gel scanning program (1981, Varian Assoc. Rev. 0.0).

1. Autoradiogram is reproduced by Graphic Arts as an 8x10 in. copy positive. This is further trimmed to a length of 20 cm or less along the axis of eventual scanning.

2. Copy positive is placed into holder with top of gel toward end of scan and emulsion side (non-glossy) toward collimator slit.

3. Collimator slit width is set to 0.2 mm.

4. Cary 219 is set on single beam operation, visible light source (485 nm, 3.6 nm band width).

5. Continue by following instructions provided in program. Usually scan 150 mm length ( $\tau = 12.8$  min) with data stored in absorbance.

#### **Generating Histogram Footprints and Determining Binding Sites**

Conversion of densitometry scans into histogram footprints on a given sequence of DNA and their eventual interpretation as binding sites completes the process for determining the preferred small molecule binding sites on heterogeneous DNA as deduced by MPE cleavage inhibition. In practice all that is needed to achieve this is an autoradiogram containing a Maxam-Gilbert base specific, a cleavage control, and a footprinting experiment lane. Densitometer scans are made of the latter two lanes. Given these, and by following the protocol exemplified below, it should be possible to derive some understanding as to the sequence specificity of DNA binding for many small molecules.

1. Densitometric scans are made of both the MPE cleavage control lane and the footprinting, small molecule containing lane as previously described.

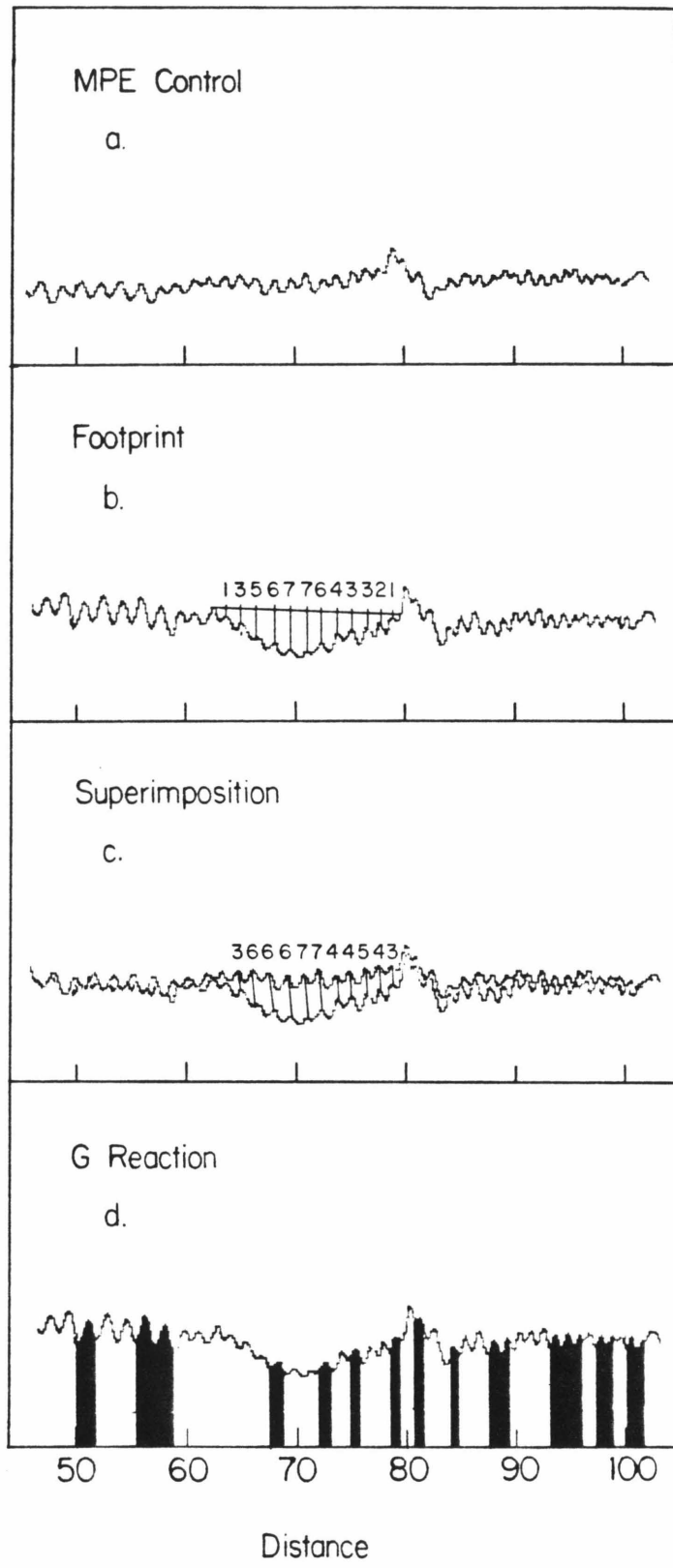
2. Using a straightedge, connect the tops of the peaks adjacent to the supposed footprinting site, such that the lines level corresponds to the anticipated average band density in the adjacent areas (see Figure 70b). Measure the difference in height from the peak top to this line and record. This method of determining footprints is called the "well method", since it is the measure of depth from an arbitrary level to the actual peak top in the well.

3. Alternatively, superimpose the footprint containing scan over the MPE cleavage control scan, usually performed with the aid of a light box. Measure the difference in height between these two sets of peaks and record (see Figure 70c). This method of determining footprints is called the "subtraction method", since it utilizes the original MPE cleavage control as its basis for cleavage inhibition quantification.

4. Given a Maxam-Gilbert G specific reaction lane on the autoradiogram as a set of markers, by reading across the lanes it is possible to determine which peaks on the densitometer scan correspond to termini ending just prior to a G nucleotide (see Figure 70a). Care must be exercised in making this comparison to take into account the differing mobilities of short DNA fragments ending in different termini. For example, a DNase I cleavage of the 5' end-labelled DNA fragment:

5' GTATCGA T ....

results in a 7 nucleotide long fragment heaving a 3'-OH terminus. A Maxam-Gilbert C+T reaction would excise out that final T, generating a 7



nucleotide long fragment having a 3'-PO<sub>4</sub> terminus. Likewise in the course of a limited MPE digestion a 7 nucleotide long fragment having either a 3'-PO<sub>4</sub> or 3'-phosphoglycolate could be generated. The relative mobilities of these 7-mers under gel electrophoresis would be MPE (3'-phosphoglycolate) > Maxam-Gilbert G, MPE (3'-PO<sub>4</sub>) > DNase I (3'-OH), with the first having the greatest mobility. Thus DNase cleavage products could appear at least a nucleotide shorter in length than its corresponding "G" marker.

5. Given that the entire nucleotide sequence is known, transfer depths of well or peak differences to their corresponding nucleotides as heights of bases in a histogram. These histograms are what we term footprints, corresponding to a quantification of the lightened regions visible in a gel autoradiogram (Figure 71, top).

6. Since most sequence specific binding small molecules bind exclusively to double stranded, non-denatured DNA, repeating these procedures on the opposite, or complementary DNA strand affords a double stranded analysis of footprinting sites on a given nucleotide sequence.

7. Applying the asymmetric cleavage model to these opposite strand footprints affords the small molecule preferred binding sites. This is performed by subtracting the two nucleotide overhang on both 3' ends of the footprints, while adding one to two nucleotides to the 5' underprotected ends. Obviously some personal judgement is employed. The product is a region of base pairs which constitute in size and location the interpreted actual small molecule binding site (see Figure 71b, bottom).

Histogram of footprint



Interpretation of binding site



**Figure 71**

Determination of footprints and binding sites (bp). Measurements from Figure 70 are located over their respective nucleotides on the DNA sequence (bottom). Application of "1/2-maximal" treatment reduces size of footprint. Repeating these procedures on the complementary DNA strand shows another footprint, offset in a 3' direction from the first. Applying the asymmetric models allows for the determination of the actual binding site, here shown as a box around the preferred sequence.

## References

- 1) Gale, E.F.; Cundliffe, E.; Reynolds, P.E.; Richmond, M.H.; Waring, M.J. (1981) The Molecular Basis of Antibiotic Action (Wiley, New York), pp. 258-401.
- 2) Wilson, W.D.; Jones, R.L. (1981) Adv. Pharmacol. Chemother. **18**, 177-222.
- 3) Neidle, S. (1979) Prog. Medicinal Chem. **16**, 151-221.
- 4) Krakow, J.S.; Kumar, S.A. (1978) Pharmac. Ther. A **2**, 261-280.
- 5) Losick, R.; Chamberlin, M. (Eds.) (1976) RNA Polymerase (Cold Spring Harbor, New York).
- 6) Kornberg, A. (1980) DNA Replication (Freeman, Oxford).
- 7) Lown, J.W. (1979) in Mitomycin C: Current Status and New Developments (Eds. S.K. Carter; S.T. Crooke, Academic Press, New York).
- 8) Prestayko, A.W.; Crooke, S.T.; Carter, S.K. (Eds.) (1980) Cisplatin, Current Status and New Developments (Academic Press, New York).
- 9) Hurley, L.H. (1977) J. Antibiotics **30**, 349.
- 10) Song, P.S.; Tapley, K.J. (1979) Photochem. Photobiol. **29**, 1177.
- 11) Connors, T.A. (1975) Handb. Exp. Pharm. **38/2**, 18.
- 12) Meeham, T.; Straub, K. (1979) Nature **277**, 410.
- 13) Akhtar, M.H.; Begleiter, A.; Johnson, D.; Lown, J.W.; McLaughlin, L.; Sim, S.K. (1975) Can. J. Chem. **53**, 2891.
- 14) Lerman, L.S. (1961) J. Mol. Biol. **3**, 18-30.
- 15) Cohen, G.; Eisenberg, H. (1969) Biopolymers **8**, 45.
- 16) Cantor, C. (1981) Cell **26**, 293-295.

- 17) Burger, R.M.; Peisach, J.; Horwitz, S.B. (1981) Life Sci. **28**, 715-727.
- 18) Lown, J.W.; Sim, S.K. (1976) Can. J. Chem. **54**, 2563.
- 19) Watson, J.D.; Crick, F.H.C. (1953) Nature **177**, 964.
- 20) Dickerson, R.E.; Drew, H.R.; Conner, B.N.; Kopka, M.L.; Pjura, P.E. (1982) Cold Spring Harbor Symp. Quant. Biol. **47**, 13-24.
- 21) Sarma, R.H., Ed. (1980) in Nucleic Acid Geometry and Dynamics (Pergamon Press, New York).
- 22) Waring, M.J. (1965) J. Mol. Biol. **13**, 269.
- 23) LePecq, J.-B.; Paoletti, C. (1967) J. Mol. Biol. **27**, 87-106.
- 24) Houssier, C.; Hardy, B.; Fredericq, E. (1974) Biopolymers **13**, 1141-1160.
- 25) Kersten, W.; Kersten, H. (1965) Biochem. Z. **341**, 174.
- 26) Vinograd, J.; Lebowitz, J.; Watson, R. (1968) J. Mol. Biol. **33**, 173-197.
- 27) Ward, D.C.; Reich, E.; Goldberg, I.H. (1965) Science **149**, 1259.
- 28) Kageyama, M.; Hasegawa, M.; Inagaki, A.; Egami, F. (1970) J. Biochem. **67**, 549-557.
- 29) Wells, R.D.; Larson, J.E. (1970) J. Mol. Biol. **319-342**.
- 30) Patel, D.J. (1982) Proc. Natl. Acad. Sci. USA **79**, 6424-6428.
- 31) Quigley, G.S.; Wang, A.H.J.; Ughetto, G., van der Marel, G.; van Boom, J.H.; Rich, A. (1980) Proc. Natl. Acad. Sci. USA **77**, 7204-7209.
- 32) Sanger, F.; Coulson, A.R. (1975) J. Mol. Biol. **94**, 441-448.

- 33) Maxam, A.M.; Gilbert, W. (1977) Proc. Natl. Acad. Sci. USA **74**, 560-564.
- 34) Sanger, F.; Nicklen, S.; Coulson, A.R. (1977) Proc. Natl. Acad. Sci. USA **74**, 5463-5467.
- 35) Maxam, A.M.; Gilbert, W. (1980) Methods Enzymol. **65**, 499-560.
- 36) D'Andrea, A.D.; Haselton, W.A. (1978) Proc. Natl. Acad. Sci. USA **75**, 3608-3612.
- 37) Takeshita, M.; Grollman, A.P.; Ohtsubo, E.; Ohtsubo, H. (1978) Proc. Natl. Acad. Sci. USA **75**, 5983-5987.
- 38) Kross, J.; Henner, W.D.; Hecht, S.M.; Haseltine, W.A. (1982) Biochemistry **21**, 4310-4318.
- 39) Berlin, V.; Haselton, W.A. (1981) J. Biol. Chem. **256**, 4747-4756.
- 40) D'Andrea, A.D.; Haseltin, W.A. (1978) Proc. Natl. Acad. Sci. USA **75**, 4120-4124.
- 41) Galas, D.J.; Schmitz, A. (1978) Nucleic Acids Res. **5**, 3157-3170.
- 42) Schmitz, A.; Galas, D.J. (1982) in Methods in DNA and RNA Sequencing (Weismann, S., Ed.) (Plenum Press, New York).
- 43) Schmitz, A.; Galas, D.J. (1979) Nucleic Acid Res. **6**, 111-137.
- 44) Schmitz, A. (1981) Nucleic Acids Res. **9**, 277-292.
- 45) Ross, W.; Landy, A.; Kikuchi, Y.; Nash, H. (1979) Cell **18** 297-307.
- 46) Simpson, R.B. (1980) Nucleic Acids Res. **8**, 759-766.
- 47) Lomonosoff, G.P.; Butler, P.J.G.; Klug, A. (1981) J. Mol. Biol. **149**, 745-760.
- 48) Blau, L.; Bittman, R. (1975) Mol. Pharmacol. **11**, 716-721.

- 49) Wartell, R.M.; Larson, J.E.; Wells, R.D. (1975) J. Biol. Chem. **250**, 2698-2702.
- 50) Krugh, T.R.; Young, M.A. (1977) Nature (London) **269**, 627-628.
- 51) Hertzberg, R.P.; Dervan, P.B. (1982) J. Amer. Chem. Soc. **104**, 313-315.
- 52) Hertzberg, R.P.; Dervan, P.B. Biochemistry, submitted for publication.
- 53) Liao, T.-H.; Salnikow, J.; Moore, S.; Stein, W.H. (1973) J. Biol. Chem. **248**, 1489-1493.
- 54) Bernardi, A.; Gaillard, C.; Bernardi, G. (1975) Eur. J. Biochem. **52**, 451-457.
- 55) Junowicz, E.; Spencer, J.H. (1973) Biochem. Biophys. Acta **312**, 72-84.
- 56) Anguili, R.; Foresti, E.; Riva di Sanseverino, L.; Isaacc, N.W.; Keinnard, O.; Motherwell, W.D.S.; Wampler, D.L.; Arcamone, F. (1971) Nature New Biol. **234**, 78.
- 57) Arcamone, F. (1978) Top. Antibiot. Chem. **2**, 99-239.
- 58) Remmers, W.A. (1979) The Chemistry of Antitumor Antibiotics Vol. 1, (Wiley, New York), pp. 63-132.
- 59) Di Marco, A.; Arcamone, F.; Zuivino, F. (1975) Antibiotics III W.W. Corcoran; F.E. Mahn, Eds. (Springer-Verlag, New York), 101-128.
- 60) Williamson, N.; Scott-Finnigan, T.J.; Hardman, M.A.; Brown, J.R. (1981) Nature (London) **292**, 466-467.
- 61) Di Marco, A.; Soldati, M.; Fioretti, A.; Dasida, T. (1964) Cancer Chemother. Rep. **38**, 39.

- 62) Tritton, T.R.; Yee, G. (1982) Science **217**, 248-250.
- 63) von Hoff, D.D.; Rozencineig, M. Slavik, M. (1978) Adv. Pharmacol. Chemother. **15**, 1-50.
- 64) Calendi, E.; Di Marco, A.; Reggiani, M.; Scarpinaot, B.; Valentini, L. (1964) Biochem. Biophys. Acta **103**, 25-49.
- 65) Waring, M. (1970) J. Mol. Biol. **54**, 247-279.
- 66) Zunino, F.; Gambetta, R., Di Marco, A.; Zaccara, A. (1972) Biochem. Biophys. Acta. **277**, 489-498.
- 67) Chaires, J.B.; Dattagupta, N.; Crothers, D.M. (1982) Biochemistry **21**, 3933-3940.
- 68) Chaires, J.B. (1983) Biochemistry **22**, 4204-4211.
- 69) Muller, W.; Crothers, D.M. (1975) Eur. J. Biochem. **54**, 267-277.
- 70) Gabbay, E.J.; Grier, D.; Fingerle, R.E.; Reimer, R.; Levy, R.; Pearce, S.W.; Wilson, W.D. (1976) Biochemistry **15**, 2062-2070.
- 71) Yen, S-F.; Germon, W.; Wilson, W.D. (1983) J. Amer. Chem. Soc. **105**, 3717-3719.
- 72) Patel, D.; Kozlowski, S.A.; Rise, J.A. (1981) Proc. Natl. Acad. Sci. USA **78**, 3333-3337.
- 73) Mayer, A.B. (1980) Top. Antibiotic. Chem. **5**, 223.
- 74) Remers, W.A. (1978) The Chemistry of Antitumor Antibiotics Vol. 1 (Wiley, New York), pp. 3-62.
- 75) Goldberg, I.H.; Robinowitz, M.; Reich, E. (1962) Proc. Natl. Acad. Sci. USA **48**, 2094-2101.
- 76) A.M.A. Drug Evaluations 2nd ed. (1973) (Publishing Sciences Group, Acton, MA), pp. 853-854.
- 77) Hyman, R.W.; Davidson, N. (1970) J. Mol. Biol. **50**, 521.

- 78) Muller, W.; Crothers, D.M. (1968) J. Mol. Biol. **35**, 251-290.
- 79) Mirau, P.A.; Shafer, R.H. (1982) Biochemistry **21**, 2626-2631.
- 80) Jain, S.C.; Sobel, H.M. (1972) J. Mol. Biol. **68**, 1-20.
- 81) Sobell, H.M.; Jain, S.C. (1972) J. Mol. Biol. **68**, 21-34.
- 82) Takusagawa, F.; Dabrow, M.; Neidle, S.; Berman, H.M. (1982)  
Nature (London) **296**, 466-469.
- 83) Krugh, T.R., Mooberry, E.S.; Chen Chiao, Y.-C. (1977)  
Biochemistry **16**, 740-747.
- 84) Krugh, T.R. (1981) in Topics in Nucleic Acid Structure ed.  
Neidle, S. (Macmillan, London), pp. 197-217.
- 85) Patel, D.J.; Kozlowski, S.A.; Rice, J.A.; Broka, C.; Itakura, K.  
(1981) Proc. Natl. Acad. Sci. USA **78**, 7281-7284.
- 86) Krey, A.K. (1980) Prog. Mol. Subcell. Biol. **7**, 43-87.,
- 87) Zimmer, C. (1975) Progr. Nucleic Acid Res. Mol. Biol. **15**,  
285-318.
- 88) Arcamone, F., Penco, S.; Orezzi, P.; Nicoletta, V.; Pirelli, A.  
(1964) Nature (London) **203**, 1064-1065.
- 89) Nakamura, S., Yowehara, H.; Umezawa, H. (1964) J. Antibiot.  
(Tokyo) Ser. A, **17**, 220-221.
- 90) Bailer, M.; Yagen, B.; Mechoulam, R. (1978) Tetrahedron **34**, 2389.
- 91) Berman, H., Neidle, S., Zimmer, C.; Thrum, H. (1979) Biochem.  
Biophys. Acta **561**, 124-131.
- 92) Hahn, F.E. (1975) in Antibiotic III J.W. Corcoran; F.E. Hahn,  
Eds., (Springer-Verlag, New York), pp. 79-100.
- 93) Zimmer, C.; Luck, G. (1970) FEBS Lett. **10**, 339-342.
- 94) Luck, G.; Triebel, H.; Waring, M.; Zimmer, C. (1974) Nucleic

- Acids Res. **1**, 503-530.
- 95) Zimmer, C., Reinert, K.E., Luck, G.; Wahwert, U.; Lober, G.; Thrum, H. (1971) J. Mol. Biol. **58**, 329-348.
- 96) Zimmer, C.; Luck, G.; Nuske, R. (1980) Nucleic Acids Res. **8**, 2999-3010.
- 97) Krylov, A.S.; Grokhovsky, S.L.; Zasedatelev, A.S.; Zhuze, A.L. Gursky, G.V.; Gottikh, B.P. (1979) Nucleic Acids Res. **6**, 289-304.
- 98) Kolchinskii, A.M.; Mirazabekov, A.D.; Zasedatelev, A.S.; Gurskii, G.V.; Grokhovskii, S.L.; Zhuze, A.L.; Gottikh, B.P. (1975) Mol. Biol. (USSR) **9**, 14-20.
- 99) Zasedatelev, A.S.; Zhuze, A.L.; Zimmer, C., Grokhovskii, S.L.; Tumaryan, V.; Gurskii, G.V.; Gottikh, B.P. (1978) Stud. Biophys. **67**, 47-48.
- 100) Dickerson, R.E. (1983), personal communication.
- 101) Remmers, W.A. (1979) The Chemistry of Antitumor Antibiotics Vol. 1, (Wiley, New York) pp. 133-175.
- 102) Kersten, W.; Kersten, H. (1974) Molec. Biol. Biochem. Biophys. **18**, 86-96.
- 103) Thiem, J.; Meyer, B. (1979) J. Chem. Soc., Perkin Trans. **2**, 1331-1336.
- 104) Thiem, J.; Meyer, B. (1981) Tetrahedron **37**, 551-558.
- 105) Thiem, J.; Schneider, G. (1983) Angew. Chem. Int. Ed. Engl. **22**, 58-59.
- 106) Slavik, M.; Carter, S.K. (1975) Adv. Pharmacol. Chemother. **12**, 1-30.
- 107) Behr, W.; Howiekl, K.; Hartmann, G. (1969) Eur. J. Biochem. **9**,

- 82-92.
- 108) Prasad, K.S.; Nayak, R. (1976) FEBS Lett. **71**, 171-174.
- 109) Katagiri, K.; Yoshida, T.; Satso, K. (1975) in Antibiotics III, J.W. Corcoran; F.E. Hah, Eds. (Springer-Verlag, New York), pp 234-251.
- 110) Dell, A.; Williams, D.H.; Morris, H.R.; Smith, G.A.; Feeney, J.; Roberts, G.C.K. (1975) J. Amer. Chem. Soc. **97**, 2497-2502.
- 111) Martin, D.G.; Mizsak, S.A.; Biles, C.; Stewart, J.C.; Baczynskyj, L.; Meulman, P.A. (1975) J. Antibiot. **28**, 332-336.
- 112) Waring, M.J. (1979) in Antibiotics Vol. 5/Part 2, F.E. Hahn, Ed., (Springer-Verlag, New York), pp. 173-194.
- 113) Waring, M.J.; Wakelin, L.P.G. (1974) Nature (London) **252** 653-657.
- 114) Wakelin, L.P.G.; Waring, M.J. (1976) Biochem. J. **157**, 721-740.
- 115) Lee, J.S.; Waring, M.J. (1978) Biochem. J. **173**, 129-144.
- 116) Fox, K.R.; Wakelin, L.P.G.; Waring, M.J. (1981) Biochemistry **20**, 5768-5779.
- 117) Cheung, H.T.; Feeney, J.; Roberts, G.C.K.; Williams, D.H.; Ughetto, G.; Waring, M.J. (1978) J. Amer. Chem. Soc. **100**, 46-54.
- 118) Ughetto, G.; Waring, M.J. (1977) Mol. Pharmacol. **13**, 579-584.
- 119) Viswamitra, M.A.; Kennard, O.; Cruse, W.B.T.; Egert, E.; Sheldrick, G.M.; Jones, P.J.; Waring, M.J.; Wakelin, L.P.G.; Olsen, R.K. (1981) Nature (London) **289**, 817-819.
- 120) Bonadonna, G.; Monfardini, S., DeLena, M.; Fossati-Bellani, F.; Beretta, G. (1970) Cancer Res. **30**, 2572-2582.
- 121) Middleman, E.; Luce, J.; Frei, E. (1971) Cancer **28**, 844-850.

- 122) Pigram, W.J.; Fuller, W.; Hamilton, L.O. (1972) Nature (London) New Biol. **35**, 17-19.
- 123) Du Vernay, Jr., V.H.; Pachter, J.A.; Crooke, S.T. (1979) Biochemistry **18**, 4024-4030.
- 124) Tsou, K.C.; Yip, K.F. (1976) Cancer Res. **36**, 3367-3373.
- 125) Wiley, P.F.; Elrod, D.W.; Houser, D.J.; Richard, F.A. (1982) J. Med. Chem. **25**, 560-567.
- 126) Das, G.C., Dasgupta, S; Dasgupta, N.N. (1974) Biochem. Biophys. Acta **353**, 274-282.
- 127) Sinha, R.K.; Talapatra, P.; Mitra, A.; Mazumder, S. (1977) Biochem. Biophys. Acta **474**, 199-209.
- 128) Bhuyan, B.K.; Smith, C.G. (1965) Proc. Natl. Acad. Sci. USA **54**, 566-572.
- 129) Bhuyan, B.K.; Neil, G.L.; Li, L.H., McGovern, J.P.; Wiley, P.F. (1980) in Anthracyclines: Current Status and New Developments Academic Press, New York, pp. 365-395.
- 130) Lee, J.S; Waring, M.J. (1978) Biochem. J. **173**, 115-128.
- 131) Personal communication from R.K. Olsen, 3/8/82.
- 132) Chandra, P.; Waltersdorf, M.; Wright, G.J. (1979) in Antibiotics V/ Part 2. Mechanism of Action of Antieucaryotic and Antiviral Compounds (Hahn, F.E., Ed.) Springer-Verlag, Berlin, pp. 385-413.
- 133) Wright, R.G. McR.; Wakelin, L.P.G.; Fields, A.; Acheson, R.M.; Waring, M.J. (1980) Biochemistry **19**, 5825-5836.
- 134) Sturm, J. (1981) Biopolymers **20**, 765-785.
- 135) Newton, B.A. (1975) Antibiotics III: Mechanism of Action of

- Antimicrobial and Antitumor Agents (Corcoran, J.W.; Hahn, F.E., Eds.), Springer-Verlag, Berlin, pp. 34-47.
- 136) Braithwaite, A.W.; Bagyley, B.C. (1980) Biochemistry **19**, 1101-1106.
- 137) Kross, J., Henner, W.D.; Haseltine, W.A.; Rodriguez, L.; Levin, M.D.; Hecht, S.M. (1982) Biochemistry **21**, 3711-3721.
- 138) Kuroda, R.; Neidle, S.; Sakai, T.T. (1982) Nucleic Acids Res. **10**, 4753-4763.
- 139) Chien, M.; Grollman, A.P.; Horwitz, S.B. (1977) Biochemistry **16**, 3641-3647.
- 140) Hecht, S.M., Ed. (1979) Bleomycin: Chemical: Biochemical and Biological Aspects (Springer-Verlag, New York).
- 141) Becker, M.M.; Dervan, P.B. (1978) J. Amer. Chem. Soc. **101**, 1968-1970.
- 142) Becker, M.M.; Dervan, P.B. (1979) J. Amer. Chem. Soc. **101**, 3664-3666.
- 143) Silver, S., Wendt, L.; Bhattacharyya, P. (1975) Antibiotics III: Mechanism of Action of Antimicrobial and Antitumor Agents (Corcoran, J.W.; Hahn, F.E., Eds.) Springer-Verlag, Berlin, pp. 614-622.
- 144) Mahler, H.R.; Green, G.; Goutarel, R.; Khoung-Huu, Q. (1968) Biochemistry **7**, 1568-1582.
- 145) Sobell, H.M.; Tsai, C.C.; Jain, S.C.; Gilbert, S.G. (1977) J. Mol. Biol. **114**, 333.
- 146) Kurnick, N.B. (1950) Exp. Cell Res. **1**, 151-158.
- 147) Krey, A.K.; Hahn, F.E. (1975) Biochemistry **14**, 5061-5067.

- 148) Wakelin, L.P.G.; Adams, A.; Hunter, C.; Waring, M.J. (1981) Biochemistry **20**, 5779-5787.
- 149) Muller, W.; Gautier, F. (1975) Eur. J. Biochem. **54**, 385-394.
- 150) Albert, A. (1973) in Selective Toxicity (5th ed.) Chapman and Hall, London.
- 151) Peacocke, A.R.; Skerrett, J.W.M. (1956) Trans. Faraday. Soc. **52**, 261.
- 152) Chan, L.M.; Van Winkle, Q. (1969) J. Mol. Biol. **40**, 491.
- 153) Schlessinger, D.; Medoff, G. (1975) in Antibiotics III: Mechanism of Action of Antimicrobial and Antitumor Agents (Corcoran, J.W. Hahn, F.E., Eds.) Springer-Verlag, pp. 535-550.
- 154) Moskowitz, M. (1963) Nature (London) **200**, 335-337.
- 155) Zimmer, C., Triebel, H.; Thrum, H. (1967) Biochem. Biophys. Acta **145**, 742-751.
- 156) Dabrowiak, J.C. (1983) Life Sci. **32**, 2915-293.
- 157) Tullius, T.D.; Lippard, S.J. (1981) J. Amer. Chem. Soc. **103**, 4620-4622.
- 158) Royer-Pokora, B.; Gordon, L.K.; Haseltine, W.A. (1981) Nucleic Acids Res. **9**, 4595-4609.
- 159) Sugiura, Y.; Suzuki, T. (1982) J. Biol. Chem. **257**, 10544-10546.
- 160) Wilkins, R.J. (1982) Nucleic Acids Res. **10**, 7273-7282.
- 161) Nosikov, V.V.; Braga, E.A.; Karlishev, A.V.; Zhurze, A.L.; Polyanovski, O.L. (1976) Nucleic Acids Res. **3**, 2293-2301.
- 162) Karia, J.; Fanning, T.G. (1976) Eur. J. Biochem. **67**, 367-371.
- 163) Ikeda, R.A.; Dervan, P.B. (1982) J. Amer. Chem. Soc. **104**, 296-297.

- 164 Lane, M.J.; Dabrowiak, J.C.; Vournakis, J.N. (1983) Proc. Natl. Acad. Sci. USA **80**, 3260-3264.
- 165 Weinstein, J.; Bielski, B.H.J. (1979) J. Amer. Chem. Soc. **101**, 58-62.
- 166 Haber, F.C.; Weiss, J. (1934) Proc. R. Soc. London, Ser. A. **147**, 332-351.
- 167 Wu, J.C.; Kozarich, J.W.; Stubbe, J. (1983) J. Biol. Chem. **258**, 4694-4697.
- 168 Dougherty, G. (1982) Int. J. Biochem. **14**, 493-504.
- 169 Van Dyke, M.W.; Hertzberg, R.P.; Dervan, P.B. (1982) Proc. Natl. Acad. Sci. USA **79**, 5470-5474.
- 170 Van Dyke, M.W.; Dervan, P.B. (1982) Cold Spring Harbor Symp. Quan. Biol. **47**, 347-353.
- 171 Van Dyke, M.W.; Dervan, P.B. (1983) Biochemistry **22**, 2373-2377.
- 172 Van Dyke, M.W.; Dervan, P.B. (1983) Nucleic Acids Res. **11**, 5555-5567.
- 173 Van Dyke, M.W.; Dervan, P.B. Proc. Natl. Acad. Sci. USA in preparation.
- 174 Pohl, F.M.; Jovin, T.M. (1972) J. Mol. Biol. **67**, 375-396.
- 175 Drew, H.; Takano, T.; Tanaka, S.; Itakura, K.; Dickerson, R.E. (198) Nature (London) **286**, 567-573.
- 176 Peck, L.J.; Nordheim, A.; Rich, A.; Wang, J.C. (1982) Proc. Natl. Acad. Sci. USA **79**, 4560-4564.
- 177 Singleton, C.K.; Klysik, J.; Stirdivant, S.M.; Wells, R.D. (1982) Nature (London) **286**, 567-573.
- 178 Klysik, J.; Stirdivant, S.M.; Larson, J.E.; Hart, P.A.; Wells,

- R.D. (1981) Nature (London) **290**, 672-677.
- 179) van de Sande, J.H.; Jovin, T.M. (1982) EMBO J. **1**, 115-120.
- 180) Mirau, P.A.; Kearns, D.R. (1983) Nucleic Acids Res. **11**, 1931-1941.
- 181) Bourgeois, S.; Pfahl, M. (1976) Adv. Protein Chem. **30**, 1-99.
- 182) Crothers, D.M. (1968) Biopolymers **6**, 575-584.
- 183) Pohl, F.; Jovin, T.M.; Baehr, W.; Holbrook, J.J. (1972)  
Proc. Natl. Acad. Sci. USA **69**, 3805-3809.
- 184) Hogan, M.; Dattagupta, N.; Crothers, D.M. (1979) Nature (London)  
**278**, 521-524.
- 185) Rosenberg, L.S.; Balakrishnan, M.S.; Graves, D.E.; Lee, K.R.;  
Winkle, S.A.; Krugh, T.R. (1982) in Biological Activities of  
Polymers (American Chemical Society) pp. 268-281.
- 186) Wilson, W.D.; Jones, R.L. (1982) Nucleic Acids Res. **10**,  
1399-1410.
- 187) Zimmer, C.; Marck, C.; Guschlbauer, W. (1983) FEBS Lett. **154**,  
156-160.
- 188) Crothers, D.M.; Fried, M. (1982) Cold Spring Harbor Symp. Quant.  
Biol. **47**, 263-269.
- 189) Dickson, R.C.; Abelson, J.; Barnes, W.M.; Reznikoff, W.S. (1975)  
Science (Washington) **187**, 27-35.
- 190) Fried, M.G.; Crothers, D.M. (1983) Nucleic Acids Res. **11**,  
141-158.
- 191) Wang, J.C.; Barkley, M.D.; Bourgeois, S. (1974) Nature (London)  
**251**, 247.
- 192) Schultz, P.G.; Taylor, J.S.; Dervan, P.B. (1982) J. Amer. Chem.  
Soc. **104**, 6861-6863.

- 193) Schultz, P.G.; Dervan, P.B. (1983) Biomolecular Structure and Dynamics in press.
- 194) Hochstein, F.A.; Stephens, C.RF.; Conover, L.H.; Regyna, P.P.; Pasternack, R.; Gordon, P.N.; Pilgrim, F.J.; Brunings, K.J.; Woodward, R.B. (1953) J. Amer. Chem. Soc. **75**, 5455-5475.
- 195) Arnott, S.; Selsing, E. (1974) J. Mol. Biol. **88**, 551-552.
- 196) Arnott, S.; Selsing, E. (1974) J. Mol. Biol. **88**, 509-521.
- 197) Ogata, R.T.; Gilbert, W. (1977) Proc. Natl. Acad. Sci. USA **74**, 4973-4976.
- 198) Smith, T.F.; Sadler, J.R. (1971) J. Mol. Biol. **59**, 273-305.
- 199) Gilbert, W.; Gralla, J.; Majors, J.; Maxam, A. (1975) in Protein-Ligand Interactions (H. Sund; G. Blauer, Eds.) (Walter-de Gruyter, Berlin), pp. 193-210.
- 200) Gilbert W.; Maxam, A.; Mirzabekov, A. (1976) in Control of Ribosome Synthesis (N.O. Kjeldgaard; O. Maaløe, Eds.) (Munksgaard, Copenhagen), pp. 139-148.
- 201) Bolivar, F.; Rodriguez, R.L.; Greene, P.J.; Betlach, M.C.; Heynecker, H.L.; Boyer, H.W. (1977) Gene **2**, 95-113.
- 202) Johnsrud, L. (1978) Proc. Natl. Acad. Sci. USA **75**, 5314-5318.
- 203) Tanaka, T.; Weisblum, B. (1975) J. Bacteriol. **121**, 354-362.
- 204) Maniatis, T.; Fritsch, E.F.; Sambrook, J. (1982) Molecular Cloning: A Laboratory Manual (Cold Spring Harbor, New York).
- 205) Sutcliffe, J.G. (1978) Cold Spring Harbor Symp. Quant. Biol. **43**, 77-90.
- 206) Haseltine, W.A.; Linden, C.P.; D'Andrea, A.D.; Johnsrud, L.

- (1980) Methods Enzymol. **65**, 235-248.
- 207) Jacobsen, H.; Klenow, H.; Overgaard-Hansen, K. (1974) Eur. J. Biochem. **45**, 623-627.
- 208) Chaconas, G.; van de Sande, J.H. (1980) Methods Enzymol. **65**, 75-85.

## APPENDIX

A series of antibiotics employed in cancer chemotherapy, including such substances as chromomycin, mithramycin, olivomycin, luteoskyrin, and kanchanomycin (albofungin) (see Figure 1 for structures), have been shown to interact with DNA in a noncovalent fashion.<sup>1</sup> All of these molecules require a stoichiometric amount of a divalent cation, usually  $Mg^{2+}$ , for the binding reaction.<sup>2</sup> The first three are of very similar structure, bind primarily to double helical DNA, and interact specifically with the 2-amino group of guanine. Luteoskyrin and albofungin have similar structural elements, yet interact with denatured DNA, RNA, and various synthetic polynucleotides while exhibiting limited base specificity. All five antibiotics are believed to evince their therapeutic abilities by interfering with the progress of RNA polymerase on an affected template.<sup>2</sup>

Recent studies on the sequence specific binding of the antibiotics chromomycin, mithramycin, and olivomycin to heterogeneous DNAs have indicated the preferred binding sites as being 2-3 base pairs in length and containing 2 or more contiguous G·C base pairs.<sup>3</sup> Earlier work by Behr et al. has indicated that the binding specificity is due to the chromomycinone chromophore and that the attached sugar side chains act to decrease the rate of complex dissociation.<sup>4</sup> Binding constants for these chromomycin analogs therefore vary with the number of sugar residues present, going from  $\sim 10^5 M^{-1}$  for a chromophore with 5 hexopyranoses attached to  $\sim 10^3 M^{-1}$  with just one. These antibiotics are anionic at pH 7, and exist as dimers in solution with  $Mg^{2+}$ .<sup>5</sup>

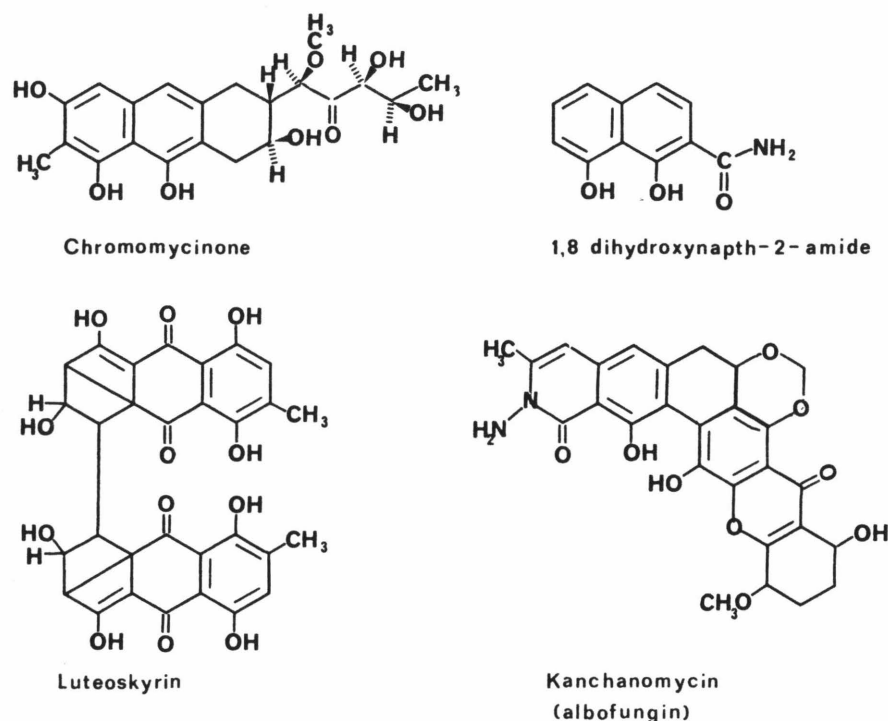


Figure 1

Structures of magnesium chelating, DNA binding antibiotics.

Divalent cations may be directly involved in binding, acting to counteract electrostatic repulsion between the negatively charged phosphate groups on the DNA and the anionic site on the antibiotic.<sup>6</sup> The actual mode of DNA binding is not understood, though intercalation is considered unlikely.<sup>7</sup>

1,8-Dihydroxy-2-naphthaldehyde, a simple model compound for these antibiotics, demonstrates a similar  $pK_a = 5$  in aqueous solutions.<sup>8</sup> The strong acidity of this compound is due to the close proximity of the

two hydroxyl functionalities, allowing stabilization of the acquired negative charge by internal hydrogen bonding. Through the use of CPK models, the binding of chromomycin-like chromophores to DNA may proceed through simultaneous chelation of a  $Mg^{2+}$  ion by an ionized hydroxyl functionality on the chromophore and by the phosphate sugar backbone. Additional hydrogen bonding between the chromophore and the amino functions of two adjacent guanines could serve to stabilize this complex. In this model the attached sugar side chains of chromomycin could stay in the minor

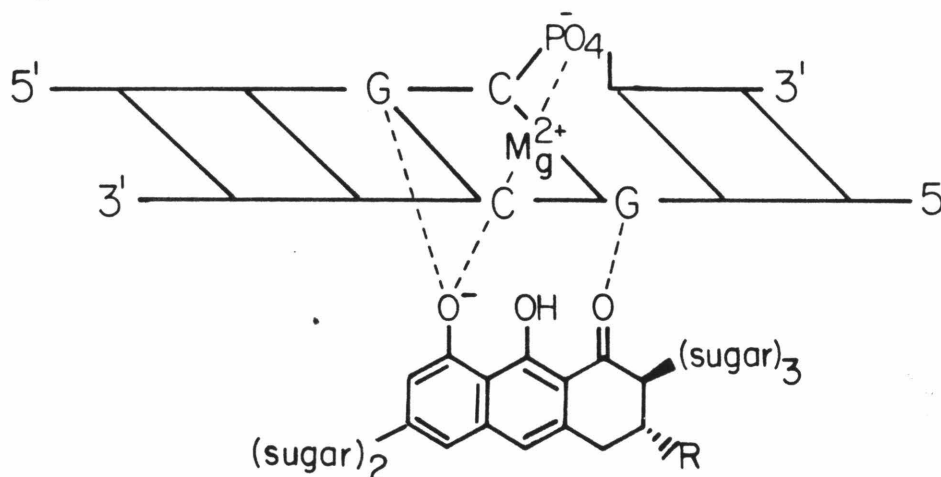


**Figure 2**  
Postulated binding model of chromomycinone-like chromophores and DNA.

groove without interfering with the binding process. Similar cases for the simultaneous chelation of  $Mg^{2+}$  by the DNA phosphate backbone and properly oriented aromatic hydroxyl substituents can also be made for luteoskyrin and albufungin.

Since the synthesis of the chromomycin chromophore has yet to be completed,<sup>8</sup> and should prove difficult to manipulate chemically I propose the design and synthesis of a similar G-specific, bis-chelating DNA binder, bis[1,8-dihydroxynaphthan-2-amide]diethylenetriamine (BDN). Its synthetic scheme is outlined in Figure 3.<sup>9</sup> The length of the linker

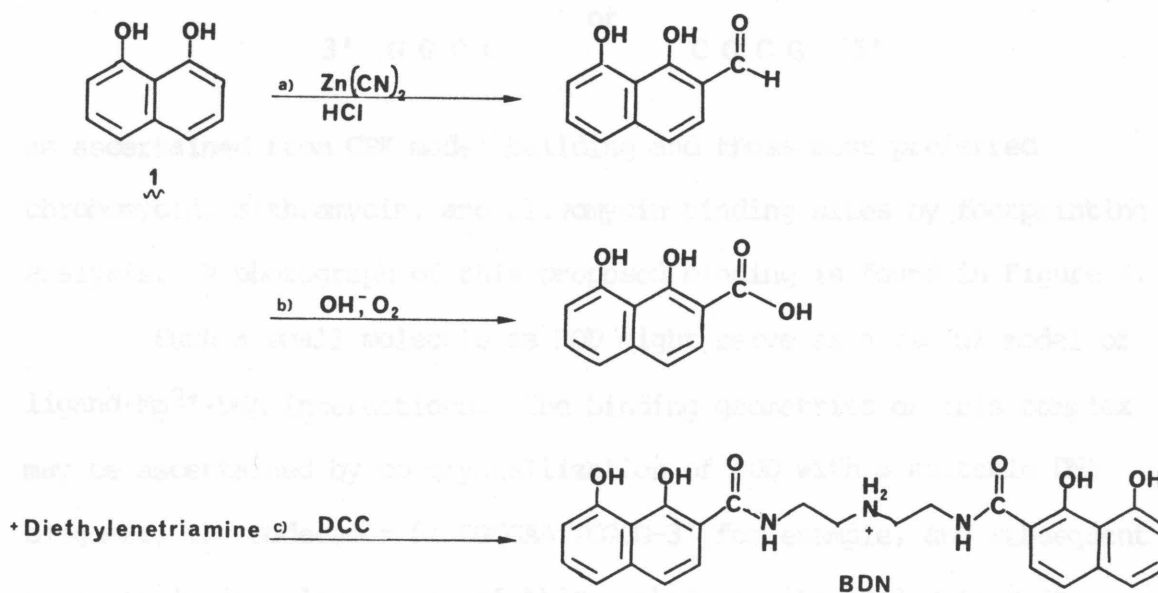
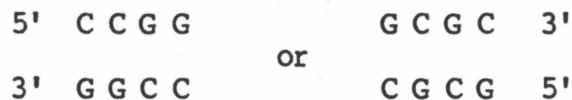


**Figure 3**

Synthetic scheme for bis[1,8-dihydroxynaphthan-2-amide] diethylenetriamine. (BDN). **1**, 1,8-dihydroxynaphthalene is commercially available. Individual reactions are: a) Gatterman reaction, formylation with  $Zn(CN)_2 + HCl$ ; b) Cannizzaro reaction, ring hydroxide oxidizes alcohol formed; c) Dicyclohexylcarbodiimide-mediated acylation of amines.

can be modified to provide optimal sequence specificity and DNA binding,

though this linker length was found ideal by CPK model studies. Given the presence of the protonated secondary nitrogen at physiological pHs and the bis-chelating abilities of the two chromophores, BDD should exhibit binding constants on the order of  $10^5 - 10^6$  in moderate salt buffer (100 mM). Such binding constants are on par with those of the echinomycin and triostin families of bisintercalators,<sup>10</sup> thus allowing the use of MPE and DNase footprinting assays for determination of binding specificity. Sequence specificity would ideally be for the double stranded sequences:



as ascertained from CPK model building and those most preferred chromomycin, mithramycin, and olivomycin binding sites by footprinting analysis. A photograph of this proposed binding is found in Figure 4.

Such a small molecule as BDD might serve as a useful model of ligand·Mg<sup>2+</sup>·DNA interactions. The binding geometries of this complex may be ascertained by co-crystallization of BDD with a suitable DNA oligomer, the dodecamer 5'-CGCGAATTGCG-3' for example, and subsequent x-ray analysis. An example of this method was its application in determining the binding of daunomycin to DNA.<sup>11</sup> With this method, the important question concerning changes in the structural conformation of the DNA substrate upon this chelation mode of binding would also be amenable to investigation. Solution studies of the interactions between these self-complementary DNA oligomers and BDD could in turn be investigated by <sup>1</sup>H and <sup>31</sup>P NMR. This was best exemplified by work

performed on the intercalators actinomycin and the minor groove binder netropsin interacting with the aforementioned dodecamer.<sup>12</sup> In fact, while this molecule BDD serves as a model for the divalent-cation chelative binding of antibiotics to DNA, it may also shed light on the greater questions of protein/DNA interactions, many of these requiring the presence of divalent cations for binding and reactivity.

References

- 1) Gale, E.F.; Cundliffe, E.; Reynold, P.E.; Richmond, M.H.; Waring, M.J. (1981) "The Molecular Basis of Antibiotics Action" (Wiley, New York), pp. 258-401.
- 2) a) Kersten, W.; Kersten, H. (1974) Molec. Biol. Biochem. Biophys. **18**, 86-96. b) Goldberg, I.H. (1975) in "Antibiotics III. Mechanism of Action of Antimicrobial and Antitumor Agents" (eds., J.W. Corcoran and F.E. Hahn), Springer-Verlag, New York, pp. 166-173.
- 3) a) Van Dyke, M.W.; Dervan, P.B. (1983) Biochemistry **22**, 2373-2377. b) Van Dyke, M.W.; Dervan, P.B. (1983) Nucleic Acids Res. **11**, 5555-5567.
- 4) Behr, W.; Honikel, K.; Hartmann, G. (1969) Eur. J. Biochem. **9**, 82-92.
- 5) Fey, G. (1973) Doctoral Dissertaion, Erlangen-Neurnberg.
- 6) Prasard, K.S.; Nayak, R. (1976) FEBS Lett. **71**, 171-174.
- 7) Waring, M.J. (1970) J. Mol. Biol. **54**, 247-279.
- 8) a) Remmers, W.A. (1979) "The Chemistry of Antitumor Antibiotics" (Wiley, New York), pp. 133-173. b) Dodd, J.H.; Garigipati, R.S.; Weinreb, S.M. (1982) J. Org. Chem. **47**, 4045-4049. c) Frank, R.W.; John, T.V. (1983) J. Org. Chem. **48**, 3269-3276.
- 9) a) Morgan, G.T.; Vining, D.C. (1921) J. Chem. Soc. **119**, 183. also see: Chen, K-M.; Joullie, M.M. (1982) Tetrehedron Lett. **23**, 4567-4568. b) Hochstein, F.A.; Stephens, C.R.; Conover, L.H.; Regna, P.P.; Pasternack, R.; Gordon, P.N.; Pilgrim, F.J.; Brunings, K.J.; Woodward, R.B. (1953) J. Amer. Chem. Soc. **75**,

- 5455-5475. c) Anderson, G.W.; Zimmerman, J.E.; Callahan, F.M. (1964) J. Amer. Chem. Soc. **86**, 1839-1842. see also: Windridge, G.C.; Jorgensen, E.C. (1971) J. Amer. Chem. Soc. **93**, 6318-5319.
- 10) Waring, M.J. (1979) in "Antibiotics, Vol. 5/Part 2. Mechanism of Action of Antieukaryotic and Antiviral Compounds" (ed., F.E. Hahn), Springer-Verlag, New York, pp. 173-194.
- 11) Quigley, G.N.; Wang, A.H.-J.; Ughetto, G.; van der Marel, G.; van Boom, J.H.; Rich, A. (1980) Proc. Natl. Acad. Sci. USA **77**, 7204-7208.
- 12) Patel, D.N.; Kozlowski, S.A.; Rice, J.A.; Broka, C.; Itakura, K. (1981) Proc. Natl. Acad. Sci. USA **78**, 7281-7284.

**Figure 4**

Corey-Pauling-Koltun (CPK) molecule model of BDD binding to DNA.  
The hydrograms of BDD have been marked for greater clarity.

